

**Low thermal expansion glass-ceramics  
in the system BaO - Al<sub>2</sub>O<sub>3</sub> - B<sub>2</sub>O<sub>3</sub>  
- crystallisation and properties-**

**Dissertation**

zur Erlangung des akademischen Grades doctor rerum naturalium  
(Dr. rer. nat.)

vorgelegt dem Rat der Chemisch-Geowissenschaftlichen Fakultät der  
Friedrich-Schiller-Universität Jena

von Dipl.-Chem. Diana Tauch  
geboren am 02.04.1977 in Jena

Gutachter:

1. Prof. Dr. C. Rüssel
2. Prof. Dr. D. Stachel

Tag der öffentlichen Verteidigung: 22.04.2005

# Contents

<b>1</b>	<b>Deutsche Zusammenfassung</b>	<b>1</b>
<b>2</b>	<b>Introduction</b>	<b>6</b>
<b>3</b>	<b>Principles and basics</b>	<b>8</b>
3.1	Low thermal expansion glass-ceramics . . . . .	8
3.2	Crystallisation of glass . . . . .	9
3.3	Incorporation of boron oxide, aluminum oxide and barium oxide in glasses	10
3.4	Crystalline phases of the composition $\text{BaAl}_2\text{B}_2\text{O}_7$ . . . . .	11
<b>4</b>	<b>Experimental procedure</b>	<b>13</b>
4.1	Preparation of glasses . . . . .	13
4.2	Preparation of glass-ceramics . . . . .	14
4.3	Preparation of sinter glass-ceramics . . . . .	14
4.4	Properties of the glasses and glass-ceramics . . . . .	15
4.4.1	Density . . . . .	15
4.4.2	Differential thermal analysis . . . . .	15
4.4.3	Dilatometry . . . . .	15
4.4.4	Hydrolytic durability . . . . .	17
4.4.5	Viscosity . . . . .	17
4.4.6	X-ray diffraction . . . . .	17
4.4.7	Optical microscopy . . . . .	18
4.4.8	Electron microscopy . . . . .	18
4.4.9	Atomic force microscopy . . . . .	18
4.5	Structure of glasses and glass-ceramics . . . . .	18
4.5.1	IR spectroscopy . . . . .	18
4.5.2	Raman spectroscopy . . . . .	19
4.6	Electrical conductivity . . . . .	19

4.6.1	Experimental setup . . . . .	19
4.6.2	Experimental procedure . . . . .	19
<b>5</b>	<b>Glass-ceramics development</b>	<b>21</b>
5.1	Stoichiometric glass BaO - Al <sub>2</sub> O <sub>3</sub> - B <sub>2</sub> O <sub>3</sub> . . . . .	21
5.1.1	Glass properties . . . . .	21
5.1.2	Bulk glass-ceramics BaO - Al <sub>2</sub> O <sub>3</sub> - B <sub>2</sub> O <sub>3</sub> . . . . .	23
5.1.3	Bulk glass-ceramics BaO - Al <sub>2</sub> O <sub>3</sub> - B <sub>2</sub> O <sub>3</sub> with platinum . . . . .	24
5.1.4	Sinter glass-ceramics BaO - Al <sub>2</sub> O <sub>3</sub> - B <sub>2</sub> O <sub>3</sub> . . . . .	25
5.1.5	Comparison of sinter and bulk glass-ceramics with and without platinum . . . . .	27
5.2	Influence of the BaO concentration on the crystallisation . . . . .	32
5.3	Influence of the B <sub>2</sub> O <sub>3</sub> concentration on the crystallisation behaviour . . . . .	39
5.3.1	Glass 0.9 BaO - 1.0 Al <sub>2</sub> O <sub>3</sub> - 1.1 B <sub>2</sub> O <sub>3</sub> - Influence of the platinum concentration . . . . .	45
5.4	Addition of TiO <sub>2</sub> . . . . .	48
5.5	Addition of TiO <sub>2</sub> / ZrO <sub>2</sub> . . . . .	58
<b>6</b>	<b>Conductivity measurements</b>	<b>65</b>
6.1	General analysis and errors of the measurements . . . . .	65
6.1.1	Analysis of the impedance measurements . . . . .	65
6.1.2	Discussion of the measurement errors . . . . .	68
6.2	BaO - Al <sub>2</sub> O <sub>3</sub> - B <sub>2</sub> O <sub>3</sub> . . . . .	69
6.3	0.9 BaO - Al <sub>2</sub> O <sub>3</sub> - B <sub>2</sub> O <sub>3</sub> . . . . .	71
6.4	Discussion - Conductivity measurements of BaO - Al <sub>2</sub> O <sub>3</sub> - B <sub>2</sub> O <sub>3</sub> and 0.9 BaO - Al <sub>2</sub> O <sub>3</sub> - B <sub>2</sub> O <sub>3</sub> . . . . .	74
6.5	Influence of MgO and Li <sub>2</sub> O additions on the miscibility gap and the conductivity of the melt . . . . .	83
6.5.1	0.1 MgO - 0.8 BaO - Al <sub>2</sub> O <sub>3</sub> - B <sub>2</sub> O <sub>3</sub> . . . . .	84
6.5.2	0.1 Li <sub>2</sub> O - 0.9 BaO - Al <sub>2</sub> O <sub>3</sub> - B <sub>2</sub> O <sub>3</sub> . . . . .	85
6.5.3	0.2 Li <sub>2</sub> O - 0.8 BaO - Al <sub>2</sub> O <sub>3</sub> - B <sub>2</sub> O <sub>3</sub> . . . . .	87
6.5.4	Summary of the conductivity measurements . . . . .	89
6.5.5	Discussion - Conductivity measurements of glasses with the additions of Li <sub>2</sub> O or MgO . . . . .	90
<b>7</b>	<b>Discussion</b>	<b>101</b>



*CONTENTS*

iii

**8 Summary**

**106**

**Bibliography**

**109**

# Chapter 1

## Deutsche Zusammenfassung

Glaskeramiken sind polykristalline Feststoffe, welche durch gesteuerte Kristallisation von Glas hergestellt werden. In der heutigen Zeit finden sie eine breite Anwendung, weil sie sich durch spezielle Eigenschaften, die außerordentlich gegenüber dem Glas sind, auszeichnen. Verwendung finden sie deshalb als hochfeste Glaskeramiken [1–3], Sinterglaskeramiken [4, 5], maschinell bearbeitbare [6–8] und biokompatible Glaskeramiken [9–11] und Glaskeramiken mit niedrigen thermischen Ausdehnungskoeffizienten [12, 13]. Glaskeramiken mit niedrigen thermischen Ausdehnungskoeffizienten basieren z.B. auf der Kristallphase  $\beta$ -Eucryptit, welche einen negativen thermischen Ausdehnungskoeffizienten aufweist [14].

Im System BaO - Al<sub>2</sub>O<sub>3</sub> - B<sub>2</sub>O<sub>3</sub> zeigen Glaskeramiken ebenfalls einen negativen linearen thermischen Ausdehnungskoeffizienten [15] und besitzen somit das Potential für einen neuen Werkstoff mit Nullausdehnung. Das Glas / Glaskeramik / System BaO - Al<sub>2</sub>O<sub>3</sub> - B<sub>2</sub>O<sub>3</sub> stand im Mittelpunkt der Untersuchungen, weil es einige vielversprechende Eigenschaften besitzt. Neben der geringen thermischen Ausdehnung der Glaskeramiken, ist die geringe Schmelztemperatur der Gläser ein weiterer Vorteil des Systems, welcher eine mögliche Produktion der Gläser und Glaskeramiken vereinfachen würde. Ein Nachteil dieses Glassystems ist die Tendenz zur Oberflächenkristallisation, die jedoch nützlich für die Herstellung von Sinterglaskeramiken ist.

Impedanzmessungen als Funktion der Frequenz wurden schon zur Untersuchung der Phasentrennung in Natriumborosilicat-Systemen verwendet [16–20]. Dies ist möglich, da die elektrische Leitfähigkeit von der Zusammensetzung jeder Phase der Probe abhängt - d.h. wenn sich die Zusammensetzung ändert, z.B. auf Grund von Phasentrennung, kann eine Änderung der Leitfähigkeit beobachtet werden. In Proben, welche eine Phasenumwandlung durchlaufen, ist der Anstieg der Arrhenius-Funktion ( $-\ln\sigma/d(1/kT)$ ) eine sensitive Größe, da sie sich verändert, wenn die Leitfähigkeit der Ausgangs- und der

Endphase unterschiedlich ist. Deshalb könnte die Impedanz nützlich zur Bestimmung der Glasübergangstemperatur sowie Kristallisations- und Schmelztemperaturen sein. Im Gegensatz zur DTA ist die Impedanz eine statische Eigenschaft und nicht die Änderung einer Eigenschaft, deshalb beeinflusst die Aufheiz- oder Abkühlrate nicht die Empfindlichkeit der Messung und kann somit wesentlich geringer gewählt werden als bei der DTA.

In dieser Arbeit wurden Gläser im System  $\text{BaO}-\text{Al}_2\text{O}_3-\text{B}_2\text{O}_3$  im Hinblick auf ihr Kristallisationsverhalten und ihre Eigenschaften untersucht. Ein Ziel der Arbeit war, im Volumen kristallisierte Glaskeramiken mit niedrigen thermischen Ausdehnungskoeffizienten zu erhalten. Die Experimente wurden mit der stöchiometrischen Zusammensetzung  $\text{BaO}-\text{Al}_2\text{O}_3-\text{B}_2\text{O}_3$  und geringfügig modifizierten Zusammensetzungen, sowie Gläsern mit  $\text{TiO}_2$ -,  $\text{TiO}_2/\text{ZrO}_2$ -Zusatz und mit Platin dotierten Gläsern durchgeführt. Von diesen Gläsern und den dazugehörigen Glaskeramiken wurden die Dichte, der lineare thermische Ausdehnungskoeffizient, die hydrolytische Beständigkeit und die Glasübergangs- und Erweichungstemperatur bestimmt. Die Ergebnisse von Licht- und Rasterelektronenmikroskopie sowie IR-Spektroskopie wurden verwendet, um den Einfluss der Zusammensetzung und der Zusätze auf die physikalischen Eigenschaften besser zu verstehen.

Im zweiten Teil dieser Arbeit wurde die elektrische Impedanz als Funktion der Temperatur von ausgewählten Gläsern untersucht. Die spezifische Leitfähigkeit wurde in die Ableitung  $(-\text{dln}\sigma/\text{d}(1/\text{kT}))$  umgewandelt, welche verwendet wurde, um die Kristallisations- und Schmelztemperatur und den Entmischungsbereich im System  $\text{BaO}-\text{Al}_2\text{O}_3-\text{B}_2\text{O}_3$  zu bestimmen.

Um zunächst die Eigenschaften des stöchiometrischen Glases und der dazugehörigen Glaskeramiken sowie das Kristallisationsverhalten näher zu bestimmen, wurde das Glas  $\text{BaO}-\text{Al}_2\text{O}_3-\text{B}_2\text{O}_3$  in verschiedene Arten von Glaskeramiken überführt (Bulkglaskeramiken mit und ohne Platinzusatz sowie Sinterglaskeramiken). Diese Untersuchungen zeigten, dass aus diesem Glas Glaskeramiken mit null oder negativer thermischer Ausdehnung hergestellt werden können. Verantwortlich für dieses Verhalten ist die rhomboedrische Kristallphase  $\text{BaAl}_2\text{B}_2\text{O}_7$  (JCPDS 86-2168), welche außerdem den besonderen Fall der Dichterniedrigung der Glaskeramik gegenüber dem Ausgangsglas bewirkt. Der thermische Ausdehnungskoeffizient hängt deutlich von der Art der Herstellung der Glaskeramik ab. In der Sinterglaskeramik und der Bulkglaskeramik mit Platin, als heterogener Keimbildner, ist der thermische Ausdehnungskoeffizient ähnlich der Ausdehnung der kristallographischen a-Achse, dies wurde durch Hochtemperatur-XRD-Messungen gezeigt. Im

Gegensatz dazu ist die thermische Ausdehnung der Bulkglaskeramik ohne Keimbildner bis zu einer Temperatur von 300 ° C nahe dem erwarteten Verlauf für eine statistische Anordnung der Kristalle, d.h. nahe der mittleren thermischen Ausdehnung der Elementarzelle.

Allerdings zeigt das stöchiometrische Glas BaO - Al<sub>2</sub>O<sub>3</sub> - B<sub>2</sub>O<sub>3</sub> eine starke Neigung zur Oberflächenkristallisation. Aus diesem Grund wurde die Zusammensetzung des Glases geringfügig in Bezug auf die BaO- und B<sub>2</sub>O<sub>3</sub>-Konzentration variiert. Die Verringerung der BaO-Konzentration resultierte in einer gesteigerten Volumenkristallisation, während die Oberflächenkristallisationsschicht deutlich abnahm. Die Gläser enthalten nach der Herstellung Kristalle, die als Al<sub>2</sub>O<sub>3</sub> identifiziert werden konnten. Weitere Untersuchungen zeigten, dass die Bildung von Al<sub>2</sub>O<sub>3</sub>-Kristallen durch einen Mangel an B<sub>2</sub>O<sub>3</sub> gefördert wird. Um dem vorzubeugen, wurde die B<sub>2</sub>O<sub>3</sub>-Konzentration erhöht. Im Glas 0,9 BaO - 1,0 Al<sub>2</sub>O<sub>3</sub> - 1,1 B<sub>2</sub>O<sub>3</sub> konnten keine Al<sub>2</sub>O<sub>3</sub>-Kristalle nach dem Schmelzprozess nachgewiesen werden. Des Weiteren sind die dazugehörigen Glaskeramiken, mit und ohne Platin, im Volumen kristallisiert und besitzen niedrige thermische Ausdehnungskoeffizienten. Folglich wurden alle weiteren Veränderungen hinsichtlich der Glaszusammensetzung mit dem Glas 0,9 BaO - 1,0 Al<sub>2</sub>O<sub>3</sub> - 1,1 B<sub>2</sub>O<sub>3</sub> als Grundzusammensetzung durchgeführt.

Um die geringe hydrolytische Beständigkeit der Gläser und Glaskeramiken zu erhöhen, wurde dem Grundglas (0,9 BaO - 1,0 Al<sub>2</sub>O<sub>3</sub> - 1,1 B<sub>2</sub>O<sub>3</sub>) TiO<sub>2</sub> unter Anwendung zweier Strategien zugesetzt. In den Gläsern Typ I wurde die TiO<sub>2</sub>-Konzentration auf Kosten der Oxide BaO und B<sub>2</sub>O<sub>3</sub> erhöht, um einen Al<sub>2</sub>O<sub>3</sub>-Überschuss zu realisieren, während in den Gläsern Typ II, dem Grundglas TiO<sub>2</sub> zugesetzt wurde und die molaren Konzentrationen der übrigen Oxide konstant gehalten wurden. Der Zusatz von TiO<sub>2</sub> verbessert die hydrolytische Beständigkeit sowohl der Gläser Typ I als auch Typ II. Allerdings verringert sich die Kristallisationsneigung der Gläser deutlich mit ansteigender TiO<sub>2</sub>-Konzentration. Aus diesem Grund wurde Platin als heterogener Keimbildner zugesetzt, aber auch dies verbesserte die Kristallisationsneigung nur geringfügig, ebenfalls in Bezug auf die Kristallisation der Phase BaAl<sub>2</sub>B<sub>2</sub>O<sub>7</sub> (JCPDS 86-2168). Der lineare thermische Ausdehnungskoeffizient der Glaskeramiken erhöhte sich mit steigender TiO<sub>2</sub>-Konzentration. Während die Glaskeramiken mit 2,5 mol% TiO<sub>2</sub> und Platin eine geringere thermische Ausdehnung als die Ausgangsglaskeramik aufweisen, steigt die thermische Ausdehnung der Glaskeramiken bei weiterer Erhöhung der TiO<sub>2</sub>-Konzentration. Die hydrolytische Beständigkeit der Glaskeramiken mit TiO<sub>2</sub> ist im Vergleich zur Ausgangsglaskeramik geringfügig besser, aber jedoch deutlich schlechter als die des dazugehörigen Glases.

Für weitere Untersuchungen zum Einfluss von TiO<sub>2</sub> und ZrO<sub>2</sub> auf das Kristallisationsverhalten, die hydrolytische Beständigkeit und den linearen thermischen Ausdehnungs-

koeffizienten wurde ein Gemisch aus  $\text{TiO}_2/\text{ZrO}_2$  mit einem molaren Verhältnis von 1:1 zugegeben. Das Gemisch aus  $\text{TiO}_2/\text{ZrO}_2$  wurde zum Grundglas  $0,9\text{BaO}-1,0\text{Al}_2\text{O}_3-1,1\text{B}_2\text{O}_3$  addiert, während das Verhältnis der molaren Konzentrationen der anderen Oxide konstant gehalten wurde. Eine deutliche Verbesserung der hydrolytischen Beständigkeit der Gläser im Vergleich zur alleinigen Zugabe von  $\text{TiO}_2$  konnte beobachtet werden. Alle Glaskeramiken mit  $\text{TiO}_2/\text{ZrO}_2$  kristallisierten im Volumen und mittels Lichtmikroskopie konnte nur eine dünne Oberflächenkristallisationsschicht festgestellt werden. Bis 7,5 mol%  $\text{TiO}_2/\text{ZrO}_2$  wurde  $\text{BaAl}_2\text{B}_2\text{O}_7$  (JCPDS 86-2168) als Hauptkristallphase detektiert, oberhalb von 7,5 mol% wurde ein Absinken der Kristallisationsneigung und die Bildung der kristallinen Phase  $\text{BaZr}(\text{BO}_3)_2$  beobachtet. Der thermische Ausdehnungskoeffizient steigt durch die Zugabe von  $\text{TiO}_2/\text{ZrO}_2$  an, allerdings zeigen die Glaskeramiken bis zu 7,5 mol%  $\text{TiO}_2/\text{ZrO}_2$  eine Nullausdehnung im Temperaturbereich von 25 bis 100 °C. Des Weiteren konnte eine Verbesserung der hydrolytischen Beständigkeit der Glaskeramiken mit 2,5 und 5,0 mol%  $\text{TiO}_2/\text{ZrO}_2$  im Vergleich zur Grundglaskeramik nachgewiesen werden.

Zusammenfassend ist dazu festzustellen, dass die Glaskeramiken  $\text{BaO}-\text{Al}_2\text{O}_3-\text{B}_2\text{O}_3$  und  $0,9\text{BaO}-\text{Al}_2\text{O}_3-\text{B}_2\text{O}_3$  mit Platin die minimale negative thermische Ausdehnung von  $-16 \cdot 10^{-7} \text{K}^{-1}$  (25 bis 307 °C) bzw.  $-7 \cdot 10^{-7} \text{K}^{-1}$  (25 bis 374 °C) zeigen. Allerdings haben diese Glaskeramiken eine sehr geringe hydrolytische Beständigkeit. Die beste hydrolytische Beständigkeit von allen untersuchten Glaskeramiken zeigt die Probe mit 5,0 mol%  $\text{TiO}_2/\text{ZrO}_2$ , welche gleichzeitig eine Nullausdehnung im Temperaturbereich von 25 bis 100 °C aufweist.

IR-Spektroskopie wurde von allen untersuchten Gläsern und Glaskeramiken durchgeführt, um Informationen über den Einbau der verwendeten Oxide in die Gläser und Glaskeramiken zu erhalten. In den Gläsern wird Bor hauptsächlich in dreifacher Koordination eingebaut, während vierfach koordiniertes Bor nur Banden sehr geringer Intensität zeigt. Die Koordination von Aluminium im Glas konnte nicht aufgeklärt werden, allerdings wird angenommen, dass Aluminium in vierfacher Koordination als weiterer Netzwerkbildner im Glas eingebaut ist. Weiterführende Untersuchungen mittels NMR-Spektroskopie sind notwendig, um diese Frage eindeutig zu klären. In Übereinstimmung mit der Kristallstruktur von  $\text{BaAl}_2\text{B}_2\text{O}_7$  (JCPDS 86-2168) [21] bestätigten die Banden in den IR-Spektren der Glaskeramiken das alleinige Auftreten von dreifach koordiniertem Bor in den Glaskeramiken. Ausserdem wurden noch Raman-Spektren vom Grundglas und den jeweiligen Glaskeramiken aufgenommen, jedoch waren die Intensitäten in den Spektren so gering, dass sie in die weiteren Betrachtungen nicht einbezogen wurden.

Im zweiten Teil der Arbeit wurde eine neue Methode entwickelt, um Kristallisations-

und Schmelztemperaturen von Gläsern mittels Impedanzmessungen zu bestimmen. Wie am Beispiel der Phasentrennung von Natriumborosilicatgläsern gezeigt wird [16–20], ist es möglich mittels Impedanzmessungen Phasenumwandlungen zu detektieren. Hier wurde die Impedanz als Funktion der Temperatur im Bereich von 550 bis 1150 °C bei konstanter Frequenz und mit unterschiedlichen Aufheiz- und Abkühlraten gemessen. Die Ableitung ( $-\ln\sigma/d(1/kT)$ ) kann mit der Aktivierungsenergie gleichgesetzt werden, wenn keine Phasenumwandlung stattfindet. Maxima und/oder Minima in der Ableitung stellen Phasenumwandlungen dar. Im Gegensatz zur Differenzthermoanalyse können Impedanzmessungen mit viel kleineren Aufheiz- und Abkühlraten durchgeführt werden. Deshalb ist es auch möglich, Kristallisations- und Schmelztemperaturen von Systemen mit geringer Kristallisationsgeschwindigkeit, wie z.B. BaO-Al<sub>2</sub>O<sub>3</sub>-B<sub>2</sub>O<sub>3</sub>, zu bestimmen. Die Kristallphase BaAl<sub>2</sub>B<sub>2</sub>O<sub>7</sub> (JCPDS 86-2168) zeigt mit der äußerst niedrigen Aktivierungsenergie (der ionischen Leitfähigkeit) von 0,50 eV eine bemerkenswerte Eigenschaft. Eine weitere Besonderheit stellt die höhere Leitfähigkeit der Glaskeramik gegenüber dem Ausgangsglas dar. Des Weiteren konnte auch mit dieser neu entwickelten Methode eine Phasentrennung detektiert werden, welche durch die Zugabe von MgO oder Li<sub>2</sub>O zum stöchiometrischen Glas BaO-Al<sub>2</sub>O<sub>3</sub>-B<sub>2</sub>O<sub>3</sub> bzw. zum geringfügig veränderten Glas 0,9 BaO-Al<sub>2</sub>O<sub>3</sub>-B<sub>2</sub>O<sub>3</sub> bewiesen werden konnte. Magnesiumoxid öffnete die Mischungslücke weiter, was in einen Shift der Kristallisationstemperatur zu niedrigeren Temperaturen resultierte. Andererseits bewirkte die Zugabe von Li<sub>2</sub>O das Schliessen der Mischungslücke und eine Verringerung der Kristallisationsneigung. Weiterhin konnte beobachtet werden, dass die Verdopplung der Li<sub>2</sub>O-Konzentration auch eine Verdopplung der Leitfähigkeit des Glases bewirkt, während solche Abhängigkeiten in den Glaskeramiken nicht auftreten. Die Aktivierungsenergie der kristallisierten Proben mit Li<sub>2</sub>O weisen den gleichen Wert auf wie die der kristallinen Phase BaAl<sub>2</sub>B<sub>2</sub>O<sub>7</sub> (JCPDS 86-2168). Dieses Verhalten zeigt, dass die Ba<sup>2+</sup>-Ionen in der kristallinen Phase über die Li<sup>+</sup>-Ionen in der Restglasphase dominieren, was sehr ungewöhnlich ist. Eine Gemeinsamkeit zeigen die Zusätze MgO and Li<sub>2</sub>O, denn sie bewirken die Senkung der Schmelztemperatur gegenüber den Grundgläsern, was auf eine Schmelzpunktdepression zurückgeführt werden kann. AFM-Messungen ermöglichten die Visualisierung der Entmischung, welche Tropfengrößen von nur einigen Nanometern aufweist.

# Chapter 2

## Introduction

Glass-ceramics are polycrystalline solids prepared by controlled crystallisation of glass. These are widely used in recent times and are distinguished due to special properties which are outstanding compared to the respective glass. They are used as tough glass-ceramics [1–3], sinter glass-ceramics [4,5], machinable [6–8] and biocompatible glass-ceramics [9–11] and low thermal expansion glass-ceramics [12,13]. Low thermal expansion glass-ceramics are commercially used as cook top panels [22] and telescope mirrors [23]. These glass-ceramics are based on a crystalline phase,  $\beta$ -eucryptite, that has a negative thermal expansion coefficient [14].

By analogy, glass-ceramics of the system BaO - Al<sub>2</sub>O<sub>3</sub> - B<sub>2</sub>O<sub>3</sub> have also a negative thermal expansion coefficient, and therefore it is a potential candidate of a zero-expansion material [15]. First research of this system with regard to the thermal expansion coefficient was carried out by MacDowell in 1989 [4, 24]. The synthesis and properties of calcium, strontium and barium aluminoborate sinter glass-ceramics were in focus of this research. A thermal expansion coefficient of  $23 \cdot 10^{-7} \text{ K}^{-1}$  (25 to 300 °C) was reported on BaAl<sub>2</sub>B<sub>2</sub>O<sub>7</sub> sinter glass-ceramics. Further investigations on alkaline earth aluminum borate in crystalline and glassy states were carried out by Hovhannisyanyan [15]. The glass-ceramics were also prepared from pressed glassy powder and showed a thermal expansion coefficient of  $14 \cdot 10^{-7} \text{ K}^{-1}$  from 20 to 300 °C for the composition BaAl<sub>2</sub>B<sub>2</sub>O<sub>7</sub>. On the other hand, low melting temperatures in the range from 1400 to 1500 °C were reported.

The glass / glass-ceramics / system BaO - Al<sub>2</sub>O<sub>3</sub> - B<sub>2</sub>O<sub>3</sub> is in the centre of attention in the following investigations, because the glass-ceramics exhibit remarkable properties. The thermal expansion coefficient of these glass-ceramics is zero or even negative in a certain temperature range [15]. A further advantage of the glass is the low melting temperature which would simplify a possible production of the glass and glass-ceramics. A disadvantage of the system is the tendency of surface crystallisation, which, however,

is useful for the preparation of sinter glass-ceramics [25, 26].

Impedance measurements as a function of frequency have already been reported to be a versatile tool to study the phase separation of sodiumborosilicate systems [16–20]. This is possible, because the electrical conductivity depends on the composition of each phase of the sample. If the composition is changed, e.g. because phase separation occurs, the conductivity also changes. Hence, the temperature below which phase separation occurs can be determined by a non-exponential change in conductivity with changing temperature. In samples, that undergo a phase transition, the slope of the Arrhenius function ( $d\ln\sigma/d(1/kT)$ ) is a sensitive measure because it changes if the conductivity of the initial and the final phase is different. Therefore impedance measurements might also be useful to determine the glass transition temperature,  $T_g$ , crystallisation and melting temperatures. In contrast to DTA, impedance is a static property and not the change of a property. Therefore the heating rate does not affect the sensitivity of the measurement and hence, can be much less than for DTA or even close to zero. This could be of special importance for the processes such as nucleation or crystal growth.

In this thesis, glasses in the system BaO-Al<sub>2</sub>O<sub>3</sub>-B<sub>2</sub>O<sub>3</sub> have been investigated with respect to their crystallisation behaviour and properties. A goal was the achievement of volume crystallised glass-ceramics with low thermal expansion coefficients. The experiments have been carried out with the stoichiometric composition BaO-Al<sub>2</sub>O<sub>3</sub>-B<sub>2</sub>O<sub>3</sub>, and with slightly modified stoichiometries as well as with TiO<sub>2</sub>, TiO<sub>2</sub>/ZrO<sub>2</sub> and platinum doped stoichiometric glasses. Density, thermal expansion coefficient, hydrolytic durability, glass transition and softening temperature were measured from the glasses and respective glass-ceramics. Optical microscopy, scanning electron microscopy and infrared spectroscopy were used to understand the effect of composition and the effects of the additives on the physical properties. In the second part of this thesis, electrical impedances of selected glasses have been studied as a function of the temperature [27]. The specific conductivities were illustrated by fitting Arrhenius functions to the data and the derivative ( $-d\ln\sigma/d(1/kT)$ ) which was used to determine the crystallisation and melting temperature and the range of immiscibility in the system BaO-Al<sub>2</sub>O<sub>3</sub>-B<sub>2</sub>O<sub>3</sub>.



# Chapter 3

## Principles and basics

### 3.1 Low thermal expansion glass-ceramics

From the well-known materials glass and ceramics, the glass-ceramics differ with respect to their production technique and the resulting properties. Therefore it is not possible to assign them either to glasses or to ceramics [28]. Glass-ceramics are produced in at least two processing steps: at first, batches of defined compositions, which depend on the aimed properties of the final product, are melted and formed. In a second step, glassy objects are transformed into polycrystalline materials through a well defined temperature-time-treatment. Beside the crystalline phases, these polycrystalline materials contain a residual glass phase up to 50%. Glass-ceramics usually are absolutely dense and non-porous in comparison to conventional ceramics. On the other hand, an additional process step in the production of glass-ceramics means increased expenditures in comparison to glasses. As a consequence, the benefits of glass-ceramic products have to be higher than those of competitive glass products.

Cooktop panels or range tops represent one of the commercially most attractive glass-ceramics product. The technical key property of these glass-ceramics is the low coefficient of thermal expansion (CTE) in the temperature range from 25 to 700 °C  $\pm 0.1 \cdot 10^{-6} \text{ K}^{-1}$  [29]. This CTE is necessary to avoid breakage of a brittle material, which is subjected to temperature gradients of some 100 K/cm and to thermal shock caused by spilling cold water on a hot cooktop panel. Materials with low CTE are also interesting for applications for which thermal dimension stability is important. Glass-ceramics have been developed for optical applications, where the thermal expansion coefficient is optimised to be as close to zero as possible in the temperature range from -50 to 100 °C. Low thermal expansion glass-ceramics are designed from a  $\text{Li}_2\text{O}-\text{Al}_2\text{O}_3-\text{SiO}_2$  based glass with small concentrations of other alkali oxides and alkaline earth oxides as well as  $\text{TiO}_2$  and  $\text{ZrO}_2$  as nucleation

agents. The outstanding property of zero thermal expansion is caused by the occurrence of crystalline phases, such as  $\beta$ -quartz-solid solution,  $\beta$ -eucryptite or  $\beta$ -spodumen [14,30], with negative thermal expansion coefficients and the residual glass phase of the system with a positive thermal expansion coefficient.

Product development is mainly focused on three product ideas: cookware, range tops for kitchen stoves and telescope mirrors blanks. For the cookware, two systems were developed and produced. Based on the keatite glass-ceramics, a porcelain appearance was possible, while the  $\beta$ -quartz glass-ceramics are a tinted, transparent variant. Both possibilities have been developed and launched to the market by Corning Inc. as well as by Schott AG. The two Corning products, Pyroceram® for the white, opaque keatite glass-ceramics and Vision® for the transparent  $\beta$ -quartz glass-ceramics are still commercially available [12]. Although these glass-ceramics withstand either high thermal gradients or thermal shock, they have one important deficiency: a low thermal conductivity in comparison to metals. The glass-ceramics Ceran® developed by Schott AG has been very successful as range tops for kitchen stoves [22]. Ceran® is a strongly tinted, partly transparent variant, based on  $\beta$ -quartz glass-ceramics. The best known low expansion optical glass-ceramics are the glass-ceramics Zerodur® produced by Schott AG [31]. While these glass-ceramics were developed for the use of large telescope mirrors, they find now applications in other areas, e.g. for laser gyros. A very demanding approach was the realisation of very large telescope mirrors of 8.2 m in diameter and only 30 cm in thickness [23].

## 3.2 Crystallisation of glass

Crystallisation of glass is one of the most important reasons for defective glass as well as the basis for the development of new materials from glass. Fundamental investigations on the crystallisation of glasses by Tammann subdivided the crystallisation process into two steps: nucleation and crystalline growth [32]. The work of nucleation consists of the difference of two energy contributions. The first is the work which is required to form a new surface, overcoming the surface tension of the surroundings, whereas the second contribution is the energy, gained through the ordering of an amorphous region to a crystalline lattice. Furthermore, the nucleation process is associated with a decrease of the free enthalpy ( $\Delta G$ ) of the system. This is the case if the gained energy of nucleation ( $\Delta G_V$ ) is higher than the contribution for overcoming of the surface tension ( $\Delta G_O$ ).

$$\Delta G = -\Delta G_V + \Delta G_O \quad (3.1)$$

The decisive parameter for the formation of a nuclei is the critical radius. If a nuclei overcomes this radius it starts to grow, while a nuclei, which is smaller than the critical radius is dissolved again. This process is called homogeneous nucleation. If the nucleation tendency is increased through the presence of some added crystalline nuclei, it is called heterogeneous nucleation. Nucleating additives are subdivided into two categories: First are those additives, which enhance the phase separation, such as fluorides and phosphates. The second group contains additives, which are soluble in the glass at high temperatures but precipitate in pure form at reduced temperatures because of strong oversaturation, e.g.  $\text{TiO}_2$ ,  $\text{ZrO}_2$  or platinum metals. These additives could be effective as heterogeneous nucleation agents. In case of a controlled primary precipitation of the heterogeneous nuclei, the starting parameters of the nuclei are equal, which leads to equal growing conditions of the crystals. A very large number of nuclei would result in very small crystallites in the final product. After the formation of nuclei in the glass, the growth of crystals starts through the addition of other structural units. Furthermore, two different types of crystallisation processes can be observed during the formation of glass-ceramics: surface and volume (or bulk) crystallisation. Most glass-ceramics are produced through controlled bulk crystallisation. The volume structure of the base glass is modified by heat treatment achieving glass-ceramics with special properties, however, at the beginning, a controlled nucleation is necessary. Two possibilities are reported to initiated controlled nucleation: by nucleating additives or by phase separation [33]. On the other hand, the development of glass-ceramics by Stookey [34] already demonstrated, that certain glasses can not be converted into glass-ceramics by controlled volume crystallisation. Further investigations were carried out with these types of glass by controlled surface crystallisation to avoid uncontrolled crystallisation [35]. Zannotto reported in 1991, that the enhanced nucleation rates at the external surfaces are the result of the catalytic effect of some solid impurity particles and faster surface diffusion rates [36].

### **3.3 Incorporation of boron oxide, aluminum oxide and barium oxide in glasses**

The incorporation and function of the oxides in glass is illustrated in this section. According to their field strength, the cations of the oxides can be classified into network-formers, network-modifiers and intermediates. On the other hand, the coordination number of a cation depends on its ionic radius, i.e. the larger the radius, the larger is the coordination number. Boric oxide is one of the best glass-formers (network-formers) beside silica

and  $P_2O_5$  [37]. Two coordinations of boron oxide are known:  $[BO_3]$  planar triangles and  $[BO_4^-]$  tetrahedra. A unique behaviour of boron oxide is the so called boron anomaly, which at first was investigated in  $Na_2O-B_2O_3$  glasses [38]. Pure  $B_2O_3$  glass consists of  $[BO_3]$  groups and with increasing alkali concentration, the first incorporation of alkali oxide leads to the coordination shift  $[BO_3]$  to  $[BO_4^-]$  with alkali ions compensating the charge of the  $[BO_4^-]$  tetrahedra. A strengthening of the structure occurs, since the points of polyhedra linkage rise from three to four. At higher alkali concentrations, the structure weakened again due to the formation of  $[BO_3]$  groups with nonbridging oxygens. This double change of coordination number explains minima or maxima of some properties which occur with increasing alkali concentration. Furthermore, this anomaly depends also on the temperature. According to Dietzel [39], the boron anomaly should not exist in glasses at temperatures above  $1000^\circ C$ , i.e. above this temperature only  $[BO_3]$  groups occur in the melt. The association of  $[BO_3]$  planar triangles with oxygen atoms into  $[BO_4^-]$  groups should, however, occur at lower temperatures. Aluminum oxide acts as an intermediate in glass. Intermediates have a mid-position between network-formers and network-modifiers. Aluminum may either form tetrahedra and so reinforce the network (coordination number 4) or loosen the network in analogy to network-modifiers (coordination number 6). The ionic radius of barium ions is much larger than of aluminum oxide and boron oxide, which results in the coordination number 8. By contrast, the field strength of barium is much smaller resulting in the behaviour as network-modifier.

### 3.4 Crystalline phases of the composition $BaAl_2B_2O_7$

Two crystalline phases of the composition  $BaAl_2B_2O_7$  are reported in literature: a monoclinic (JCPDS 29-0144) [40] and a rhombohedral (JCPDS 86-2168) phase [21]. According to Hübner, the monoclinic symmetry with  $a = 24.98 \text{ \AA}$ ,  $b = 4.85 \text{ \AA}$ ,  $c = 18.85 \text{ \AA}$  and  $\beta = 120.31^\circ$  belongs to the space group  $C_{1h}^2$ -P2 [40]. Single crystals of this compound were produced and investigated by X-ray diffraction. However, the precise crystal structure was not determined.

On the other hand, the rhombohedral structure has a unit cell dimension of  $a = 5.001 \text{ \AA}$  and  $c = 24.378 \text{ \AA}$  and belongs to the space group R32 (No. 155). In Ref. [21], the crystal structure of rhombohedral  $BaAl_2B_2O_7$  is determined by single crystal method. The structure of the crystal lattice is presented in Fig. 3.1 showing  $[BO_3]^-$  triangles,  $[AlO_4]^-$  tetrahedra and  $Ba^{2+}$ , which is coordinated by twelve oxygen atoms.

Furthermore, strong displacement effects are suggested for Al and  $O_1$  atoms [21]. The

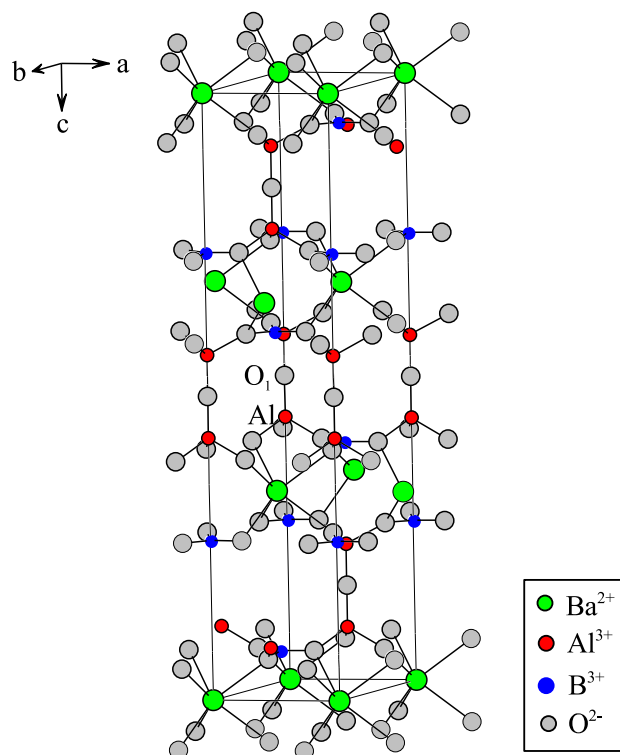


Figure 3.1: Crystal structure of the rhombohedral phase  $\text{BaAl}_2\text{B}_2\text{O}_7$ .

centred triangles of  $[\text{BO}_3]^-$  are bridged to aluminum atoms to the nearly planar  $[\text{AlBO}_3]^{2+}$  network with  $[\text{BO}_3]^-$  groups perpendicular to the c-axis. Neighbouring planes are connected by oxygen to form a three-dimensional framework.

Finally, the two allotrops of  $\text{BaAl}_2\text{B}_2\text{O}_7$  exhibit not only a different structure, but also different densities. The (X-ray) density of the rhombohedral and the monoclinic phase were reported to be 3.065 [21] and 3.559  $\text{g}/\text{cm}^3$  [40], respectively.

# Chapter 4

## Experimental procedure

### 4.1 Preparation of glasses

The glasses were melted using the pure grade raw materials  $\text{BaCO}_3$ ,  $\text{Al}(\text{OH})_3$ ,  $\text{H}_3\text{BO}_3$ , as well as  $\text{TiO}_2$ ,  $\text{ZrO}_2$ ,  $\text{ZnO}$ ,  $\text{Li}_2\text{CO}_3$  and  $\text{MgCO}_3$ . After homogenisation, the batch was melted in a platinum crucible using an induction furnace. The melt was stirred during the melting process. The different melting temperatures and times are listed in Table 4.1. Finally, the melt was casted in a steel mould and given to a muffle furnace preheated to the temperatures shown in Table 4.1. Then the furnace was switched off and the sample allowed to anneal. The compositions of the investigated glasses are listed in chapter 5.

Table 4.1: Melting temperatures and times as well as annealing temperatures of the different glass types.

Glass type	$T_{\text{melting}}$ in $^{\circ}\text{C}$	$t_{\text{melting}}$ in h	$T_{\text{annealing}}$ in $^{\circ}\text{C}$
Basic glasses	1480-1500	1	654
Addition of $\text{TiO}_2$	1450	1	620
Addition of $\text{TiO}_2/\text{ZrO}_2$	1500	1.25	620

One part of the glass was crushed  $< 1$  mm and 0.01 wt% platinum, as  $\text{PtCl}_4/\text{acetone}$  solution, was added as nucleation agent. After homogenising and subsequent drying, the mixture was given to a platinum crucible, heated to  $1480^{\circ}\text{C}$  and stirred at  $1450^{\circ}\text{C}$  for 30 min, to ensure a homogeneous distribution of the platinum. Afterwards the melt was casted and cooled as described above.

The pure and doped glasses were used for different experiments to determine their properties, e.g. density, thermal expansion coefficient and hydrolytic durability.

## 4.2 Preparation of glass-ceramics

One part of the pure and doped glasses was used to produce glass-ceramics by thermal treatment. The thermal treatment was done in a muffle furnace (Linn Elektrotherm). The temperature was controlled by a second thermocouple placed next to the sample. Bulk samples, cut from a glass bar without further polishing, were used for the experiments. All samples were thermally treated at 720 °C for 24 h and 780 °C for 8 h using heating and cooling rates of 10 K/min. Other programs are described in the following chapters.

## 4.3 Preparation of sinter glass-ceramics

For the preparation of sinter glass-ceramics, glass was produced as described in section 4.1, but was quenched in cold water instead of annealed. The quenched glass was minced < 710  $\mu\text{m}$  with a steel mortar and the obtained glass frit was milled in a planetary mill (Pulverisette, Fritsch) without adding liquid. The grinding devices are corundum beaker and balls of different sizes. The glass powder was sieved through a 25  $\mu\text{m}$  metal mesh. The received glass powder was used to make pellets with the aid of an isostatic press (Wickert). The pellets were thermally treated in a furnace (Ivoclar Programat P80) using the parameters listed in Table 4.2.

Table 4.2: Thermal treatment parameters of the sinter glass-ceramics.

Parameters	Value
Holding temperature in °C	700 - 1000, every 50 K
Holding time in min	40
Heating rate in K/min	100
Cooling time in min	10

Afterwards the sinter glass-ceramics were characterised. The density of the powder and the crystalline phase consistence were determined and micrographs of selected samples were made by scanning electron microscopy. For the measurement of the thermal expansion coefficient, it was necessary to make larger pellets. The strengthening of the structure was accomplished by addition of a plasticiser. 20 g of the glass powder (< 25  $\mu\text{m}$ ) was homogenised with 10 g of 1 % polyvinylalcohol (PVA) solution. After drying in air, pellets with a diameter of 40 mm and a thickness of 10 mm were prepared by uniaxial pressing (5 MPa). To remove the PVA, the pellets were heated with 5 K/min to 600 °C for 1.5 h. In a second step, the sample was further heated to 850 °C or 900 °C for 40 min

with a heating rate of 20 K/min. Afterwards the density, crystalline phases and thermal expansion coefficient of these sinter glass-ceramics were determined.

## 4.4 Properties of the glasses and glass-ceramics

### 4.4.1 Density

The densities of the glasses and glass-ceramics were determined using two different procedures. All samples were measured via pycnometry. Additionally, some samples were measured using the floatation weight loss method to compare the results. A helium pycnometer (AccuPyc 1330, Micromeritics) was used to determine density and volume of powder and bulk samples by measuring the pressure change of helium in a calibrated volume. The computer calculates a mean value from five single measurements. For the Archimedes method, a precision balance (MC1 Analytik, Sartorius), chloroform and pieces of bulk glass or glass-ceramics were used. Each sample is measured four times to get a statistically reliable result.

### 4.4.2 Differential thermal analysis

The differential thermal analysis (DTA) was carried out with devices from Shimadzu DTA 50 or Netzsch STA 429. The samples had a grain size between 250 to 315  $\mu\text{m}$  and alumina was used as reference. Holder for sample and reference were platinum crucibles. The heating rate was 10 K/min. The DTA curves of glasses usually show the glass transition temperature ( $T_g$ ) as well as exothermic (crystallisation) and endothermic (melting of crystalline phases, phase transition) peaks. The values are shown in Fig. 4.1.

For further discussions, the onset temperature of the glass transition temperature, the peak maximum for the crystallisation temperature and the peak minimum for the liquidus temperature are used.

### 4.4.3 Dilatometry

The thermal expansion coefficient (TEC) of the glasses and glass-ceramics was measured by dilatometry (Netzsch 402E) with a heating rate of 5 K/min. The samples for the measurement were polished bulk specimens with sizes of approximately  $10 \cdot 10 \cdot 20 \text{ mm}^3$ . Due to the preparation, the surface layer of the original samples was removed.

Figure 4.2 shows an example of a dilatometry measurement. The thermal expansion coefficients were calculated for a temperature range between 100 to 300 °C and from 100



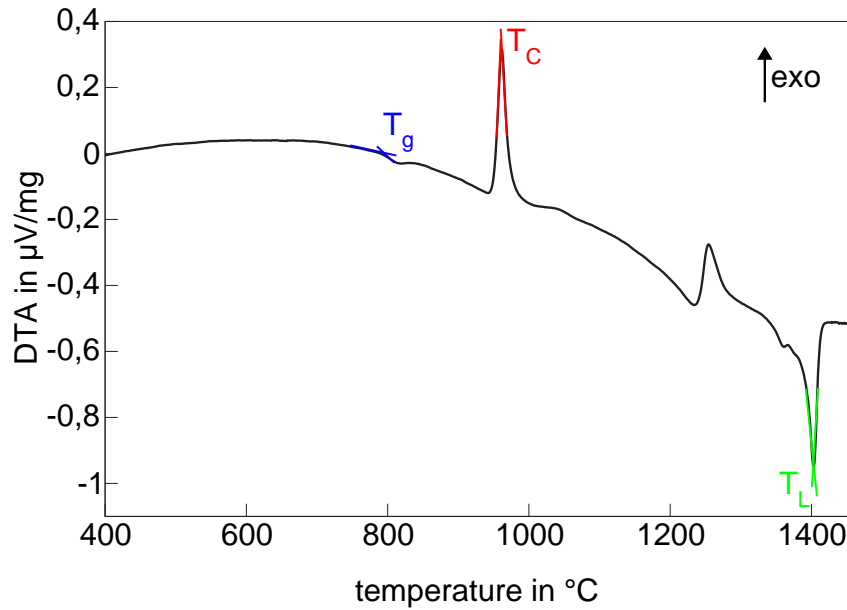


Figure 4.1: DTA curve with glass transition temperature ( $T_g$ ), crystallisation temperature ( $T_C$ ) and liquidus temperature ( $T_L$ ).

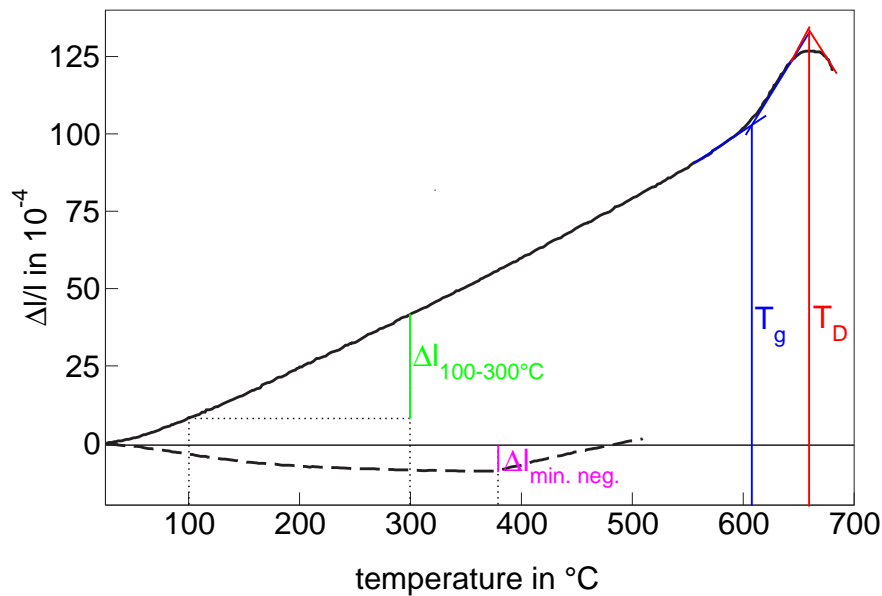


Figure 4.2: Curve of dilatometry measurement: solid line: glass, dashed line: glass-ceramics.

to 500 °C. Also, the temperature and the most negative coefficient was determined as shown in Fig. 4.2. The linear coefficient of thermal expansion  $\alpha$  is defined by:

$$\alpha_{\Delta T} = \frac{\Delta l}{l_0 \Delta T} \quad (4.1)$$

where  $l_0$  is the initial length of the sample and  $\Delta l$  is the change of length with the change of temperature  $\Delta T$  [41]. Furthermore, the glass transition temperature,  $T_g$ , and the softening temperature,  $T_D$ , of the glass can be determined.

#### 4.4.4 Hydrolytic durability

The determination of the hydrolytic durability of the glasses and glass-ceramics was carried out after DIN ISO 719 [42]. Glass fraction from 315 to 500  $\mu\text{m}$  was produced by crushing with a steel mortar and sieving with metal meshes. Afterwards this fraction was washed with acetone to remove the remaining fine glass powder. Three samples, each of 2 g of glass, were boiled in 50 ml deionized water for 1 h at 98 °C. 25 ml of the solution were taken and titrated with 0.01 N hydrochloric acid against methyl red. The quantity of 0.01 N hydrochloric acid added serves as the indicator of the division in the different hydrolytic classes, see Table 4.3.

Table 4.3: Hydrolytic classes after DIN ISO 719.

Hydrolytic Class	Volume of 0.01 N HCl in ml
1	0 to 0.10
2	above 0.10 to 0.20
3	above 0.20 to 0.85
4	above 0.85 to 2.00
5	above 2.00 to 3.50

#### 4.4.5 Viscosity

The viscosity of the glasses was determined with a rotary viscometer (Typ 403, Bähr Thermoanalysengeräte) and a beam bending viscometer (Typ 401, Bähr Thermoanalysengeräte). The rotary viscometer is used in the viscosity range from  $10^2$  to  $10^5$  dPas with glass powder as sample, while the beam bending viscometer enables to determine the viscosity from  $10^9$  to  $10^{15}$  dPas. Glass blocks of  $4 \cdot 5 \cdot 45 \text{ mm}^3$  or  $5 \cdot 5 \cdot 45 \text{ mm}^3$  were needed for the measurement of the beam bending viscosity. The results were referenced against a standard glass (DGG I).

#### 4.4.6 X-ray diffraction

X-ray diffraction (XRD) was used for the identification of crystalline phases. The XRD measurements were carried out with a diffractometer (D5000, Siemens) applying  $\text{Cu}_{K\alpha}$  radiation on the powdered samples. To measure the samples, the Bragg-Brentano-geometry was used, for the identification of the crystalline phases the JCPDS database (Joint Committee on Powder Diffraction Standards). Some crystallised samples were also studied by high temperature X-ray diffraction using a heating chamber (PAR HTK 10, Siemens).

The XRD of the samples were measured every 50 K from 25 to 500 °C in the 2 Theta range from 8 to 40 °.

#### 4.4.7 Optical microscopy

To investigate the structure of the glass-ceramics, an optical microscope (Jenapol and NU2, Zeiss) was deployed. Polished thin sections with a thickness of around 60  $\mu\text{m}$  were used. Using this kind of samples, the contrast is improved and the shape of the crystals can be better identified. The micrographs were taken with polarised and transmitted light.

#### 4.4.8 Electron microscopy

Electron microscopy uses the interaction of electron radiation with the object to show the object with a high magnification. Two different types of microscopes were used: a scanning electron microscope (SEM) and a transmission electron microscope (TEM). The scanning electron microscope (DSM 940A, Zeiss) was used to study polished bulk pieces and fracture surfaces. The surfaces of the samples were vapour-coated with carbon (EDX analysis) or sputtered with gold (micrographs). An integrated energy dispersive X-ray analysis (EDX) (eXL, Oxford Instruments) was used for qualitative and quantitative analysis. The transmission electron microscopy were done on a 200 kV equipment (H-8100, Hitachi). The replica technique was used to prepare the samples.

#### 4.4.9 Atomic force microscopy

The atomic force microscopy (AFM) was carried out with an ultraobjective (SIS - survive imaging system) on surfaces of glasses and thermally treated glasses. The samples were polished on pitch with  $\text{Ce}_2\text{O}_3$  and chemically etched.

### 4.5 Structure of glasses and glass-ceramics

#### 4.5.1 IR spectroscopy

An infrared spectrometer (IFS66, Bruker) was used to record IR-reflectance spectra of glasses and glass-ceramics. The spectra were measured from 100 to 6000  $\text{cm}^{-1}$  with a spectral resolution of 2  $\text{cm}^{-1}$ . The angle of incident was 20 ° and the light was either

parallel or perpendicular polarised. Polished glasses and glass-ceramics were used for the measurements to maximise the specular reflectance.

## 4.5.2 Raman spectroscopy

A raman spectrometer (T64000, Jobin-Yvon) with microscope top (Olympus, spot-size 1 micron) was used to record raman spectra of the glasses and glass-ceramics. The spectra were measured using the 514.5 nm emission wavelength of an Ar-Kr gas laser in the range from 50 to 2600  $\text{cm}^{-1}$  with a spectral resolution of 1.18  $\text{cm}^{-1}$ . Measurements were carried out on the samples for IR spectroscopy using polished glasses and glass-ceramics.

## 4.6 Electrical conductivity

### 4.6.1 Experimental setup

Figure 4.3 shows the experimental setup which was used to measure the impedance. The glass samples were cut into disks with 10 mm diameter and 5 mm height and subsequently polished. A ring of alumina (spacer) with an inner diameter of 10.4 mm and a height of 5 to 10 % less than the sample was cut from a tube, ground and polished on both sides. On top and bottom of the sample, platinum disks, 12 mm in diameter and 1 mm in thickness, were attached. The wiring to the impedance analyser (Zahner IM 5d, Zahner Elektrik) consists of 0.35 mm platinum wires occupying 2 of the 4 holes in an alumina tube, which were connected to the impedance analyser as shown in Fig. 4.3. To control the furnace temperature (dc power supply), a type N thermocouple was inserted into one of the remaining holes of the alumina tube and placed as close as possible to the sample without electrical contact.

### 4.6.2 Experimental procedure

The measurement of the impedance was done in two steps: at first, the contact was established and subsequently the measurement was carried out. To establish the contact, the sample was heated to 650 °C (all samples except 0.9 BaO - Al<sub>2</sub>O<sub>3</sub> - B<sub>2</sub>O<sub>3</sub>) or 670 °C (sample 0.9 BaO - Al<sub>2</sub>O<sub>3</sub> - B<sub>2</sub>O<sub>3</sub>), held for 10 min and then cooled down to 550 °C with a rate of 10 K/min. After this procedure, the diameter and the height of the samples were equal to the inner diameter and the height of the spacer, furthermore the contact to the platinum disks was well established. After initial measurements of the impedance spectra between 0.05 Hz and 1 MHz at 550 °C, a frequency (3.7 s<sup>-1</sup>) was selected at

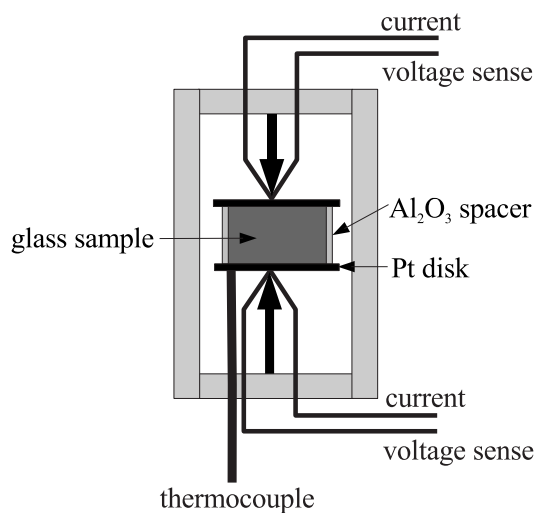


Figure 4.3: Experimental arrangement of the impedance measurements.

which the phase angle (around  $0^\circ$ ) is controlled by the resistive part of the sample at any temperature. The frequency was  $3.7 \text{ s}^{-1}$ , the AC amplitude was 50 mV, and 66 cycles were measured for averaging. The absolute magnitudes of the impedance,  $|Z|$ , and the phase angle,  $|\varphi|$ , as function of the temperature, were measured in the range from  $550^\circ \text{ C}$  to  $1150^\circ \text{ C}$  during heating and cooling using rates of 0.167, 0.5, 1 and 2 K/min. The sample was kept at the maximum temperature for 6 min. After the measurements of the impedance were completed, the XRD patterns were recorded from powdered samples. Additionally, the cross-sections of the samples were studied by optical microscopy.

# Chapter 5

## Glass-ceramics development

### 5.1 Stoichiometric glass BaO - Al<sub>2</sub>O<sub>3</sub> - B<sub>2</sub>O<sub>3</sub>

#### 5.1.1 Glass properties

The methodical investigations of the glass system BaO-Al<sub>2</sub>O<sub>3</sub>-B<sub>2</sub>O<sub>3</sub> were started from the stoichiometric composition, i.e. 33.3 mol% BaO, Al<sub>2</sub>O<sub>3</sub> and B<sub>2</sub>O<sub>3</sub>. This glass system was chosen after intensive literature research, as former investigations showed that glass-ceramics of this system have a low thermal expansion coefficient [4, 15, 24].

The glass BaO-Al<sub>2</sub>O<sub>3</sub>-B<sub>2</sub>O<sub>3</sub> was melted under the conditions shown in section 4.1, and a vitreous and transparent glass was obtained. Furthermore, the properties of the glass were determined. The DTA shows a  $T_g$  of 620 °C, but no exothermic peak indicating crystallisation of the glass. The thermal expansion coefficient of the glass is  $68 \cdot 10^{-7} \text{ K}^{-1}$  from 100 to 300 °C and  $71 \cdot 10^{-7} \text{ K}^{-1}$  from 100 to 500 °C. The dilatometric measurement shows the  $T_g$  at 585 °C and the  $T_D$  at 660 °C. The difference of 35 K between the  $T_g$  values of DTA and dilatometry results from the different sample geometry. While the DTA sample is a powder with a grain size fraction of 250 to 315  $\mu\text{m}$ , the dilatometry sample is a block with  $10 \cdot 10 \cdot 20 \text{ mm}^3$  dimension. Therefore, the heat transfer is different during the measurements and leads to the difference in the  $T_g$  values. Another reason is the heating rate which is 5 K/min for the dilatometry and 10 K/min for the DTA. The heating rate influences  $T_g$ , i.e.  $T_g$  is shifted to higher temperatures with an increased heating rate. The density of the glass was determined by helium pycnometry and shows a value of  $3.37 \text{ g/cm}^3$ . The Archimedes method gives a density value of  $3.35 \text{ g/cm}^3$ .

Another important material property is the hydrolytic durability (determination see section 4.4.4) which shows a volume of 23 ml 0.01 N HCl for the BaO-Al<sub>2</sub>O<sub>3</sub>-B<sub>2</sub>O<sub>3</sub> glass. While the glass is soaked in water (98 °C), it starts to dissolve. After one hour of

heat treatment precipitation can be seen in the solution, indicating a very low hydrolytic durability. On the other hand, the glass is stable in air, because no surface corrosion through humidity was observed after 2 years of storage.

The results of the different viscosity measurements are shown in Fig. 5.1. A gap was observed between the two rotary viscometric measurements with different velocities (10 and 250 l/min), while the measurement curves of the bending viscometry match. The difference between the two curves of rotary viscometry might be caused through crystallisation in the glass. Another peculiarity is observed comparing both viscosity measurements, bending and rotary viscometry. The curve of the viscosity versus temperature decreases discontinuously. A reason for this behaviour is discussed in section 6.5.5.

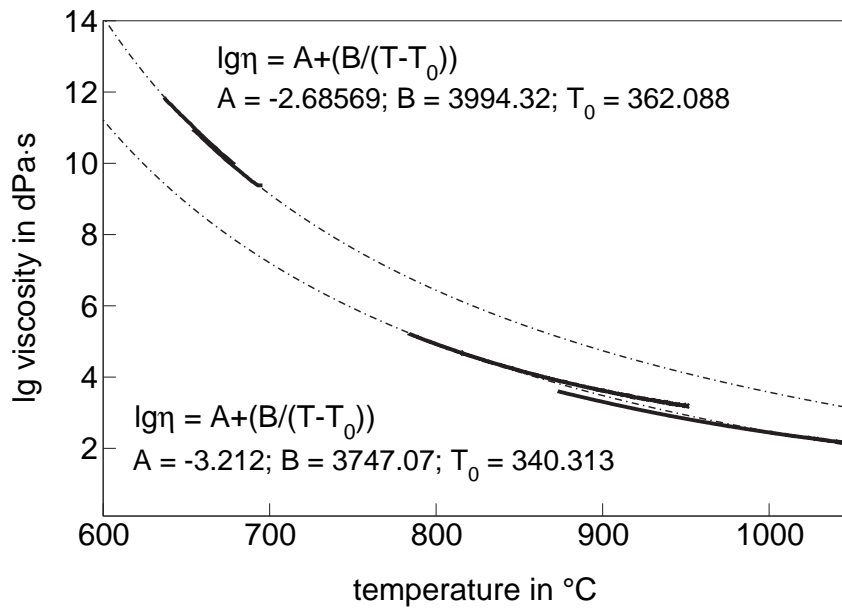


Figure 5.1: Viscosity of glass BaO - Al<sub>2</sub>O<sub>3</sub> - B<sub>2</sub>O<sub>3</sub>; thick solid lines: measured viscosities, dash dotted lines: upper curve: FVT-fit to data from bending viscometry, lower curve: FVT-fit to data from rotary viscometry.

The experimental results were fitted to the Vogel-Fulcher-Tammann-(VFT)-equation [37]:

$$\lg \eta = A + \frac{B}{T - T_0} \quad (5.1)$$

The fit was used to extrapolate the temperatures at viscosities of 10<sup>4</sup> and 10<sup>13</sup> dPa·s for the glass BaO - Al<sub>2</sub>O<sub>3</sub> - B<sub>2</sub>O<sub>3</sub> showing a temperature of 864 °C at 10<sup>4</sup> dPa·s and 617 °C at 10<sup>13</sup> dPa·s.

The chemical analysis of the glass BaO - Al<sub>2</sub>O<sub>3</sub> - B<sub>2</sub>O<sub>3</sub> is very difficult and shows no satisfactory result. The analysis was carried out by EDX-SEM and wet chemical analysis. Unfortunately, an energy dispersive detector can detect barium, aluminum and oxygen but

not boron, because its radiation is too low in energy (185 eV) and the absorption is high. So a line broadening occurs and the concentration can not be determined. The line would be preciser through an extension of the measuring time, but this results in destruction of the glass. Therefore, the boron concentration was calculated to 100 %, which is inaccurate and does not give the real concentration in the glass. The quantitative determination of boron by wet chemical analysis was also not possible, as the high alumina concentration in the glass disturbs the analysis of boron. For this method, the boron concentration was also calculated to 100%. There is no analytical method reported in literature to determine the boron in such high concentration directly if simultaneously high alumina concentrations are present. For this reason no additional analysis of the glass was carried out and the theoretical composition of the glasses will be used for all further discussions.

### 5.1.2 Bulk glass-ceramics BaO - Al<sub>2</sub>O<sub>3</sub> - B<sub>2</sub>O<sub>3</sub>

First experiments showed that a two step thermal treatment is necessary to get completely crystallised glass-ceramics. The following program for the thermal treatment was determined to crystallise the glass BaO - Al<sub>2</sub>O<sub>3</sub> - B<sub>2</sub>O<sub>3</sub>: 720 °C, 24 h and 780 °C, 8 h, heating rate 10 K/min. The glass-ceramics exhibit a white appearance, the surfaces are smooth and the dimensions of the bulk sample remain nearly constant. The cross-section of the bulk shows a crystallised material with small parts of glass phase at the crystal borders. In comparison to the glass with the same chemical composition, glass-ceramics with the composition BaO - Al<sub>2</sub>O<sub>3</sub> - B<sub>2</sub>O<sub>3</sub> exhibit a smaller density of 3.10 g/cm<sup>3</sup>. Hence, a volume expansion takes place during the crystallisation. It should be noted, that at most glass compositions, volume contraction is observed during crystallisation, caused by a more ordered and denser packed structure [43]. The crystal structure formed here seems to have a less dense packing, which is why a density decrease is observed. This behaviour is unusual but not unique, e.g. it is also observed during the crystallisation of cordierite glass [44]. Figure 5.2 shows the XRD patterns of the glass-ceramics; only one crystalline phase BaAl<sub>2</sub>B<sub>2</sub>O<sub>7</sub> (JCPDS 86-2168) is detected. This crystalline phase has a rhombohedral structure and a (X-ray) density of 3.065 g/cm<sup>3</sup> [21].

Furthermore, the XRD patterns from the surface and the cross-section of the glass-ceramics show a different orientation of the crystals. The crystals at the surface indicate a strong orientation with respect to the [003] plane which can be seen in the larger peak intensity in comparison to the others, while the orientation of the crystals in the bulk (see cross-section) is random. This result is supported by the optical micrographs (see Fig. 5.3). These pictures show two types of crystals. A thin surface crystallisation layer



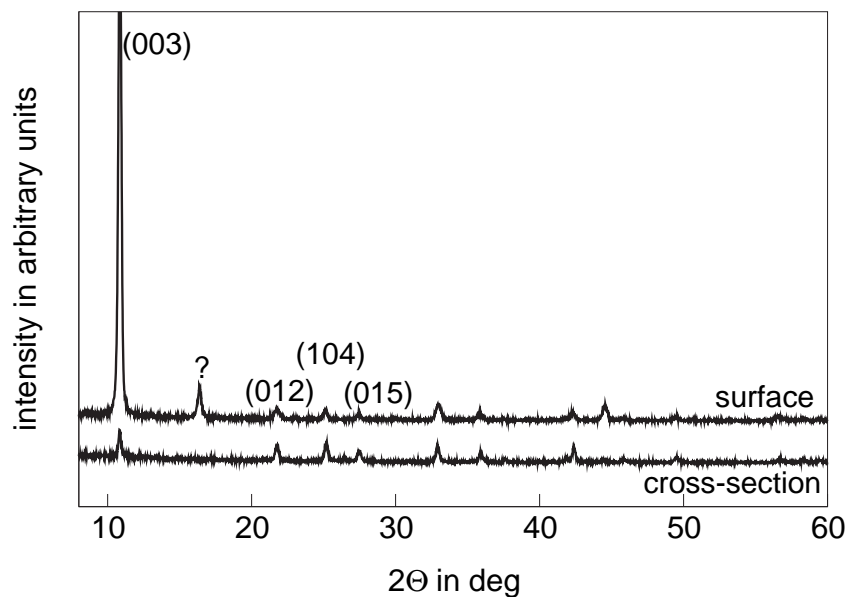


Figure 5.2: XRD pattern of the bulk glass-ceramics  $\text{BaO} - \text{Al}_2\text{O}_3 - \text{B}_2\text{O}_3$  measured at the surface and the cross-section (crystalline phase: ? - unknown, other peaks -  $\text{BaAl}_2\text{B}_2\text{O}_7$  (JCPDS 86-2168) with indication of the crystal plane orientation.

is formed beside the crystallisation in the volume. At the surface, the crystals are needle-like and oriented perpendicular to the surface, while the crystals in the volume have an ellipsoide shape and seem to be randomly distributed.

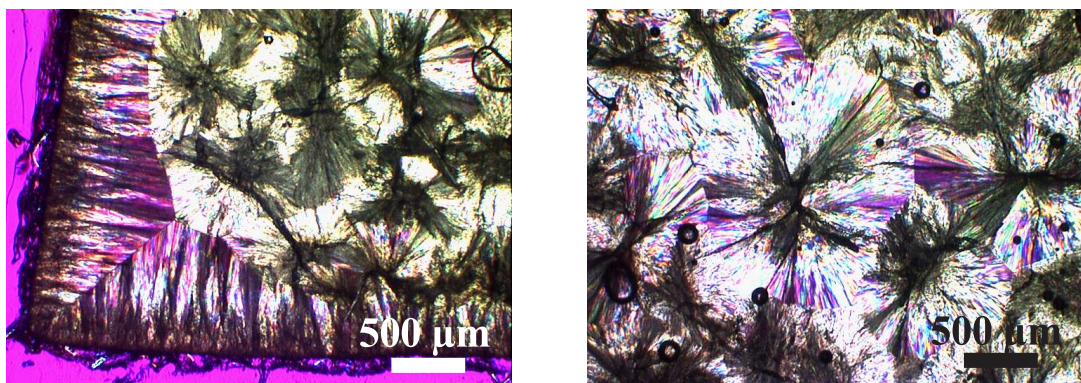


Figure 5.3: Optical micrographs of the bulk glass-ceramics  $\text{BaO} - \text{Al}_2\text{O}_3 - \text{B}_2\text{O}_3$ .

The thermal expansion of the bulk glass-ceramics is discussed in section 5.1.5 together with other glass-ceramics in the system  $\text{BaO} - \text{Al}_2\text{O}_3 - \text{B}_2\text{O}_3$ . The hydrolytic durability was not determined as the remaining glass phase may influence the result.

### 5.1.3 Bulk glass-ceramics $\text{BaO} - \text{Al}_2\text{O}_3 - \text{B}_2\text{O}_3$ with platinum

Since the bulk glass-ceramics of  $\text{BaO} - \text{Al}_2\text{O}_3 - \text{B}_2\text{O}_3$  show a combination of surface and volume crystallisation, platinum was added as nucleation agent to achieve complete vol-

ume crystallisation [45]. The obtained glass did not contain crystals and was light grey in colour. A homogenous distribution of the platinum was observed by visual inspection. The density of the glass is  $3.38 \text{ g/cm}^3$  and the glass-ceramics (standard crystallisation program) have a density of  $3.10 \text{ g/cm}^3$ . A density decrease is also monitored during crystallisation which verifies the results of the bulk glass-ceramics without platinum. The XRD pattern of the bulk glass-ceramics with platinum can also be attributed to  $\text{BaAl}_2\text{B}_2\text{O}_7$  (JCPDS 86-2168). Figure 5.4 presents the optical micrographs of the glass-ceramics.

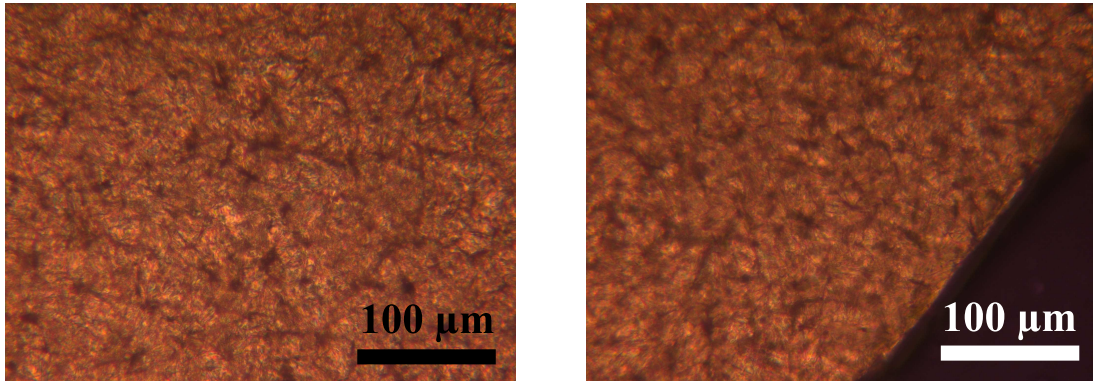


Figure 5.4: Optical micrographs of the bulk glass-ceramics  $\text{BaO} - \text{Al}_2\text{O}_3 - \text{B}_2\text{O}_3$  with platinum.

The micrographs show a homogeneously crystallised glass-ceramics with much smaller crystals than the bulk glass-ceramics without platinum (compare Fig. 5.3). A surface layer could not be detected, i.e. the glass  $\text{BaO} - \text{Al}_2\text{O}_3 - \text{B}_2\text{O}_3$  doped with platinum indicates volume crystallisation. The thermal expansion coefficient of the glass-ceramics with platinum was also measured and the results are discussed in section 5.1.5. Additionally, the hydrolytic durability was determined from this completely crystallised material. The volume of 0.01 N HCl, used for the titration against methyl red, was 36.5 ml. This result shows that the durability of the glass-ceramics is even lower than of the original glass.

#### 5.1.4 Sinter glass-ceramics $\text{BaO} - \text{Al}_2\text{O}_3 - \text{B}_2\text{O}_3$

The experiments for making sinter glass-ceramics with the composition  $\text{BaO} - \text{Al}_2\text{O}_3 - \text{B}_2\text{O}_3$  were carried out to reproduce the results of MacDowell [4, 24] and to compare them with the bulk glass-ceramics with and without platinum of the same composition.

The preparation procedure of the sinter glass-ceramics is described in section 4.3. In a first step, the crystallisation temperature was varied to find the optimum temperature. The resulting samples had different appearances. In Fig. 5.5, the XRD patterns of the sinter glass-ceramics at different crystallisation temperatures are shown. At  $700^\circ \text{C}$ , the

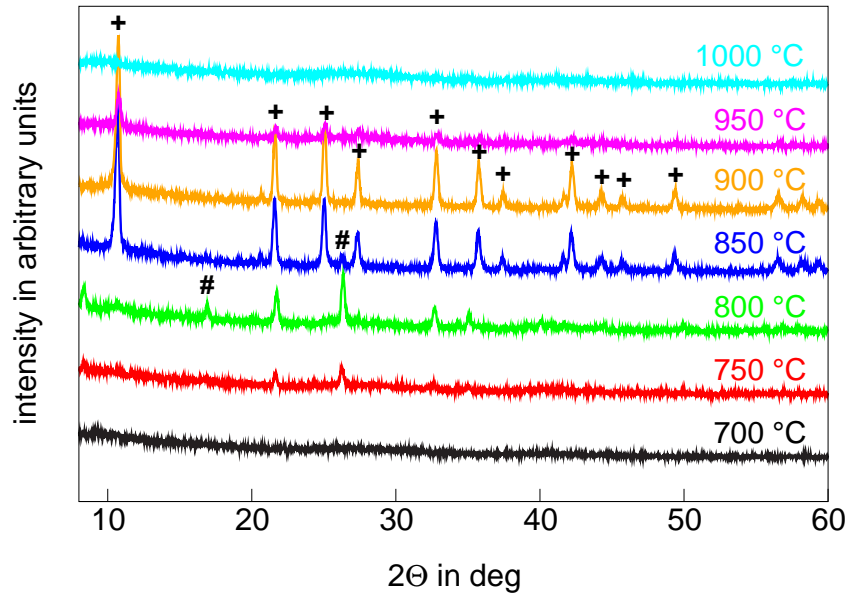


Figure 5.5: XRD patterns of sinter glass-ceramics prepared from the glass  $\text{BaO} - \text{Al}_2\text{O}_3 - \text{B}_2\text{O}_3$  using different crystallisation temperatures (crystalline phases: + -  $\text{BaAl}_2\text{B}_2\text{O}_7$  (JCPDS 86-2168), # -  $\text{BaB}_8\text{O}_{13}$ ) (JCPDS 23-0042).

sample is amorphous and no crystalline phase is formed. The sample tempered at  $750^\circ\text{C}$  shows small peaks belonging to the crystalline phase  $\text{BaB}_8\text{O}_{13}$  (JCPDS 23-0042), but the glass phase is still dominant. At  $800^\circ\text{C}$ , the crystalline phase  $\text{BaAl}_2\text{B}_2\text{O}_7$  (JCPDS 86-2168) is detected beside  $\text{BaB}_8\text{O}_{13}$ . After tempering at increased temperature ( $850$  and  $900^\circ\text{C}$ ), only the crystalline phase  $\text{BaAl}_2\text{B}_2\text{O}_7$  (JCPDS 86-2168) is detected. Further increase of the temperature resulted in the melting of the phase and no other phases crystallised (see  $950$  and  $1000^\circ\text{C}$ ).

SEM micrographs (see Fig. 5.6) were used to analyse the porosity of the samples and the morphology of the crystals. At  $700^\circ\text{C}$ , the sintered sample is still amorphous and some small holes are formed during thermal treatment. With increasing temperature, the porosity increases and the sintered glass starts to crystallise (see sample prepared at  $800^\circ\text{C}$ ). At  $850^\circ\text{C}$ , the sample completely consists of needle-like crystals which are randomly oriented. On the other hand, the number and size of the holes increases. The sample prepared at  $950^\circ\text{C}$ , shows only cavities and the crystals are already melted. After these experiments, larger pellets were produced to measure the thermal expansion coefficient (see section 4.3). The results of density, XRD and TEC measurement are described and discussed in comparison to two other types of glass-ceramics in section 5.1.5.

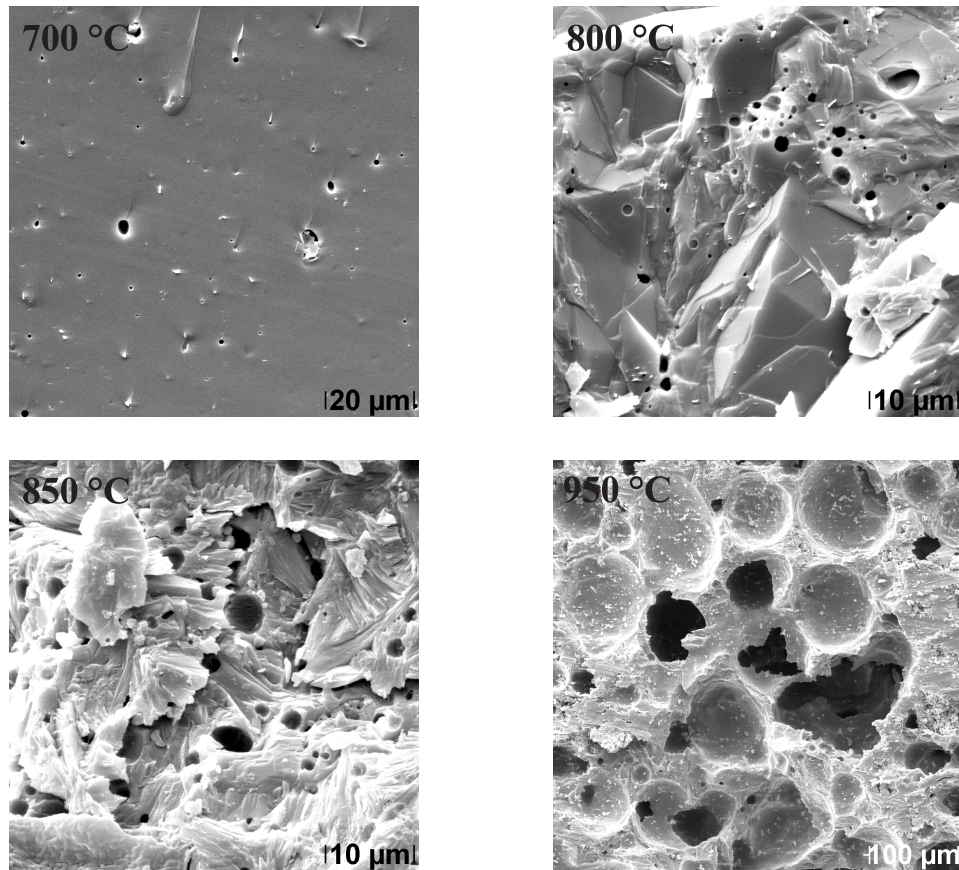


Figure 5.6: SEM micrographs of the sinter glass-ceramics  $\text{BaO} - \text{Al}_2\text{O}_3 - \text{B}_2\text{O}_3$  at different temperatures of heat treatment.

### 5.1.5 Comparison of sinter and bulk glass-ceramics with and without platinum

This section deals with the comparison of the surface and bulk crystallised glass-ceramics as well as the sinter glass-ceramics prepared from the glass  $\text{BaO} - \text{Al}_2\text{O}_3 - \text{B}_2\text{O}_3$ . Figure 5.7 shows the XRD patterns of the prepared crystallised samples recorded at room temperature.

The XRD line pattern of the rhombohedral  $\text{BaAl}_2\text{B}_2\text{O}_7$  crystalline phase (JCPDS 86-2168) is at the bottom of the graph. All three glass-ceramics show the lines attributed to the  $\text{BaAl}_2\text{B}_2\text{O}_7$  crystalline phase (JCPDS 86-2168). But the relative intensities of respective XRD lines are different, e.g. in bulk glass-ceramics (sample A), the intensity of the line at  $10.8^\circ$  is larger in comparison to those of the bulk glass-ceramics with Pt (sample B) and the sinter glass-ceramics (sample C). Furthermore, the ratio between the 100 % line ( $10.8^\circ$ ) and the other lines is in agreement with JCPDS data for the bulk glass-ceramics with Pt and the sinter glass-ceramics, i.e., the orientation of the crystals is random. The bulk glass-ceramics without platinum, however, show an orientation in the



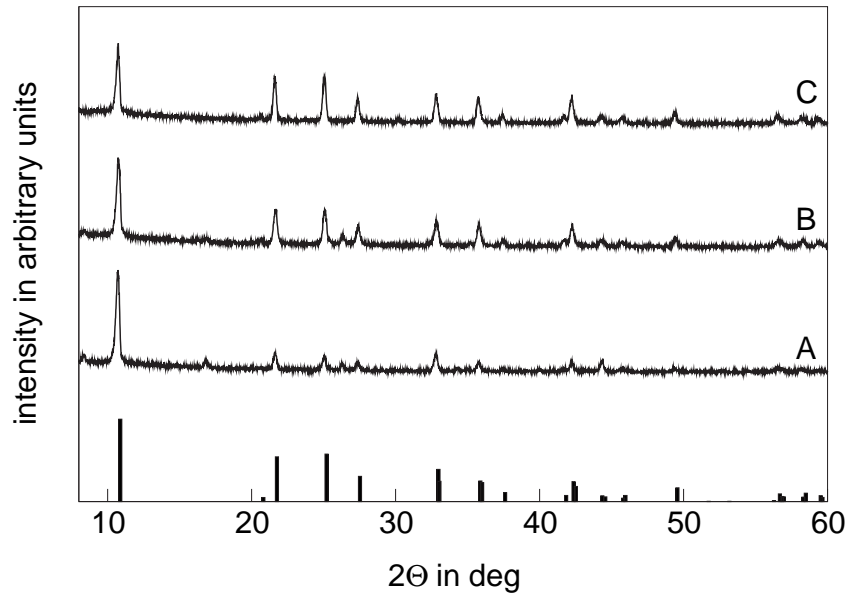


Figure 5.7: XRD patterns of the different types of glass-ceramics  $\text{BaO} - \text{Al}_2\text{O}_3 - \text{B}_2\text{O}_3$ ; A: bulk glass-ceramics, B: bulk glass-ceramics with Pt, C: sinter glass-ceramics; and the line pattern of the  $\text{BaAl}_2\text{B}_2\text{O}_7$  crystalline phase (JCPDS 86-2168).

[003] plane which can be derived from the higher intensity of the line at  $10.8^\circ$ .

In Fig. 5.8, the dilatometric measurements of the different glass-ceramics are shown. The bulk glass-ceramics exhibit a negative thermal expansion coefficient in the temperature range from 25 to  $390^\circ\text{C}$  in sample A (without Pt) and up to around  $115^\circ\text{C}$  in the Pt-containing sample (sample C), while the thermal expansion coefficient of the sinter glass-ceramics (sample C) is approximately zero up to  $80^\circ\text{C}$ . Above these temperatures, the expansion coefficients are positive for all studied samples.

To verify the XRD results regarding the orientation of the crystals, pictures of the morphology of the glass-ceramics were taken. Figure 5.9 presents the micrographs of the different types of glass-ceramics (sample A to C). Bulk glass-ceramics (sample A) show a surface crystallisation layer of 500 to  $700\ \mu\text{m}$  in thickness. The surface layer is highly oriented and the crystallographic c-axis is perpendicular to the surface (see XRD). In the bulk, large spheroidal crystals with a mean diameter from 500 to  $700\ \mu\text{m}$  are observed. The bulk glass-ceramics with Pt (sample B) do not exhibit a surface layer and the crystals are notably smaller than in sample A. Sample C, the sinter glass-ceramics, still has some porosity, with crystals around 20 to  $30\ \mu\text{m}$  long, as well as some spheroidal crystals.

Figure 5.10 presents results from the high temperature XRD up to  $500^\circ\text{C}$ , illustrated by the dependency of the [003] peak at around  $10.8^\circ$  and the [012] peak at around  $21.6^\circ$  on temperature. The peak at  $10.8^\circ$  is directly attributed to the crystallographic c-axis, and with increasing temperature, gets shifted to larger  $2\theta$ -values, i.e.

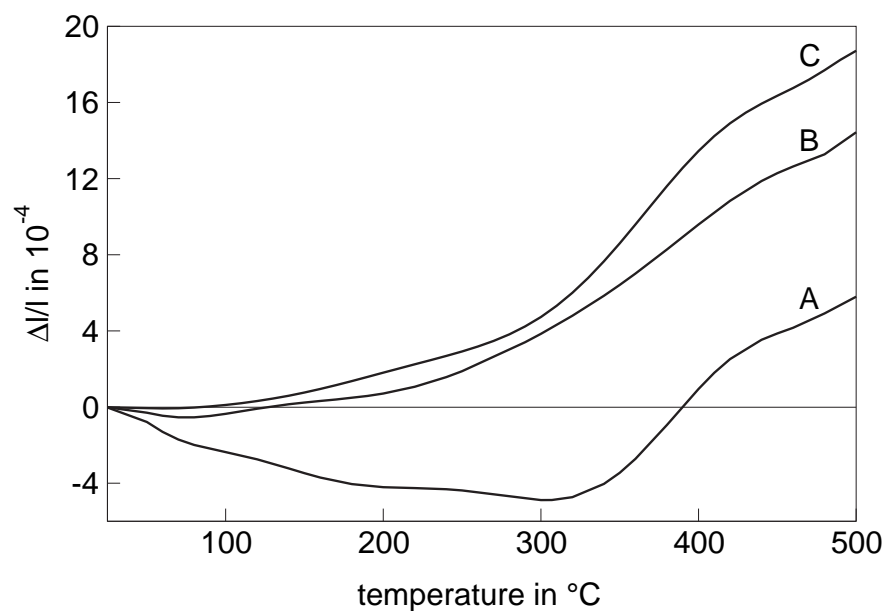


Figure 5.8: Dilatometry measurements of the different types of glass-ceramics BaO-Al<sub>2</sub>O<sub>3</sub>-B<sub>2</sub>O<sub>3</sub>; A: bulk glass-ceramics, B: bulk glass-ceramics with Pt, C: sinter glass-ceramics.

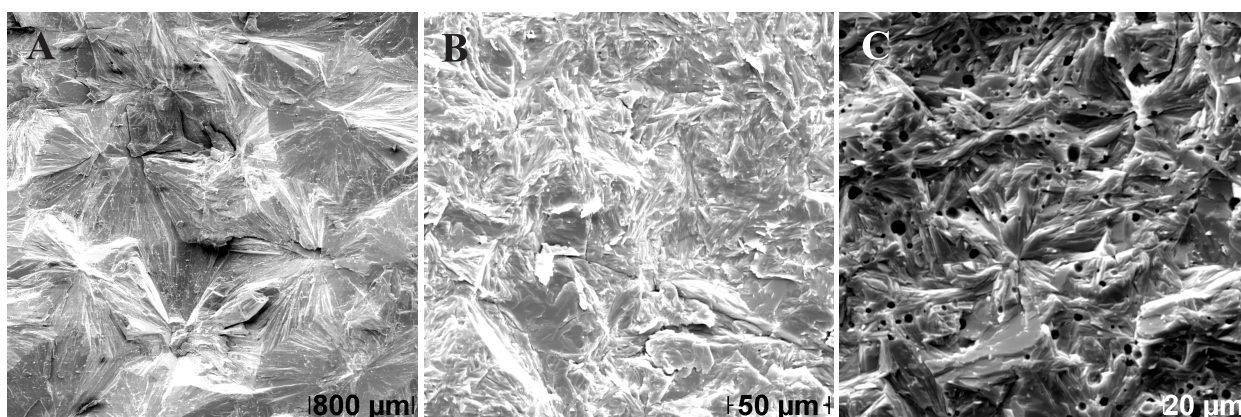


Figure 5.9: SEM micrographs of the different types of glass-ceramics BaO-Al<sub>2</sub>O<sub>3</sub>-B<sub>2</sub>O<sub>3</sub>; A: bulk glass-ceramics, B: bulk glass-ceramics with Pt, C: sinter glass-ceramics.

the *c*-axis gets shorter. The peak at 21.6 deg is observed at approximately the same  $2\Theta$ -values up to a temperature of 250 °C and with further increasing temperature, it is shifted to smaller  $2\Theta$ -values. From the temperature dependency of these two peaks and others observed in Fig. 5.7, the lengths of the crystallographic *a*- and *c*-axis were calculated as a function of temperature. The results of the calculation are shown in Fig. 5.11. With increasing temperature, the *c*-axis gets continuously shorter, while the *a*-axis remains approximately constant up to 150 °C and increases above this temperature.

The unusual density behaviour is already described in section 5.1.2 and could also be verified for the glass-ceramics doped with platinum and the sinter glass-ceramics. An-

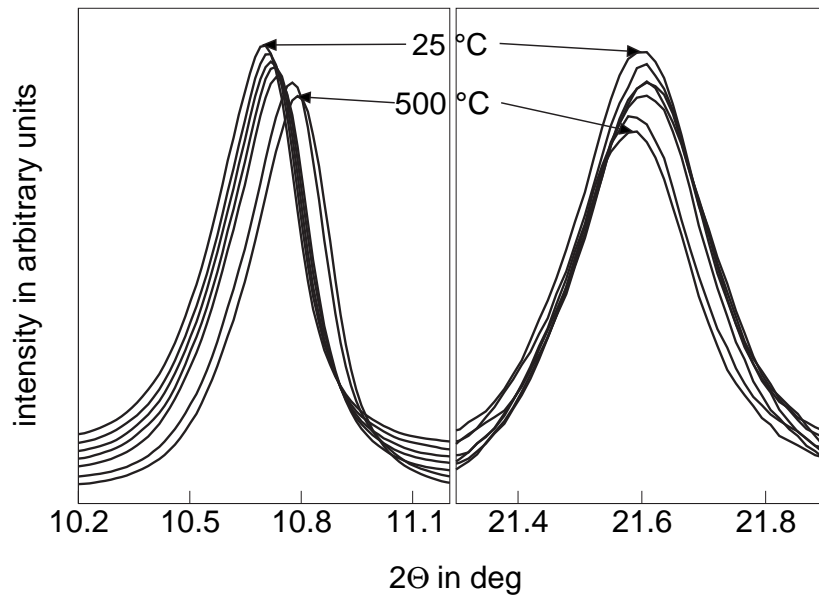


Figure 5.10: XRD patterns of the [003] and [012] peaks as function of the temperature.

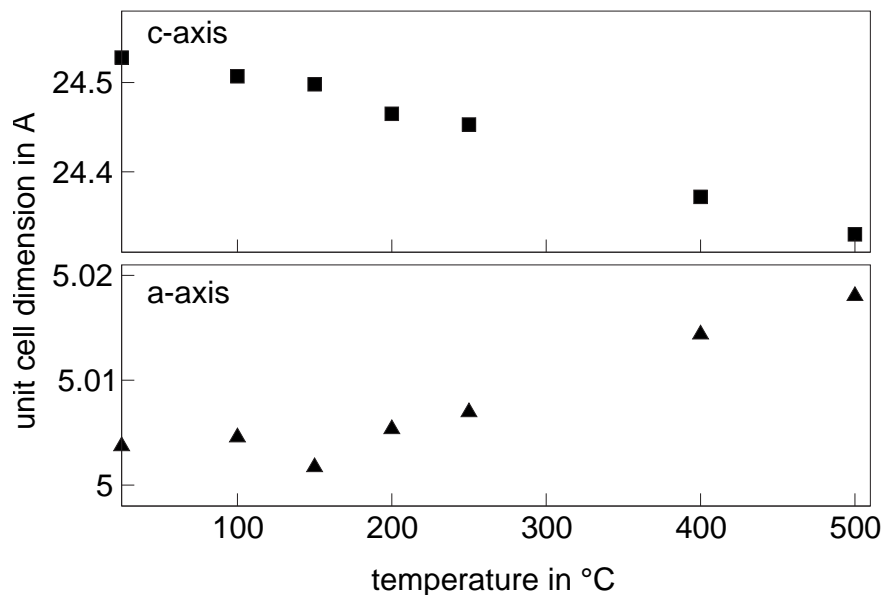


Figure 5.11: Temperature dependence of the a and c-axis of the crystalline phase  $\text{BaAl}_2\text{B}_2\text{O}_7$  (JCPDS 86-2168).

other quite uncommon property of the  $\text{BaAl}_2\text{B}_2\text{O}_7$  crystalline phase (JCPDS 86-2168) is the negative thermal expansion coefficient. It is predominantly caused by the strongly negative expansion in the crystallographic c-axis of  $-174 \cdot 10^{-7} \text{ K}^{-1}$  in the temperature range from 25 to 500 °C (as shown in Fig. 5.11). In the same temperature range, the crystallographic a-axis has a mean thermal expansion coefficient of  $58 \cdot 10^{-7} \text{ K}^{-1}$ .

The glass has the same chemical composition as the glass-ceramics. As the density of the glass-ceramics with and without platinum and the sinter glass-ceramics is approxi-

mately the same as that of the pure crystalline phase, the glass seems to be crystallised quantitatively. Furthermore, any hint at the occurrence of a residual glassy phase was not obtained from the XRD patterns and the SEM micrographs.

Dilatometric measurements of the crystallised samples (see Fig. 5.8) show that the thermal expansion coefficient of all crystallised samples is negative or at least zero up to a temperature of around 80 °C. However, notable deviations were obtained between the different types of glass-ceramics. The thermal expansion of the bulk glass-ceramics is minimum, of the sinter glass-ceramics is maximum and the bulk glass-ceramics with platinum lies in between. As the only detected phase in all three samples is  $\text{BaAl}_2\text{B}_2\text{O}_7$  (JCPDS 86-2168), the differences have to be explained by the respective microstructures. Figure 5.12 shows the dilatometric curves of the three glass-ceramics, the relative change of the crystallographic a- and c-axis and the changes of the mean length of the unit cell ( $l = \sqrt[3]{V}$ ,  $V$  = volume of the unit cell) with temperature.

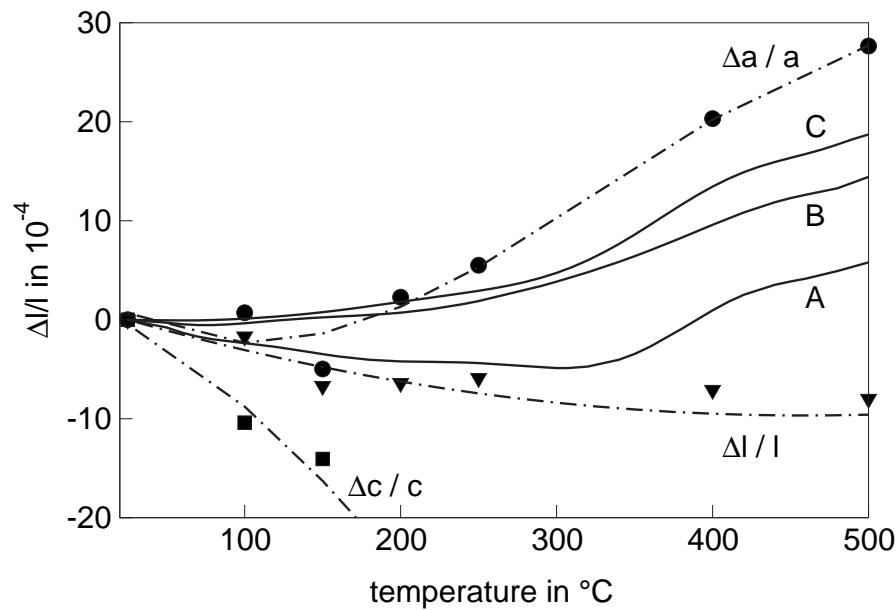


Figure 5.12: Dilatometric curves of the bulk glass-ceramics with (A) and without platinum (B) and the sinter glass-ceramics (C) in comparison to the a ( $\Delta a/a$ ) and c-axis ( $\Delta c/c$ ) as well as the mean length of the unit cell ( $\Delta l/l$ ).

It is shown, that the thermal expansion coefficient of the bulk glass-ceramics (sample A) is close to  $\Delta l/l$  up to temperature of 300 °C. In a first approximation, this should be expected from a sample with statistically arranged crystals. Above 300 °C, the relative change of the mean length of the unit cell,  $\Delta l/l$ , is further decreasing while the curve of the bulk glass-ceramics starts to increase. The bulk glass-ceramics with platinum (sample B) and the sinter glass-ceramics (sample C) exhibit a thermal expansion close to  $\Delta a/a$



up to a temperature of around 250 °C. Here, only the expansion in the crystallographic a-axis seems to be decisive for the macroscopic expansion. At higher temperatures, the experimentally observed thermal expansions of all glass-ceramics differ from the obtained values of  $\Delta a/a$ ,  $\Delta c/c$  and  $\Delta l/l$ .

## 5.2 Influence of the BaO concentration on the crystallisation

Pre-examinations have shown that the BaO concentration influences the crystallisation of the glasses, therefore glasses with BaO concentration deviating from the BaO - Al<sub>2</sub>O<sub>3</sub> - B<sub>2</sub>O<sub>3</sub> stoichiometry were melted. The compositions of the studied glasses are shown in Table 5.1 as well as the glass transformation temperatures,  $T_g$ , and softening temperatures,  $T_D$ .

Table 5.1: Chemical composition, glass transformation and softening temperature of the glasses with varied BaO concentration.

Sample name	BaO in mol%	Al <sub>2</sub> O <sub>3</sub> in mol%	B <sub>2</sub> O <sub>3</sub> in mol%	$T_g$ in °C	$T_D$ in °C
0.80 BaO - Al <sub>2</sub> O <sub>3</sub> - B <sub>2</sub> O <sub>3</sub>	28.6	35.7	35.7	600	665
0.90 BaO - Al <sub>2</sub> O <sub>3</sub> - B <sub>2</sub> O <sub>3</sub>	31.0	34.5	34.5	609	662
0.95 BaO - Al <sub>2</sub> O <sub>3</sub> - B <sub>2</sub> O <sub>3</sub>	32.2	33.9	33.9	605	667
1.00 BaO - Al <sub>2</sub> O <sub>3</sub> - B <sub>2</sub> O <sub>3</sub>	33.3	33.3	33.3	585	660
1.10 BaO - Al <sub>2</sub> O <sub>3</sub> - B <sub>2</sub> O <sub>3</sub>	35.5	32.3	33.3	573	634

The preparation of the glasses caused problems, because the tendency of crystallisation increased with decreasing BaO concentration. Vitreous and transparent glasses were obtained from all compositions except sample 0.80 BaO - Al<sub>2</sub>O<sub>3</sub> - B<sub>2</sub>O<sub>3</sub>, which contained some crystals. The analysis of the crystals is described later in this section. One part of each glass was doped with 0.01 wt% platinum. A decrease in the BaO concentration results in increased  $T_g$  and  $T_D$ . The densities of the glassy samples are summarised in Table 5.2, column 2, ranging from 3.24 to 3.40 g/cm<sup>3</sup>. They decrease with decreasing BaO concentration.

The standard thermal treatment (section 4.2) was carried out with all glasses and the investigated properties are shown in Table 5.2. The densities of the glass-ceramics are around 3.10 g/cm<sup>3</sup>. Like already mentioned in section 5.1.2, the density decrease

Table 5.2: Densities and thermal expansion coefficients of the glasses and glass-ceramics with varied BaO concentration.

Sample name	$\rho_{glass}$ in g/cm <sup>3</sup>	$\rho_{glass-ceramics}$ in g/cm <sup>3</sup>	$\alpha_{min.neg.}$ in 10 <sup>-7</sup> K <sup>-1</sup>	$\alpha_{100-300\text{ }^\circ\text{C}}$ in 10 <sup>-7</sup> K <sup>-1</sup>
0.80 BaO - Al <sub>2</sub> O <sub>3</sub> - B <sub>2</sub> O <sub>3</sub>	3.24	3.05	-1.6 (76 °C)	26
0.80 BaO - Al <sub>2</sub> O <sub>3</sub> - B <sub>2</sub> O <sub>3</sub> +Pt	3.28	3.10	-	24
0.90 BaO - Al <sub>2</sub> O <sub>3</sub> - B <sub>2</sub> O <sub>3</sub>	3.33	3.07	-1.4 (90 °C)	20
0.90 BaO - Al <sub>2</sub> O <sub>3</sub> - B <sub>2</sub> O <sub>3</sub> +Pt	3.36	3.06	-6.7 (374 °C)	-6
0.95 BaO - Al <sub>2</sub> O <sub>3</sub> - B <sub>2</sub> O <sub>3</sub>	3.34	3.29	-	-
0.95 BaO - Al <sub>2</sub> O <sub>3</sub> - B <sub>2</sub> O <sub>3</sub> +Pt	3.34	3.07	0 (85 °C)	21
1.00 BaO - Al <sub>2</sub> O <sub>3</sub> - B <sub>2</sub> O <sub>3</sub>	3.37	3.10	-15.9 (307 °C)	-12
1.00 BaO - Al <sub>2</sub> O <sub>3</sub> - B <sub>2</sub> O <sub>3</sub> +Pt	3.38	3.10	-5.5 (100 °C)	19
1.10 BaO - Al <sub>2</sub> O <sub>3</sub> - B <sub>2</sub> O <sub>3</sub>	3.39	3.44	-	-
1.10 BaO - Al <sub>2</sub> O <sub>3</sub> - B <sub>2</sub> O <sub>3</sub> +Pt	3.40	3.29	-	44

from the glass to the glass-ceramics indicates that the main crystalline phase should be BaAl<sub>2</sub>B<sub>2</sub>O<sub>7</sub> (JCPDS 86-2168). Only the glass-ceramics 0.95 BaO - Al<sub>2</sub>O<sub>3</sub> - B<sub>2</sub>O<sub>3</sub> and 1.10 BaO - Al<sub>2</sub>O<sub>3</sub> - B<sub>2</sub>O<sub>3</sub> with and without platinum have higher densities, which might result from an insufficient crystallisation. The XRD patterns of the glass-ceramics prove this assumption, see Fig. 5.13. Except for the glass-ceramics 0.95 BaO - Al<sub>2</sub>O<sub>3</sub> - B<sub>2</sub>O<sub>3</sub> and 1.10 BaO - Al<sub>2</sub>O<sub>3</sub> - B<sub>2</sub>O<sub>3</sub>, lines of the crystalline phase BaAl<sub>2</sub>B<sub>2</sub>O<sub>7</sub> (JCPDS 86-2168) can be seen in all samples. The XRD pattern of the sample 1.10 BaO - Al<sub>2</sub>O<sub>3</sub> - B<sub>2</sub>O<sub>3</sub> with platinum is of lower intensity compared to the other platinum doped samples resulting from a lower crystallinity. This fact is also indicated by the higher density of the glass-ceramics. An unknown crystalline phase was also detected in the samples with 0.95, 1.0 and 1.1 mol BaO. Furthermore, all samples without platinum show lines of lower intensities than the respective platinum containing glass-ceramics.

In Fig. 5.14, the thermal expansion coefficient versus the temperature is presented for all sufficiently crystallised samples with varied BaO concentration. The thermal expansion coefficient is around zero or negative up to 90 °C for all shown samples. The glass-ceramics BaO - Al<sub>2</sub>O<sub>3</sub> - B<sub>2</sub>O<sub>3</sub> and 0.90 BaO - Al<sub>2</sub>O<sub>3</sub> - B<sub>2</sub>O<sub>3</sub> with platinum have minimum negative thermal expansion coefficients of  $-15.9 \cdot 10^{-7} \text{ K}^{-1}$  from 25 to 307 °C, and  $-6.7 \cdot 10^{-7} \text{ K}^{-1}$  from 25 to 374 °C, respectively. These values are much lower in comparison to the other glass-ceramics. Here, the TEC lies between 19 and  $26 \cdot 10^{-7} \text{ K}^{-1}$  from 100 to 300 °C, except 1.10 BaO - Al<sub>2</sub>O<sub>3</sub> - B<sub>2</sub>O<sub>3</sub> with platinum. The crystallised sample

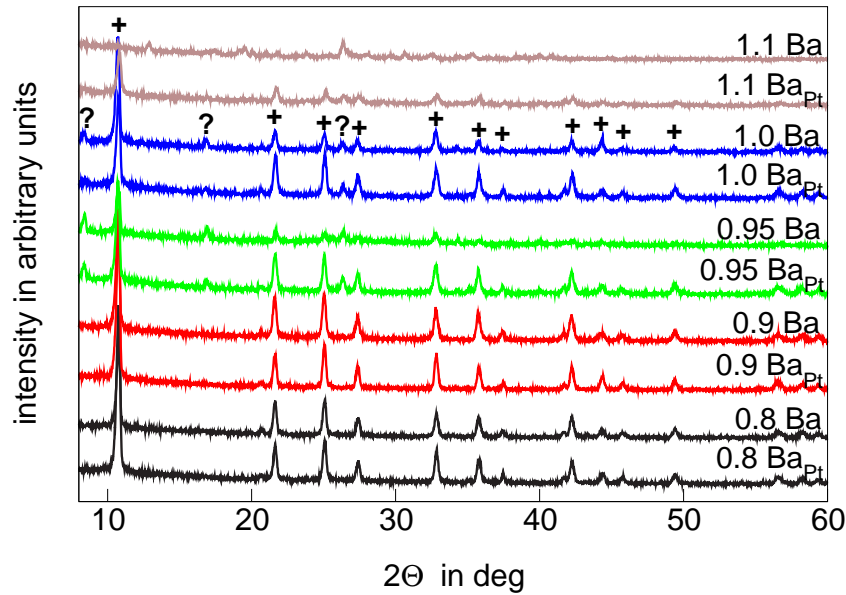


Figure 5.13: Crystalline phase consistence in dependence on the BaO concentration (crystalline phases: + - BaAl<sub>2</sub>B<sub>2</sub>O<sub>7</sub> (JCPDS 86-2168), ? - unknown).

1.10 BaO - Al<sub>2</sub>O<sub>3</sub> - B<sub>2</sub>O<sub>3</sub> with platinum has a much larger thermal expansion coefficient which is  $44 \cdot 10^{-7} \text{ K}^{-1}$  from 100 to 300 °C. This increase in the TEC of the glass-ceramics results from the insufficient crystallisation of BaAl<sub>2</sub>B<sub>2</sub>O<sub>7</sub> (JCPDS 86-2168), i.e. the glassy phase seems to be still dominant at temperatures above 80 °C.

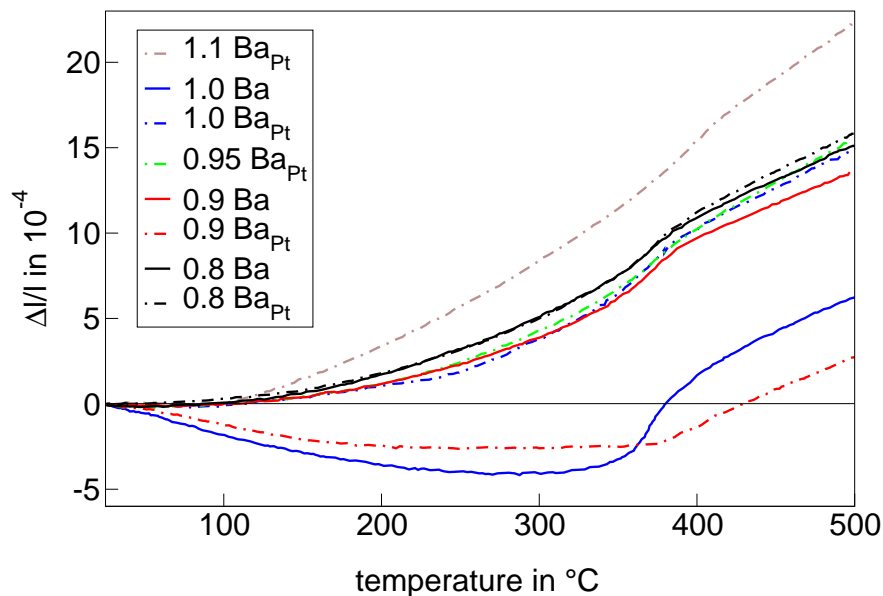


Figure 5.14: Thermal expansion of the glass-ceramics with varied BaO concentration.

Figure 5.15 shows optical micrographs of the glass-ceramics. The effect of the varied BaO concentration can be seen in these micrographs. For the samples without platinum, the decreased BaO concentration results in a better volume crystallisation. A surface

crystallisation layer is not observed for the sample  $0.80 \text{ BaO} - \text{Al}_2\text{O}_3 - \text{B}_2\text{O}_3$  and  $0.90 \text{ BaO} - \text{Al}_2\text{O}_3 - \text{B}_2\text{O}_3$ , while the base glass  $\text{BaO} - \text{Al}_2\text{O}_3 - \text{B}_2\text{O}_3$  has a layer of  $500$  to  $700 \mu\text{m}$  thickness. The crystals in the volume are much smaller in the samples with smaller BaO concentration than in  $\text{BaO} - \text{Al}_2\text{O}_3 - \text{B}_2\text{O}_3$  and are randomly oriented. A further increase of the BaO concentration results in a glass crystallising only at the surface, as shown for sample  $1.10 \text{ BaO} - \text{Al}_2\text{O}_3 - \text{B}_2\text{O}_3$ . The preparation of a polished thin section for optical microscopy was not possible of this sample.

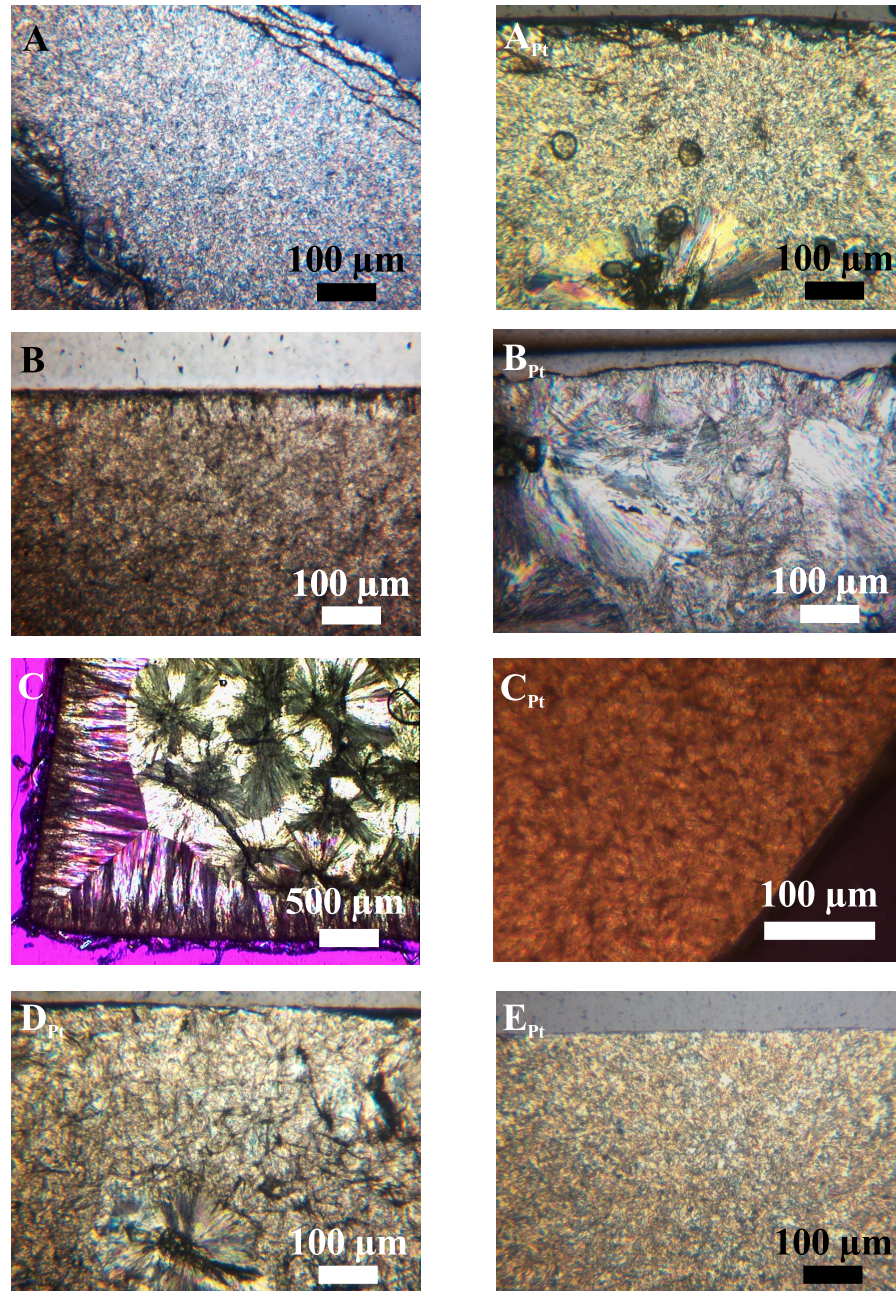


Figure 5.15: Optical micrographs of glass-ceramics with varied BaO concentration (A:  $0.80 \text{ BaO} - \text{Al}_2\text{O}_3 - \text{B}_2\text{O}_3$ , B:  $0.90 \text{ BaO} - \text{Al}_2\text{O}_3 - \text{B}_2\text{O}_3$ , C:  $\text{BaO} - \text{Al}_2\text{O}_3 - \text{B}_2\text{O}_3$ , D:  $0.95 \text{ BaO} - \text{Al}_2\text{O}_3 - \text{B}_2\text{O}_3$ , E:  $1.10 \text{ BaO} - \text{Al}_2\text{O}_3 - \text{B}_2\text{O}_3$ ), index Pt: addition of platinum.



All prepared glasses doped with platinum could be transformed into glass-ceramics. The microstructures of these samples look slightly different in comparison to the samples without platinum. All samples are completely crystallised in the volume, i.e. a surface crystallisation layer could not be observed. The micrographs of all glass-ceramics, except 0.90 BaO - Al<sub>2</sub>O<sub>3</sub> - B<sub>2</sub>O<sub>3</sub> + Pt, show very fine randomly oriented crystals. Glass-ceramics 0.90 BaO - Al<sub>2</sub>O<sub>3</sub> - B<sub>2</sub>O<sub>3</sub> + Pt consist of very fine crystals and long needle-like crystals with spheroidal shape. The samples 0.80 BaO - Al<sub>2</sub>O<sub>3</sub> - B<sub>2</sub>O<sub>3</sub> + Pt and 0.95 BaO - Al<sub>2</sub>O<sub>3</sub> - B<sub>2</sub>O<sub>3</sub> + Pt have occasionally such spheroidal crystals.

IR-reflectance spectra were recorded from the glasses as well as from the crystallised samples with various BaO concentration, as shown in Fig. 5.16, to achieve half quantitative structure informations, especially on the boron coordination. The measurements were carried out using the equipment and parameters described in section 4.5.1 and the signed peak positions were read from the spectrum, band separation was not carried out.

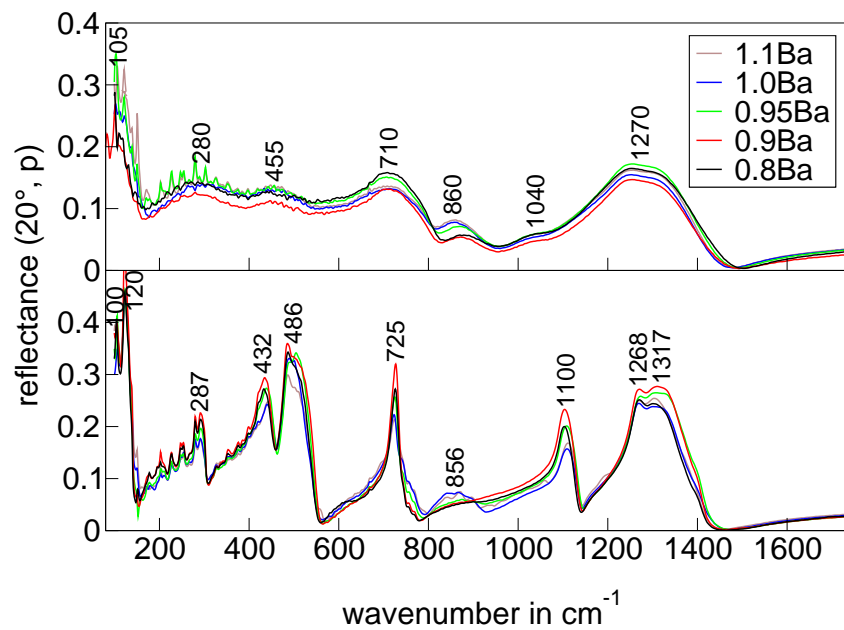


Figure 5.16: IR-reflectance spectra of the glasses (upper part) and glass-ceramics (lower part) with varied BaO concentration (incidence angle 20°, parallel polarised radiation).

The spectra exhibit, in the examined wavenumber region (100 to 1750 cm<sup>-1</sup>), broad reflection bands typical for glass samples. On the other hand, the linewidth of the reflection bands of the crystalline samples is smaller and the peaks exhibit higher intensities than those of the respective glasses. A further effect influencing the widths of the peaks is the crystal size, i.e. sharper peaks are due to larger crystals [46]. In Table 5.3, the assignment of the bands to the wavenumbers is listed representative for all measured spectra. The assignment of the bands is not unambiguous to clarify without deconvolution of the

spectra, but it shows tendentially the incorporation of the different oxides in the glasses and glass-ceramics.

Table 5.3: Assignment of the IR-reflectance bands by means of the glasses and glass-ceramics with varied BaO concentration ( $^{[x]}$ -coordination number).

Glass wavenumber in $\text{cm}^{-1}$	Band assignment	Glass-ceramics wavenumber in $\text{cm}^{-1}$	Reference
105	$\nu$ (Ba-O)	100	[47]
-	$\nu$ (Ba-O)	120	[47]
280	$\delta$ ( $^{[4]}$ Al-O); $\delta$ ( $^{[6]}$ Al-O); lattice vibration	287	[48]
455	$\delta$ ( $^{[4]}$ Al-O); $\nu$ ( $^{[6]}$ Al-O); lattice vibration	432	[48, 49]
-	$\delta$ ( $^{[4]}$ Al-O); $\delta$ ( $^{[6]}$ Al-O); lattice vibration	486	[48]
710	$\delta$ ( $^{[3]}$ B-O); $\nu$ ( $^{[4]}$ Al-O)	725	[48, 50, 51]
860	$\delta$ ( $^{[4]}$ B-O)	856	[52]
1040	$\nu$ ( $^{[4]}$ B-O)	-	[53]
-	$\nu$ ( $^{[3]}$ B-O)	1100	[48]
1270	$\nu$ ( $^{[3]}$ B-O)	1268	[48, 50, 51]
-	$\nu$ ( $^{[3]}$ B-O)	1317	[48]

The bands at around  $100 \text{ cm}^{-1}$  in the glass and glass-ceramic samples can be attributed to Ba-O stretching vibrations [47]. At  $280$  and  $455 \text{ cm}^{-1}$ , the bands are broad and of small intensity in the spectra of the glasses. An exact assignment of these bands can not be done, because bands of lattice vibrations as well as of stretching and/or bending vibrations of four- and/or sixfold coordinated aluminum are possible in this range [48]. Moreover, according to Ref. [49], the low intensity reflection band of the glass spectra at wavenumbers around  $455 \text{ cm}^{-1}$  may be assigned to the Al-O stretching vibrations in  $[\text{AlO}_6]$  groups. The spectra of the crystallised samples show in this region two bands at  $432$  and at  $486 \text{ cm}^{-1}$ , which could also be attributed to different vibrations as explained for the glasses. With regard to the crystal structure of  $\text{BaAl}_2\text{B}_2\text{O}_7$  (JCPDS 86-2168) (see section 3.4), the aluminum should be fourfold coordinated in the crystallised samples. Therefore, it is assumed that the band at  $710 \text{ cm}^{-1}$  might be assigned to the stretching vibration of fourfold coordinated aluminum [48]. However, these assumptions can not be proved with these measurements. Further investigations of the structure, with e.g. NMR

spectroscopy, would be necessary to clarify this problem. In analogy to Ref. [48, 50, 51], the bands at 710 and 1270  $\text{cm}^{-1}$  can be assigned to  $\text{BO}_3$  groups, while the band at 1040  $\text{cm}^{-1}$  belongs to tetrahedral  $\text{BO}_4$  [53]. The band at 860  $\text{cm}^{-1}$  also corresponds to tetrahedral  $\text{BO}_4$  unit as reported in Ref. [52]. The crystallisation of the glasses results in a slight shift in the position of the boron bands, but the assignment is analogous. However, three bands are observed at larger wavenumbers, 1100, 1268 and 1317  $\text{cm}^{-1}$ , which can be attributed to  $\text{BO}_3$  groups with different coordination sphere or symmetrical and asymmetrical stretching vibration.

The spectra of glasses and glass-ceramics with varied BaO concentration show only small differences. In the spectra of the glasses, the band at 860  $\text{cm}^{-1}$  is slightly shifted to higher wavenumbers and becomes less pronounced with decreasing BaO concentration. In contrast to previous reports [50], this behaviour is correlated to a decreasing  $\text{BO}_4$  coordination with decreased BaO concentration. The IR-reflectance spectrum of the glass-ceramics is that of the crystalline phase  $\text{BaAl}_2\text{B}_2\text{O}_7$  (JCPDS 86-2168) according to XRD measurements. However, the spectra of the glass-ceramics show also differences at 856  $\text{cm}^{-1}$ ; with increasing BaO concentration a pronounced band is observed at this wavenumber. While the samples 0.8 to 0.95 BaO show only a shoulder, the samples 1.0 and 1.1 BaO exhibit a small peak indicating a higher  $\text{BO}_4$  concentration. A reason for this behaviour could be a higher amount of glassy phase in these samples as already observed in the XRD measurements.

In addition, raman spectroscopy was carried out with the base glass and the respective glass-ceramics  $\text{BaO} - \text{Al}_2\text{O}_3 - \text{B}_2\text{O}_3$  to receive further information about the structure. The spectra could not be analysed due to very low intensities. The reason for this behaviour is probably that the system  $\text{BaO} - \text{Al}_2\text{O}_3 - \text{B}_2\text{O}_3$  is a poor scatterer. Raman spectra were not further considered.

As already mentioned, the glasses 0.80 BaO -  $\text{Al}_2\text{O}_3$  -  $\text{B}_2\text{O}_3$  and 0.90 BaO -  $\text{Al}_2\text{O}_3$  -  $\text{B}_2\text{O}_3$  already contained some crystals after the preparation. Reasons for these crystals could be an increased tendency to crystallisation with a decreased BaO concentration or an excess of an oxide, which could not be completely dissolved during the melting process. Figure 5.17 presents micrographs of crystals in the glass 0.80 BaO -  $\text{Al}_2\text{O}_3$  -  $\text{B}_2\text{O}_3$ . In the optical micrograph, the crystals have a hexagonal shape and are of different sizes. On the other hand, in the SEM micrograph, the crystals are thin and needle-like, probably consisting of elements with a low average atomic number, as indicated by the darker colour in comparison to the base glass. The crystals were studied by EDX analysis; solely aluminum and oxygen were detected. A problem is that unfortunately the EDX analysis

can not detect boron oxide which hence, might also be a component of the crystal. That is why the characterisation of the crystalline phase was also carried out by XRD. Due to the low amount of crystalline phase with respect to the surrounding glass, the analysis proves to be difficult. The XRD measurement was done by grazing incidence on a thin section with the unknown crystals at the surface. The XRD patterns show the lines of the crystalline phase  $\text{Al}_2\text{O}_3$  (JCPDS 10-0173) and hence, confirm the EDX analysis.

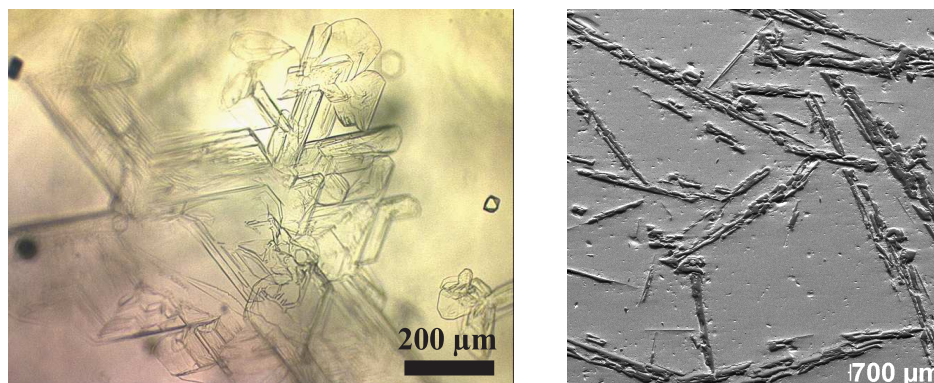


Figure 5.17: Optical microscopy (left picture) and SEM micrographs (right picture) of the crystals in glass 0.80 BaO -  $\text{Al}_2\text{O}_3$  -  $\text{B}_2\text{O}_3$ .

These alumina crystals are formed during melting, because the alumina was not dissolved completely. The formation of the alumina results probably from a lack of boron oxide, which vaporises during melting. There are two possible ways how the boron oxide could vaporise during the melting process. In the first phase of the melting process, the boron oxide is carried away with the steam and above  $900^\circ\text{C}$ , it starts to vaporise as  $\text{B}_2\text{O}_3$  or  $\text{B}(\text{OH})_3$  [54–56].

For this reason, the concentration of  $\text{Al}_2\text{O}_3$  and  $\text{B}_2\text{O}_3$  was changed. On one hand, a glass with higher  $\text{B}_2\text{O}_3$  concentration was prepared and on the other hand, a glass with lower  $\text{Al}_2\text{O}_3$  concentration. The initial composition for both glasses was the glass 0.90 BaO -  $\text{Al}_2\text{O}_3$  -  $\text{B}_2\text{O}_3$  and the results are presented in section 5.3.

### 5.3 Influence of the $\text{B}_2\text{O}_3$ concentration on the crystallisation behaviour

In the previous section the experiments showed that the decreased BaO concentration improves the crystallisation of the glasses, but also results in the formation of  $\text{Al}_2\text{O}_3$  during the melting process. The formation of  $\text{Al}_2\text{O}_3$  crystals could have been promoted through a too low  $\text{B}_2\text{O}_3$  concentration, thus, the increase of the boron oxide and the subsequent



decrease of the alumina concentration is evaluated in this chapter. In Table 5.4, the chemical composition of the glasses with varied  $B_2O_3$  concentration as well as the glass transformation and the softening temperatures are listed. At first the glasses 0.90 BaO - 0.90  $Al_2O_3$  - 1.00  $B_2O_3$ , with decreased alumina concentration, and 0.90 BaO - 1.00  $Al_2O_3$  - 1.10  $B_2O_3$ , with increased boron oxide concentration were prepared. Additionally, the glasses 0.88 BaO - 0.98  $Al_2O_3$  - 1.14  $B_2O_3$  and 0.85 BaO - 0.95  $Al_2O_3$  - 1.20  $B_2O_3$  were prepared, with further increased boron oxide concentration, while the ratio of the other oxides is kept constant starting from the glass 0.90 BaO - 1.00  $Al_2O_3$  - 1.10  $B_2O_3$ .

Table 5.4: Chemical composition, glass transformation and softening temperature of the glasses with varied  $B_2O_3$  concentration.

Sample name	BaO in mol%	$Al_2O_3$ in mol%	$B_2O_3$ in mol%	$T_g$ in °C	$T_D$ in °C
0.90 BaO - 0.90 $Al_2O_3$ - 1.00 $B_2O_3$	32.1	32.1	35.7	566	642
0.90 BaO - 1.00 $Al_2O_3$ - 1.10 $B_2O_3$	30.0	33.3	36.7	585	644
0.88 BaO - 0.98 $Al_2O_3$ - 1.14 $B_2O_3$	29.3	32.7	38.0	583	641
0.85 BaO - 0.95 $Al_2O_3$ - 1.20 $B_2O_3$	28.3	31.7	40.0	574	629

A part of each obtained glass was doped with platinum to investigate the influence of a nucleation agent on these glasses. All glasses with as well as without platinum were vitreous and transparent and showed no alumina crystals, which proves the assumption that a lack of boron oxide caused the formation of alumina crystals in the previous glasses.

In order to compare the glass transformation and the softening temperatures, the base glass 0.90 BaO -  $Al_2O_3$  -  $B_2O_3$  with a  $T_g$  of 600 °C and a  $T_D$  of 660 °C will be included. The decrease of the alumina concentration (glass 0.90 BaO - 0.90  $Al_2O_3$  - 1.00  $B_2O_3$ ) results in a decrease of the glass transition and the softening temperature. By analogy, the increase of the boron oxide concentration (glass 0.90 BaO - 1.00  $Al_2O_3$  - 1.10  $B_2O_3$ ) causes also a decrease of  $T_g$  and  $T_D$ . The glasses with further increasing  $B_2O_3$  concentration show the same behaviour. The densities of the glasses decrease with increasing  $B_2O_3$  concentration, see Table 5.5, while the density of glass 0.90 BaO - 0.90  $Al_2O_3$  - 1.00  $B_2O_3$  remains constant in comparison to the starting glass 0.90 BaO -  $Al_2O_3$  -  $B_2O_3$  with 3.33 g/cm<sup>3</sup>.

The standard heat treatment (see section 4.2) was carried out with all described glasses with and without platinum as nucleation agent. In Table 5.5, the properties of the obtained glass-ceramics are listed. All glass-ceramics show lower densities than the respective glasses, but only the glass-ceramics 0.90 BaO - 1.00  $Al_2O_3$  - 1.10  $B_2O_3$  with and without platinum show such low densities as the (X-ray) density of the pure crystalline

Table 5.5: Densities and thermal expansion coefficients of the glasses and glass-ceramics with varied  $B_2O_3$  concentration.

Sample name	$\rho_{glass}$ in $g/cm^3$	$\rho_{glass-ceramics}$ in $g/cm^3$	$\alpha_{min.neg.}$ in $10^{-7} K^{-1}$	$\alpha_{100-300} \text{ } ^\circ C$ in $10^{-7} K^{-1}$
0.90 BaO - 0.90 $Al_2O_3$ - 1.00 $B_2O_3$	3.33	3.20	-	-
0.90 BaO - 0.90 $Al_2O_3$ - 1.00 $B_2O_3$ +Pt	3.32	3.12	-9 (365 $^\circ C$ )	-4
0.90 BaO - 1.00 $Al_2O_3$ - 1.10 $B_2O_3$	3.25	3.07	-	24
0.90 BaO - 1.00 $Al_2O_3$ - 1.10 $B_2O_3$ +Pt	3.26	3.06	-2 (130 $^\circ C$ )	16
0.88 BaO - 0.98 $Al_2O_3$ - 1.14 $B_2O_3$	3.23	3.20	-	-
0.88 BaO - 0.98 $Al_2O_3$ - 1.14 $B_2O_3$ +Pt	3.23	3.15	-	13
0.85 BaO - 0.95 $Al_2O_3$ - 1.20 $B_2O_3$	3.19	3.17	-	-
0.85 BaO - 0.95 $Al_2O_3$ - 1.20 $B_2O_3$ +Pt	3.19	3.17	-	-

phase  $BaAl_2B_2O_7$  (JCPDS 86-2168) ( $3.065 g/cm^3$ ). The densities of the other glass-ceramics are higher, i.e. the glasses crystallised not completely or other crystalline phases with higher densities were formed. Figure 5.18 shows photographs of all heat treated glasses, except 0.90 BaO - 1.00  $Al_2O_3$  - 1.10  $B_2O_3$  with and without platinum. The thin sections of these samples are discussed later. During the heat treatment of the glass 0.90 BaO - 0.90  $Al_2O_3$  - 1.00  $B_2O_3$ , glassy parts flowed outside of the sample and remained there slightly crystallised. The cross section of the sample showed a glass-ceramics consisting of a thick surface crystallisation layer and only a small part of glassy phase left in the middle of the block (see photograph A). These glass-ceramics were porous and fragile and could not be used for further experiments, e.g. dilatometric measurement. The respective glass-ceramics with platinum (see photograph  $A_{Pt}$ ) were completely crystallised, but two types of crystals were observed - a light grey surface layer of approximately 1 mm thickness and a dark grey volume inside the block. These glass-ceramics were also fragile and the preparation of a thin section was not possible. Sample 0.88 BaO - 0.98  $Al_2O_3$  - 1.14  $B_2O_3$  with and without platinum (see photographs B and  $B_{Pt}$ ) shows also two types of crystallisation. In both cases, a surface layer is formed, but in the middle of the block the heat treated samples seem only partially crystallised. Finally, the samples 0.85 BaO - 0.95  $Al_2O_3$  - 1.20  $B_2O_3$  with and without platinum have only a thin surface crystallisation layer and show numerous cracks in the bulk. Inside, the broken glass looks translucent, which could be an indication of phase separation. In conclusion, the increased  $B_2O_3$  concentration reduces the ability of the glasses to crystallise in the volume.

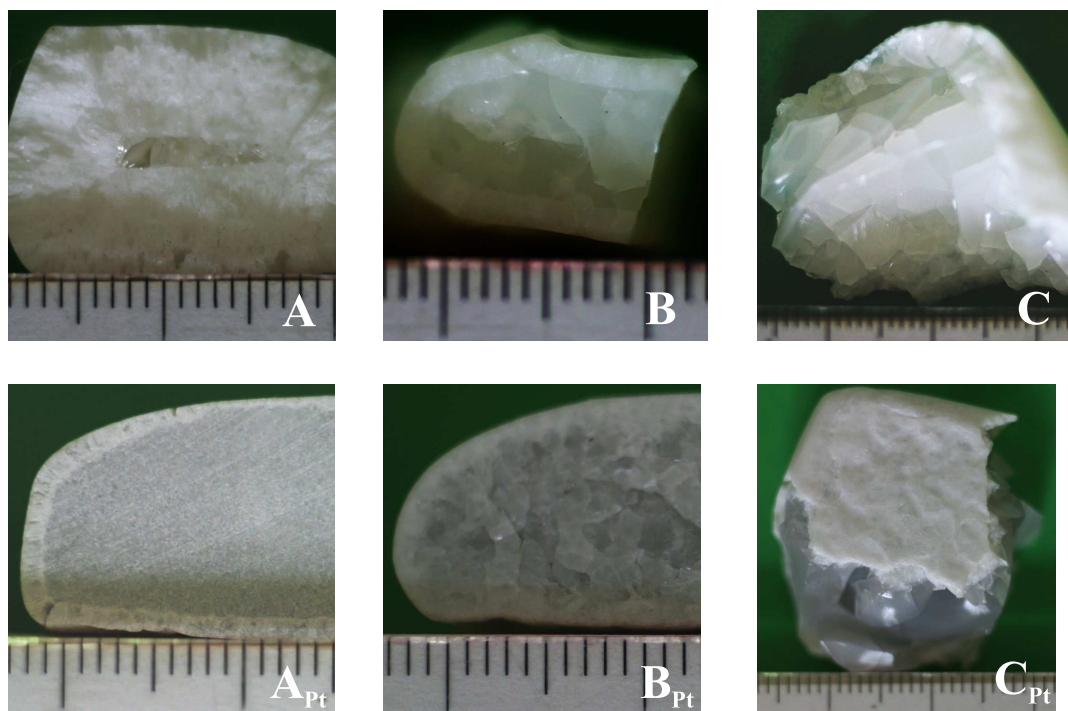


Figure 5.18: Photographs of the glass-ceramics with varied  $B_2O_3$  concentration (A:  $0.90 BaO - 0.90 Al_2O_3 - 1.00 B_2O_3$ , B:  $0.88 BaO - 0.98 Al_2O_3 - 1.14 B_2O_3$ , C:  $0.85 BaO - 0.95 Al_2O_3 - 1.20 B_2O_3$ ); 1 scale graduation = 1 mm.

Figure 5.19 presents the XRD patterns of the glass-ceramics with varied  $B_2O_3$  concentration. The XRD patterns of the different heat treated samples support the conclusion drawn from the photographs. In the samples  $0.85 BaO - 0.95 Al_2O_3 - 1.20 B_2O_3$  with and without platinum, a crystalline phase could not be detected, i.e. the concentration should be very low if there is any crystalline phase. The heat treated samples  $0.88 BaO - 0.98 Al_2O_3 - 1.14 B_2O_3$  with and without platinum show lines of the crystalline phase  $BaAl_2B_2O_7$  (JCPDS 86-2168), but the intensities of the peaks are small. In the glass-ceramics  $0.90 BaO - 1.00 Al_2O_3 - 1.10 B_2O_3$  with and without platinum, only one crystalline phase,  $BaAl_2B_2O_7$  (JCPDS 86-2168), is detected; the intensities of the peaks are larger than in the samples with  $1.14 B_2O_3$ . Furthermore, the sample  $0.90 BaO - 0.90 Al_2O_3 - 1.00 B_2O_3$  shows three different crystalline phases. The lines of the XRD patterns of  $BaAl_2B_2O_7$  (JCPDS 86-2168) and  $Ba_{10}Al_2B_2O_{16}$  (JCPDS 30-0112) are very low, while the lines of the unknown crystalline phase show a higher intensity. In the glass  $0.90 BaO - 0.90 Al_2O_3 - 1.00 B_2O_3$  doped with platinum the  $BaAl_2B_2O_7$  phase (JCPDS 86-2168) crystallises and the lines of the other crystalline phases have low intensities. These results confirm the former conclusions, that a higher boron oxide concentration hampers the volume crystallisation and also the crystallisation of the  $BaAl_2B_2O_7$  phase (JCPDS

86-2168).

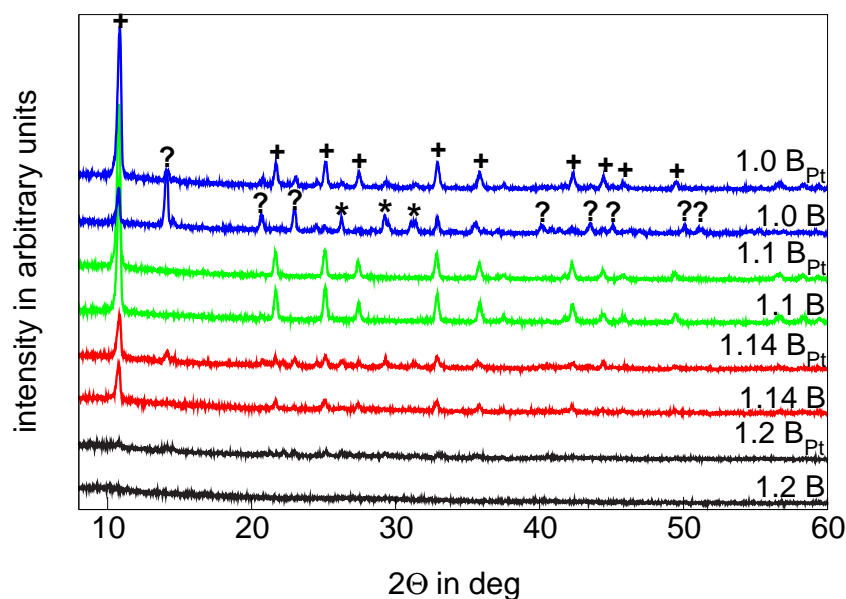


Figure 5.19: Crystalline phase consistence in dependence on the  $B_2O_3$  concentration (crystalline phases: + -  $BaAl_2B_2O_7$  (JCPDS 86-2168), \* -  $Ba_{10}Al_2B_2O_{16}$  (JCPDS 30-0112), ? - unknown).

In Fig. 5.20, the thermal expansion of the glass-ceramics with varied  $B_2O_3$  concentrations are illustrated. Caused by insufficient crystallisation of the glasses, only the four shown samples could be studied by dilatometry. The exact values of the thermal expansion coefficients are listed in Table 5.5. Sample  $0.90 BaO - 0.90 Al_2O_3 - 1.00 B_2O_3$  with platinum has the lowest thermal expansion and has the minimum negative TEC of  $-9 \cdot 10^{-7} K^{-1}$  (up to  $365^\circ C$ ). The other measured glass-ceramics have a zero expansion in the range from 25 to  $100^\circ C$ . Above these temperatures the shape of the curves are similar, but the thermal expansions of the glass-ceramics with platinum are lower than for the glass-ceramics  $0.90 BaO - 1.00 Al_2O_3 - 1.10 B_2O_3$  without platinum. This tendency is supported by the thermal expansion coefficients from 100 to  $300^\circ C$ , which are  $24 \cdot 10^{-7} K^{-1}$  for  $0.90 BaO - 1.00 Al_2O_3 - 1.10 B_2O_3$ , and  $13 \cdot 10^{-7} K^{-1}$  or  $16 \cdot 10^{-7} K^{-1}$  for the glass-ceramics with platinum  $0.90 BaO - 1.00 Al_2O_3 - 1.10 B_2O_3$  and  $0.88 BaO - 0.98 Al_2O_3 - 1.14 B_2O_3$ , respectively.

The lowest thermal expansion coefficients of these glass-ceramics were observed in the samples  $0.90 BaO - 0.90 Al_2O_3 - 1.00 B_2O_3$  and  $0.88 BaO - 0.98 Al_2O_3 - 1.14 B_2O_3$ , both doped with platinum. But these samples could not further be used as the mechanical strength was very low, e.g. the glass-ceramics broke during preparation of thin sections.

The structure of the glasses with varied  $B_2O_3$  concentration was also investigated using IR-reflectance spectroscopy. In Fig. 5.21, the spectra of these glasses are shown. IR-

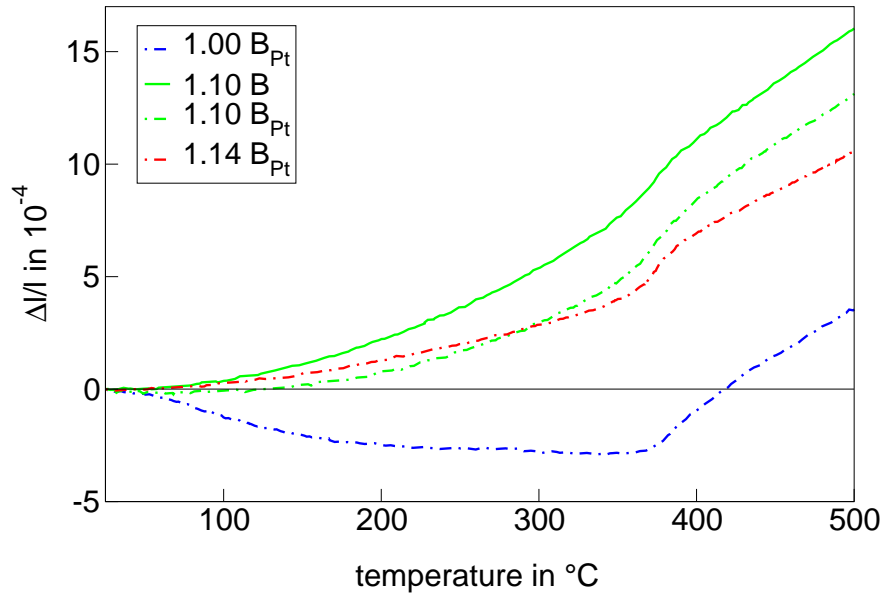


Figure 5.20: Thermal expansion of the glass-ceramics with varied  $B_2O_3$  concentration.

spectra of the respective thermally treated samples were not recorded because of the occurrence of surface crystallised layers, which did not allow the preparation of suitable IR-reflectance samples.

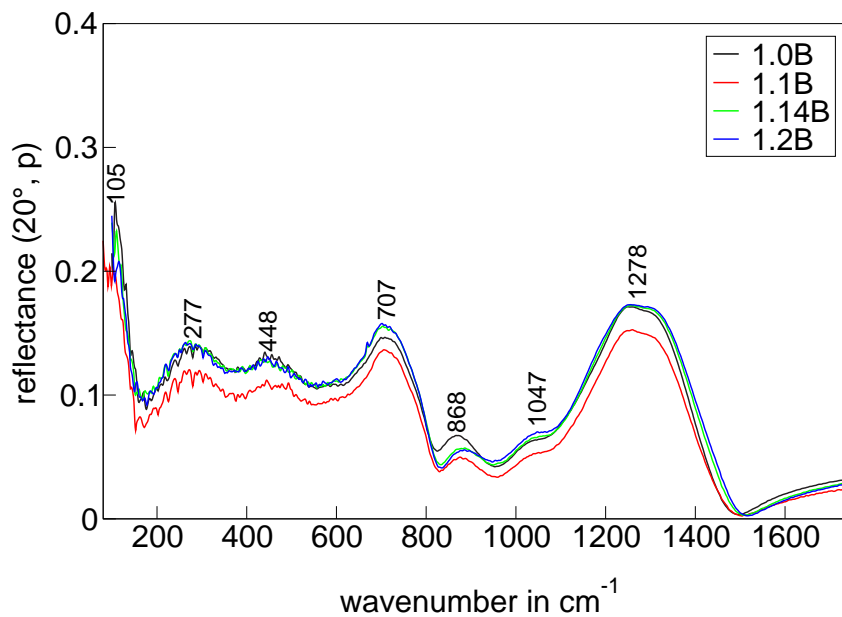


Figure 5.21: IR-reflectance spectra of the glasses with varied  $B_2O_3$  concentration (incidence angle  $20^\circ$ , parallel polarised radiation).

The band assignment of the glasses with varied  $B_2O_3$  concentration is analogous to glasses with varied  $BaO$  concentration (see Table 5.3 at page 37). In agreement with the glasses with varied  $BaO$  concentration, the only band that is shifted while varying the concentration is located at  $868\text{ cm}^{-1}$ . With increasing  $B_2O_3$  concentration, the band is



slightly shifted to higher wavenumbers, which could be caused by a changed coordination sphere of the  $\text{BO}_4$  groups.

Sample 0.90 BaO - 1.00  $\text{Al}_2\text{O}_3$  - 1.10  $\text{B}_2\text{O}_3$  shows overall good results. Alumina crystals are not observed in the glass after the melting process. The glass-ceramics with as well as without platinum are volume crystallised (see Fig. 5.22) and compact with a sufficient mechanical strength. Furthermore, the thermal expansion of the glass-ceramics is low. Hence, for all further variations in the glass composition the glass 0.90 BaO - 1.00  $\text{Al}_2\text{O}_3$  - 1.10  $\text{B}_2\text{O}_3$  was used as base glass.

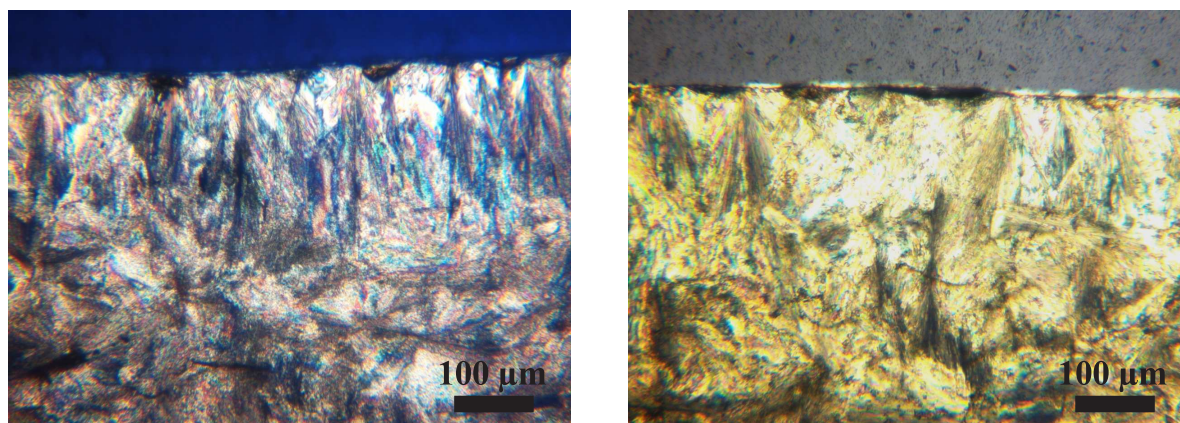


Figure 5.22: Optical micrographs of the glass-ceramics 0.9 BaO - 1.0  $\text{Al}_2\text{O}_3$  - 1.1  $\text{B}_2\text{O}_3$  with and without platinum.

### 5.3.1 Glass 0.9 BaO - 1.0 $\text{Al}_2\text{O}_3$ - 1.1 $\text{B}_2\text{O}_3$ - Influence of the platinum concentration

In this section, the influence of the platinum concentration on the crystallisation of 0.9 BaO - 1.0  $\text{Al}_2\text{O}_3$  - 1.1  $\text{B}_2\text{O}_3$  glass is discussed. Another important aspect is the influence on the thermal expansion coefficient and the morphology of the glass-ceramics.

After the glass 0.9 BaO - 1.0  $\text{Al}_2\text{O}_3$  - 1.1  $\text{B}_2\text{O}_3$  was prepared, platinum was added in different concentrations. Three glasses doped with 0.005, 0.01 and 0.02 wt% platinum were examined. All glasses were vitreous and transparent after the addition of platinum. In analogy to the base glass 0.9 BaO - 1.0  $\text{Al}_2\text{O}_3$  - 1.1  $\text{B}_2\text{O}_3$ , the doped glasses were subjected to the standard thermal treatment (see section 4.2) and the received glass-ceramics were analysed.

The glasses with different platinum concentration exhibit equal densities of  $3.26 \text{ g/cm}^3$ . As expected, the obtained glass-ceramics show lower densities with  $3.08 \text{ g/cm}^3$  indicating the presence of the crystalline phase  $\text{BaAl}_2\text{B}_2\text{O}_7$  (JCPDS 86-2168). However, the similar

densities of these glass-ceramics indicate also that the formed crystalline phase should be the same.

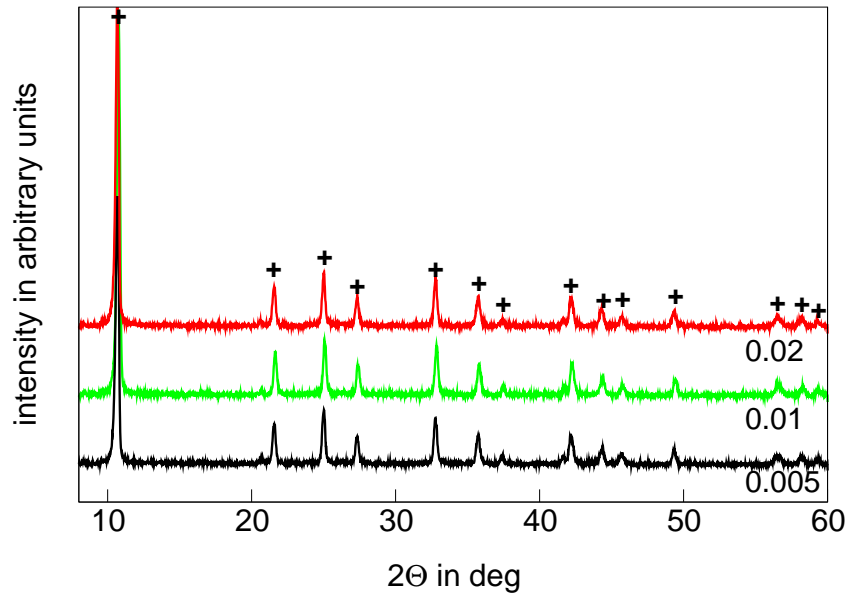


Figure 5.23: XRD patterns of the glass-ceramics  $0.90 \text{ BaO} - 1.00 \text{ Al}_2\text{O}_3 - 1.10 \text{ B}_2\text{O}_3$  with various platinum concentration (crystalline phase:  $+ - \text{BaAl}_2\text{B}_2\text{O}_7$  (JCPDS 86-2168);  $0.005 = 0.005 \text{ wt}\% \text{ Pt}$ ).

In Fig. 5.23, the XRD patterns of the glass-ceramics with various platinum concentrations are presented to confirm the assumptions made above. The XRD patterns show well defined lines of the crystalline phase  $\text{BaAl}_2\text{B}_2\text{O}_7$  (JCPDS 86-2168) in the investigated glass-ceramics proving that the variation of the platinum concentration did not influence the type of crystal formed. Furthermore, the intensities of the lines are similar in the compared samples, i.e. the XRD measurements show no differences between the glass-ceramics. As a result of this, samples for optical microscopy were prepared to get informations about whether the type of crystallisation is surface or volume.

Figure 5.24 shows the micrographs obtained by optical microscopy of the glass-ceramics with varied platinum concentrations. The samples are completely crystallised showing volume crystallisation and a surface crystallisation layer with a thickness between 50 and 150  $\mu\text{m}$ . The crystals of the surface layer are grown perpendicular to the surface, while the crystals in the volume are randomly oriented. The varied platinum concentration does not lead to notable differences in the morphology of the glass-ceramics.

The glasses and glass-ceramics with different platinum concentrations present similar densities, crystalline phase consistence as well as microstructures. Therefore, it is expected that the dilatometric measurements should show no differences between the samples. The thermal expansion coefficient of the glasses is around  $70 \cdot 10^{-7} \text{ K}^{-1}$  from

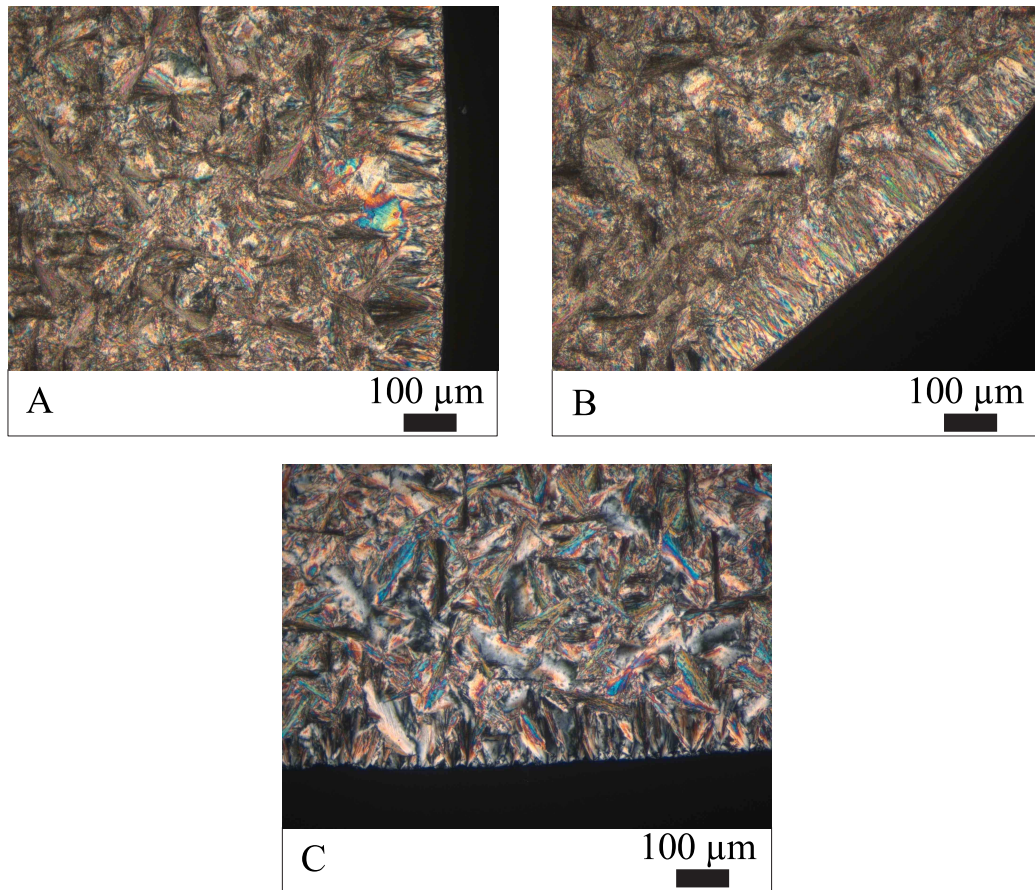


Figure 5.24: Optical micrographs of the glass-ceramics  $0.90 \text{ BaO} - 1.00 \text{ Al}_2\text{O}_3 - 1.10 \text{ B}_2\text{O}_3$  with varied platinum concentration; A: 0.005 wt% Pt, B: 0.01 wt% Pt, C: 0.02 wt% Pt.

100 to 300 °C and shows only slight differences between the samples. In Fig. 5.25, the thermal expansions of the glass-ceramics are plotted as function of the temperature. As expected, the glass-ceramics show similar thermal expansions within small variations. The expansion is around zero in the temperature range from 25 to 85 °C and increases above 85 °C with increasing temperature. At higher temperatures, the thermal expansions of the glass-ceramics are slightly decreased with increasing platinum concentration.

Finally, the obtained results show that the variation of platinum as nucleation agent did not alter the crystalline phase consistence or the microstructure of the glass-ceramics. Furthermore, the influence on the thermal expansion coefficient is marginally. The addition of platinum will be 0.01 wt% in further experiments, in order to compare the results with former experiments without changing this parameter.



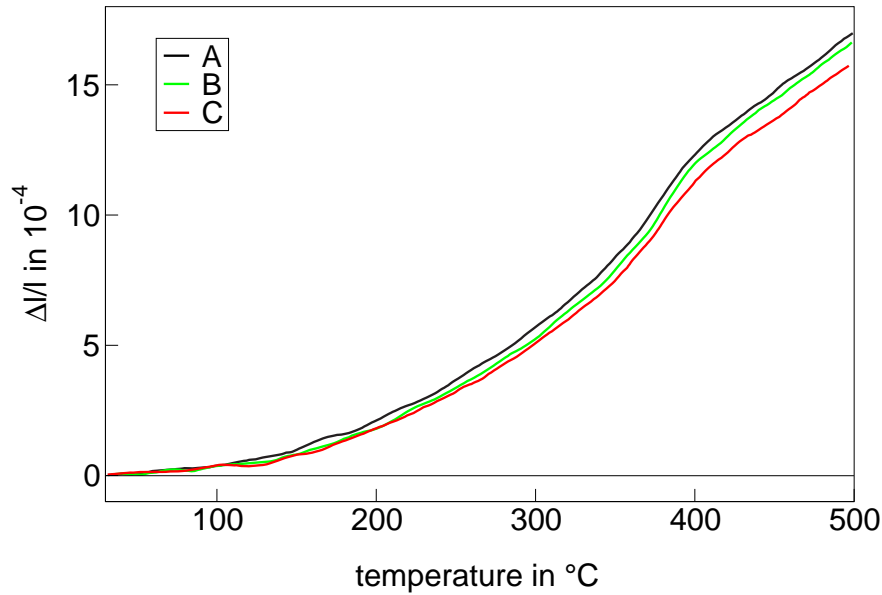


Figure 5.25: Dilatometric measurements of glass-ceramics  $0.9 \text{ BaO} - 1.0 \text{ Al}_2\text{O}_3 - 1.1 \text{ B}_2\text{O}_3$  with varied platinum concentration; A: 0.005 wt% Pt, B: 0.01 wt% Pt, C: 0.02 wt% Pt.

## 5.4 Addition of $\text{TiO}_2$

It is expected that the addition of  $\text{TiO}_2$  should improve the hydrolytic durability of the glasses and glass-ceramics as shown in earlier research [57,58]. In principle, two strategies are possible to achieve an increase in the hydrolytic durability of the glass-ceramics in the system  $\text{BaO} - \text{Al}_2\text{O}_3 - \text{B}_2\text{O}_3$ . First, the durability of the glass can be improved and subsequently the ratio of glassy to crystalline phase will be adjusted to achieve a higher hydrolytic durability of the glass-ceramics. The second possibility would be the crystallisation of a more durable crystalline phase in the glass-ceramics. For instance, the crystallisation of  $\text{Al}_2\text{O}_3 \cdot \text{TiO}_2$  should positively influence the hydrolytic durability, but not interfere with the thermal expansion coefficient of the glass-ceramics, because the crystalline phase  $\text{Al}_2\text{O}_3 \cdot \text{TiO}_2$  exhibits also a negative thermal expansion coefficient of  $-20 \cdot 10^{-7} \text{ K}^{-1}$  in the temperature range from 50 to 400 °C [59,60].

Thus, titanium oxide was added to the base glass  $0.9 \text{ BaO} - 1.0 \text{ Al}_2\text{O}_3 - 1.1 \text{ B}_2\text{O}_3$  using two strategies. In the glasses type I, the  $\text{TiO}_2$  concentration was increased, while the concentrations of  $\text{BaO}$  and  $\text{B}_2\text{O}_3$  were decreased, realising an excess of  $\text{Al}_2\text{O}_3$ , which might give raise to the crystallisation of  $\text{Al}_2\text{O}_3 \cdot \text{TiO}_2$ . In the glasses type II,  $\text{TiO}_2$  was added to the base glass, while the ratio of the molar concentrations of the other oxides was kept constant. The chemical compositions, glass transformation temperatures,  $T_g$ , and softening temperatures,  $T_D$ , of the glasses type I and II are summarised in Table 5.6.

During preparation of the glasses first differences between the two types were observed.

Table 5.6: Chemical composition, glass transformation and softening temperatures of the glasses with TiO<sub>2</sub> as additive (I- addition TiO<sub>2</sub>, decrease BaO, B<sub>2</sub>O<sub>3</sub>; II- addition TiO<sub>2</sub>, decrease BaO, Al<sub>2</sub>O<sub>3</sub>, B<sub>2</sub>O<sub>3</sub>).

Sample name	BaO in mol%	Al <sub>2</sub> O <sub>3</sub> in mol%	B <sub>2</sub> O <sub>3</sub> in mol%	TiO <sub>2</sub> in mol%	T <sub>g</sub> in °C	T <sub>D</sub> in °C
base glass	30.0	33.3	36.7	-	585	644
I- 2.5 TiO <sub>2</sub>	28.8	33.3	35.5	2.5	588	641
I- 5.0 TiO <sub>2</sub>	27.5	33.3	34.2	5.0	590	648
I- 7.5 TiO <sub>2</sub>	26.3	33.3	33.0	7.5	595	650
II- 2.5 TiO <sub>2</sub>	29.3	32.5	35.8	2.4	582	637
II- 5.0 TiO <sub>2</sub>	28.6	31.7	35.0	4.8	582	627
II- 7.5 TiO <sub>2</sub>	27.9	31.0	34.1	7.0	584	628
II- 10.0 TiO <sub>2</sub>	27.3	30.3	33.4	9.1	586	635
II- 12.5 TiO <sub>2</sub>	26.7	29.6	32.6	11.1	587	637

All prepared glasses, except I- 7.5 TiO<sub>2</sub> and II- 12.5 TiO<sub>2</sub>, were vitreous and transparent but included some crystals. The amount of crystals was low in comparison to the surrounding glassy phase, therefore an analysis by XRD or EDX was not possible. By contrast, the glasses I- 7.5 TiO<sub>2</sub> and II- 12.5 TiO<sub>2</sub> started to crystallise from the centre of the glass block during cooling. XRD measurements of the crystallised region could not detect the type of crystalline phase, as the ratio glass/crystals was still too high. Consequently, the glasses type I could be melted up to only 5 mol% TiO<sub>2</sub> and the glasses type II up to 10.0 mol% TiO<sub>2</sub> without strong crystallisation.

In analogy to former investigations, the properties of the glasses were analysed. The glasses type I show higher T<sub>g</sub> and T<sub>D</sub> with increasing TiO<sub>2</sub> concentration due to the increased Al<sub>2</sub>O<sub>3</sub> concentration in these glasses. For the glasses type II, the glass transition temperature is nearly the same (between 582 and 587 °C) as for the base glass 0.9 BaO - 1.0 Al<sub>2</sub>O<sub>3</sub> - 1.1 B<sub>2</sub>O<sub>3</sub>. A dependence between T<sub>D</sub> and the composition of glasses type II is not unambiguous. The addition of TiO<sub>2</sub>, up to 5 mol%, results in a decrease of the softening temperature. Further increase of the TiO<sub>2</sub> concentration leads to an increase in T<sub>D</sub>, so that T<sub>D</sub> of sample II- 12.5 TiO<sub>2</sub> is the same as of sample II- 2.5 TiO<sub>2</sub> (637 °C). One part of each glass was doped with 0.01 wt% platinum (see section 4.1). The densities of the glasses slightly increase with increasing TiO<sub>2</sub> concentration as well as with the addition of platinum and are in the range of 3.25 to 3.36 g/cm<sup>3</sup>. Furthermore, the thermal expansion coefficient from 100 to 300 °C of all studied glasses with TiO<sub>2</sub> as additive is shown in

Fig. 5.29 at page 54. The TECs of the glasses with  $\text{TiO}_2$  addition have approximately the same values and are in the range from  $68$  to  $74 \cdot 10^{-7} \text{ K}^{-1}$  from  $100$  to  $300^\circ \text{ C}$ .

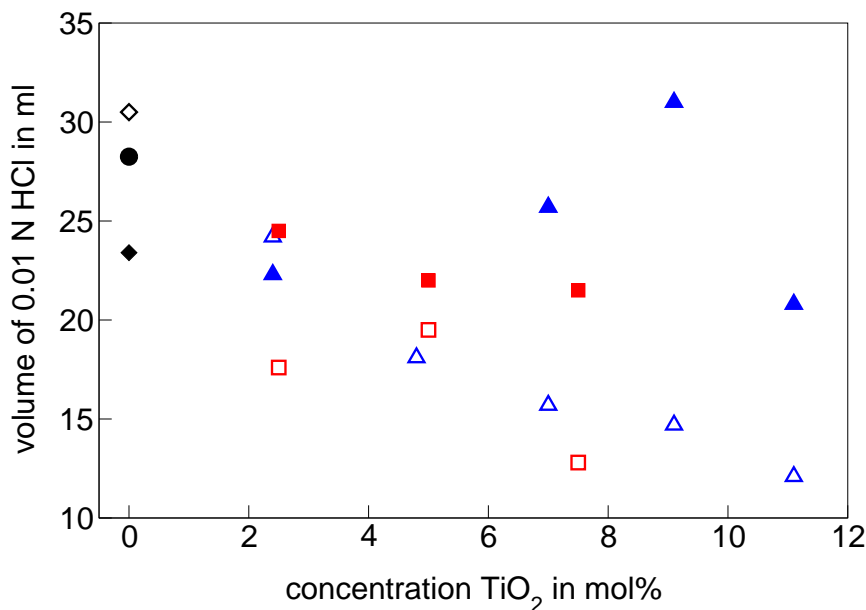


Figure 5.26: Hydrolytic durability of the glasses and glass-ceramics with  $\text{TiO}_2$  addition; ( $\diamond$ ): base glass, ( $\bullet$ ): base glass-ceramics, ( $\blacklozenge$ ): base glass-ceramics with Pt, ( $\square$ ): glasses type I, ( $\blacksquare$ ): glass-ceramics type I with Pt, ( $\triangle$ ): glasses type II, ( $\blacktriangle$ ): glass-ceramics type II with Pt.

Another property of interest is the hydrolytic durability of the glasses, the results are shown in Fig. 5.26. The volume of hydrochloric acid indicates the hydrolytic durability of the sample and is used to classify it (see section 4.4.4). A volume of 30.5 ml 0.01 N HCl is needed for the determination of the hydrolytic durability of the base glass  $0.9 \text{ BaO} - 1.0 \text{ Al}_2\text{O}_3 - 1.1 \text{ B}_2\text{O}_3$ . While the glass is boiled in water, it starts to dissolve and a subsequent precipitation is formed. This is all attributed to a low hydrolytic durability. On the other hand, it has to be clarified that the glass is stable against humidity in air. With increasing  $\text{TiO}_2$  concentration, an improvement of the hydrolytic durability of the glasses could be obtained, although differences were expected between the two types of glasses caused by the different ratios of  $\text{BaO}$ ,  $\text{Al}_2\text{O}_3$  and  $\text{B}_2\text{O}_3$ . The hydrolytic durability of glass type I with the addition of only 2.5 mol% of  $\text{TiO}_2$  is strongly improved to a volume of 17.5 ml HCl. Further addition of  $\text{TiO}_2$  leads to a small increase in the volume of HCl, sample I-5.0  $\text{TiO}_2$ , but afterwards it decreases further, sample I-7.5  $\text{TiO}_2$ . The volume of 0.01 N HCl needed for the glasses type II decreases linearly within the  $\text{TiO}_2$  concentration in the investigated range. For the sample II-12.5  $\text{TiO}_2$ , the lowest volume of 0.01 N HCl is achieved with 12 ml. As expected, the glasses type I, except I-5.0  $\text{TiO}_2$ , show an improved hydrolytic durability compared to the glasses type II. According to the

lower concentration of BaO and the higher concentration of Al<sub>2</sub>O<sub>3</sub> in the glasses type I, this effect is observed.

After the characterisation of the glasses, the standard thermal treatment (see section 4.2) was carried out in order to obtain glass-ceramics. The crystallisation of the glasses proved to be difficult, only glass I-2.5TiO<sub>2</sub> could be transformed to the glass-ceramics through volume crystallisation. All other glasses showed surface crystallisation layers and were translucent in the volume. Further investigations with other crystallisation programs, e.g. 620 °C for 24 h and 780 °C for 8 h, caused only surface crystallisation as well. The addition of TiO<sub>2</sub> to the glass 0.9 BaO - 1.0 Al<sub>2</sub>O<sub>3</sub> - 1.1 B<sub>2</sub>O<sub>3</sub> diminishes the volume crystallisation instead of promoting it as was expected from a nucleation agent [33].

In a second step, the standard thermal treatment (see section 4.2) was carried out with all glasses doped with platinum as heterogeneous nucleation agent. All glass-ceramics of type I are completely volume crystallised, but some small cracks are visible in the bulk. On the other hand, the appearance of the glass-ceramics type II varies with the increase of the TiO<sub>2</sub> concentration. The glass-ceramics II-2.5 TiO<sub>2</sub>+Pt are completely crystallised in the volume, while the sample II-5.0 TiO<sub>2</sub>+Pt shows a thick surface crystallisation layer and the centre of the block is translucent. With further increasing the TiO<sub>2</sub> concentration, the obtained glass-ceramics consist of some glassy parts beside the crystals. The samples II-10.0 TiO<sub>2</sub>+Pt and II-12.5 TiO<sub>2</sub>+Pt also formed thin surface crystallisation layers. These results are confirmed by the density measurements of the thermally treated samples. Beside the base glass-ceramics with platinum (3.06 g/cm<sup>3</sup>), only the glass-ceramics I-2.5 TiO<sub>2</sub>+Pt (3.11 g/cm<sup>3</sup>) and II-2.5 TiO<sub>2</sub>+Pt (3.09 g/cm<sup>3</sup>), show low densities similar to the (X-ray) density (3.065 g/cm<sup>3</sup>) of the crystalline phase BaAl<sub>2</sub>B<sub>2</sub>O<sub>7</sub> (JCPDS 86-2168). The other heat treated samples also have lower densities than the respective glasses, but do not reach the density of the crystalline phase BaAl<sub>2</sub>B<sub>2</sub>O<sub>7</sub> (JCPDS 86-2168). Another point of interest is the linear increase of the densities of the glass-ceramics type I with increasing TiO<sub>2</sub> concentration (I-5.0 TiO<sub>2</sub>: 3.13 g/cm<sup>3</sup>, I-7.5 TiO<sub>2</sub>: 3.17 g/cm<sup>3</sup>). The densities of the glass-ceramics type II increase also with increasing TiO<sub>2</sub> concentration, except sample II-5.0 TiO<sub>2</sub>+Pt. By contrast, the density of sample II-5.0 TiO<sub>2</sub>+Pt (glass: 3.28 g/cm<sup>3</sup>, glass-ceramics: 3.23 g/cm<sup>3</sup>) decreases in a smaller extend compared to the others of type II according to an insufficient crystallisation as the appearance already showed. The higher densities of the other samples might result from the formation of a different crystalline phase or the insufficient crystallisation of the samples, i.e. a high amount of glassy phase.

By means of XRD measurements the crystalline phase consistence of the heat treated

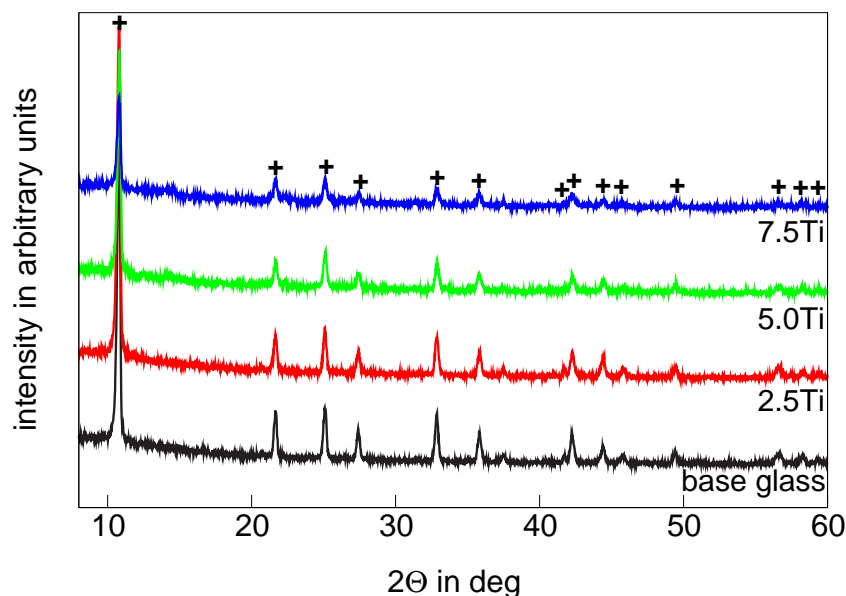


Figure 5.27: XRD patterns of the glass-ceramics with  $\text{TiO}_2$  and Pt addition, type I (crystalline phase:  $\text{BaAl}_2\text{B}_2\text{O}_7$  (JCPDS 86-2168); base glass =  $0.9 \text{BaO} - 1.0 \text{Al}_2\text{O}_3 - 1.1 \text{B}_2\text{O}_3$ ,  $\text{Ti} = \text{TiO}_2$ ).

samples were analysed. In Fig. 5.27, the XRD patterns of the glass-ceramics type I with platinum are presented. All studied glass-ceramics show lines corresponding to the crystalline phase  $\text{BaAl}_2\text{B}_2\text{O}_7$  (JCPDS 86-2168), while another crystalline phase could not be detected. As it can be seen in Fig. 5.27, the intensities of the XRD patterns differ between the samples of type I. The glass-ceramics I-2.5  $\text{TiO}_2 + \text{Pt}$  show the same intensities of the lines attributed to  $\text{BaAl}_2\text{B}_2\text{O}_7$  (JCPDS 86-2168) as the base glass-ceramics  $0.9 \text{BaO} - 1.0 \text{Al}_2\text{O}_3 - 1.1 \text{B}_2\text{O}_3 + \text{Pt}$ . Further addition of  $\text{TiO}_2$  causes a decrease of the intensity, which is associated to the amount of crystalline phase. These measurements confirm the results of the density showing a decrease of crystallinity of the glass-ceramics with increasing  $\text{TiO}_2$  concentration.

Figure 5.28 presents the XRD patterns recorded from the heat treated samples type II with platinum. Only sample II-2.5  $\text{TiO}_2 + \text{Pt}$  shows XRD patterns of the crystalline phase  $\text{BaAl}_2\text{B}_2\text{O}_7$  (JCPDS 86-2168) with high intensity, while the other samples are insufficiently crystallised. The heat treated samples II-7.5  $\text{TiO}_2 + \text{Pt}$ , II-10.0  $\text{TiO}_2 + \text{Pt}$  and II-12.5  $\text{TiO}_2 + \text{Pt}$  show lines of very low intensity attributable to  $\text{BaAl}_2\text{B}_2\text{O}_7$  (JCPDS 86-2168) and an unknown crystalline phase. Furthermore, the low intensities of the XRD patterns are caused by the high amount of glassy phase.

In good agreement to the density measurements, these results confirm a diminution of the glass crystallisation through the addition of  $\text{TiO}_2$ . Even platinum as nucleation agent could not stop this tendency.

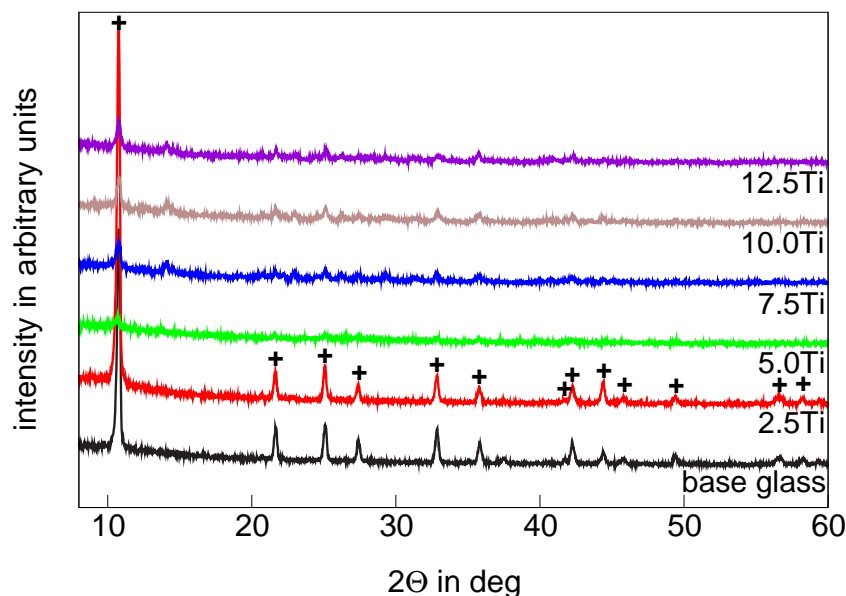


Figure 5.28: XRD patterns of the glass-ceramics with  $\text{TiO}_2$  and Pt addition, type II (crystalline phase:  $\pm\text{-BaAl}_2\text{B}_2\text{O}_7$  (JCPDS 86-2168); base glass =  $0.9\text{BaO} - 1.0\text{Al}_2\text{O}_3 - 1.1\text{B}_2\text{O}_3$ ,  $\text{Ti} = \text{TiO}_2$ ).

Besides these results, the properties of the heat treated samples were analysed. Figure 5.29 presents the thermal expansion coefficient from 100 to 300 °C of the glass-ceramics with  $\text{TiO}_2$  and platinum addition. The base glass-ceramics  $0.9\text{BaO} - 1.0\text{Al}_2\text{O}_3 - 1.1\text{B}_2\text{O}_3$  without platinum show a TEC of  $24 \cdot 10^{-7} \text{K}^{-1}$  from 100 to 300 °C, while the glass-ceramics with platinum have a lower TEC of  $16 \cdot 10^{-7} \text{K}^{-1}$ . The addition of  $\text{TiO}_2$  results in a decreasing thermal expansion coefficient. A thermal expansion coefficient of  $5 \cdot 10^{-7} \text{K}^{-1}$  and  $7 \cdot 10^{-7} \text{K}^{-1}$  was measured for the glass-ceramics I-2.5  $\text{TiO}_2 + \text{Pt}$ , and II-2.5  $\text{TiO}_2 + \text{Pt}$ , respectively. Further increase of the  $\text{TiO}_2$  concentration causes an increase of the thermal expansion coefficient of the glass-ceramics type I as well as II. While the TEC of sample I-5.0  $\text{TiO}_2 + \text{Pt}$  is slightly below the value of the base glass-ceramics with platinum, it is shifted to larger values for samples with increased  $\text{TiO}_2$  concentration.

In Fig. 6.11, the thermal expansion of the glass-ceramics is plotted as a function of the temperature. These curves are recorded for the range of 25 to 500 °C and are used to define the temperature range of zero expansion of the investigated glass-ceramics. While the base glass-ceramics with platinum show a zero expansion up to 120 °C, this region could be extended up to 200 °C for the glass-ceramics with 2.5 mol%  $\text{TiO}_2$  (type I and II). In analogy to Fig. 5.29, the curves of the thermal expansion are continuously shifted to higher values with increasing  $\text{TiO}_2$ . Another interesting aspect is the decrease in the thermal expansion due to the addition of platinum as heterogeneous nucleation agent, which could be observed for the base glass-ceramics  $0.9\text{BaO} - 1.0\text{Al}_2\text{O}_3 - 1.1\text{B}_2\text{O}_3$  as well

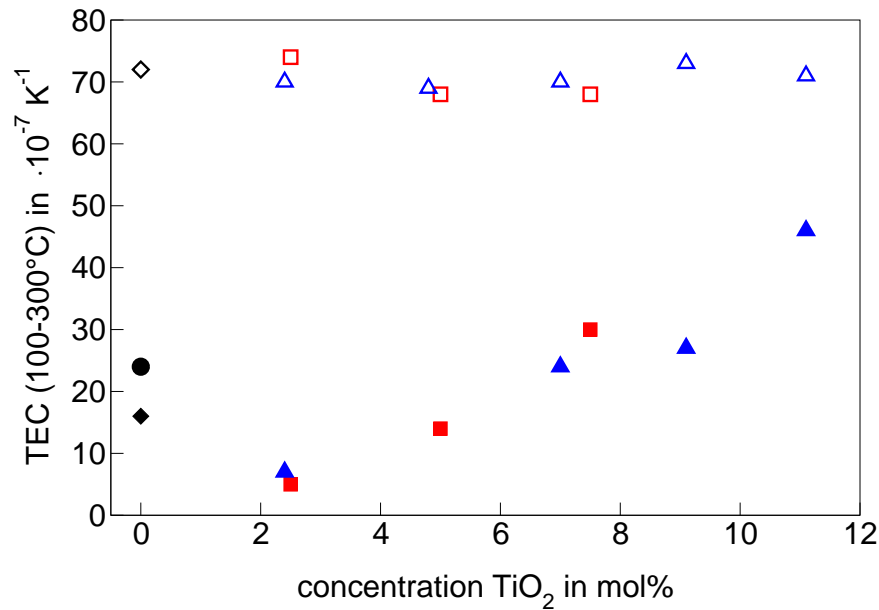


Figure 5.29: Thermal expansion coefficient from 100 to 300 °C of the glasses and glass-ceramics with TiO<sub>2</sub> addition; (◇): base glass, (●): base glass-ceramics, (◆): base glass-ceramics with Pt, (□): glasses type I, (■): glass-ceramics type I with Pt, (△): glasses type II, (▲): glass-ceramics type II with Pt.

as for the glass-ceramics I- 2.5 TiO<sub>2</sub>.

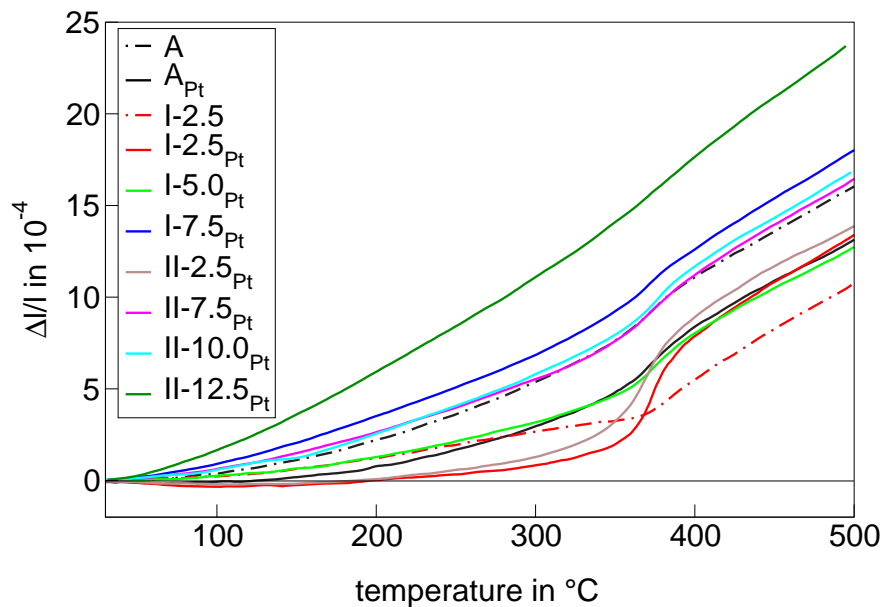


Figure 5.30: Thermal expansion of the glass-ceramics with TiO<sub>2</sub> and Pt addition and the base glass-ceramics 0.9 BaO - 1.0 Al<sub>2</sub>O<sub>3</sub> - 1.1 B<sub>2</sub>O<sub>3</sub> without (A) and with (A<sub>Pt</sub>) platinum.

The increase of the thermal expansion coefficient is caused by an insufficient crystallisation of the glass-ceramics, see sample I- 7.5 TiO<sub>2</sub>+Pt, II - 7.5 TiO<sub>2</sub>+Pt, II - 10.0 TiO<sub>2</sub>+Pt and II-12.5 TiO<sub>2</sub>+Pt, whereas the crystallisation of the crystalline phase BaAl<sub>2</sub>B<sub>2</sub>O<sub>7</sub>

(JCPDS 86-2168) results in a lower TEC, see I-2.5 TiO<sub>2</sub>+Pt, I-5.0 TiO<sub>2</sub>+Pt and II-2.5 TiO<sub>2</sub>+Pt.

The hydrolytic durability of the glass-ceramics with TiO<sub>2</sub> and platinum addition is displayed in Fig. 5.26 at page 50. The base glass-ceramics with (23 ml 0.01 N HCl) and without platinum (28 ml 0.01 N HCl) show a higher hydrolytic durability than the respective glass (30 ml 0.01 N HCl), i.e. the crystallisation of the glass results in an increase of the durability. Furthermore, the result shows that the crystalline phase BaAl<sub>2</sub>B<sub>2</sub>O<sub>7</sub> (JCPDS 86-2168) is more durable than the glassy phase. At first, the glass-ceramics type I will further be discussed. The addition of TiO<sub>2</sub> causes a slight decrease of the hydrolytic durability, see sample I-2.5 TiO<sub>2</sub>+Pt with 24.5 ml 0.01 N HCl. Further addition of TiO<sub>2</sub> results in a, within the limits of error, linear decrease of hydrochloric acid added, see sample I-5.0 TiO<sub>2</sub>+Pt and I-7.5 TiO<sub>2</sub>+Pt, where 22 and 21.5 ml, respectively, were determined. A slight improvement in the hydrolytic durability of the glass-ceramics type I is detected with regard to the base glass-ceramics, although the durability decreases compared to the respective glasses. The glass-ceramics of type II have a different hydrolytic behaviour with respect to the TiO<sub>2</sub> concentration. Glass-ceramics II-2.5 TiO<sub>2</sub>+Pt show an even higher hydrolytic durability than the respective glass. Further addition of TiO<sub>2</sub> decreases the hydrolytic durability for the heat treated sample II-10.0 TiO<sub>2</sub>+Pt (31 ml 0.01 N HCl). The sample II-12.5 TiO<sub>2</sub>+Pt with an addition of 12.5 mol% TiO<sub>2</sub> shows again a higher hydrolytic durability, i.e. the volume of 0.01 N HCl decreases (to 21 ml).

Due to the insufficient crystallisation of the glass-ceramics with higher TiO<sub>2</sub> concentration, only the micrographs of the glass-ceramics I-2.5 TiO<sub>2</sub>+Pt and II-2.5 TiO<sub>2</sub>+Pt are presented in Fig. 5.31. In order to enable the direct comparison, the micrograph of the base glass-ceramics with platinum is also shown in Fig. 5.31. The base glass-ceramics were randomly crystallised in the volume and exhibited a surface crystallisation layer of approximately 200 μm thickness. Glass-ceramics I-2.5 TiO<sub>2</sub>+Pt also formed a surface crystallisation layer of 200 μm, but in the volume, large spheroidal crystals were observed beside randomly oriented ones. By contrast, the glass-ceramics II-2.5 TiO<sub>2</sub>+Pt consisted of long needle-like crystals which were randomly oriented. In agreement, both glass-ceramics with 2.5 mol% TiO<sub>2</sub> addition exhibit another type of crystals with the shape of thick needles. These crystals were already observed in section 5.2 and were identified as Al<sub>2</sub>O<sub>3</sub> crystals.

The glasses and glass-ceramics with the addition of TiO<sub>2</sub> were studied by IR spectroscopy to obtain structure information and informations on the incorporation of titanium in the network. Figure 5.32 presents IR-reflectance spectra of the glasses and



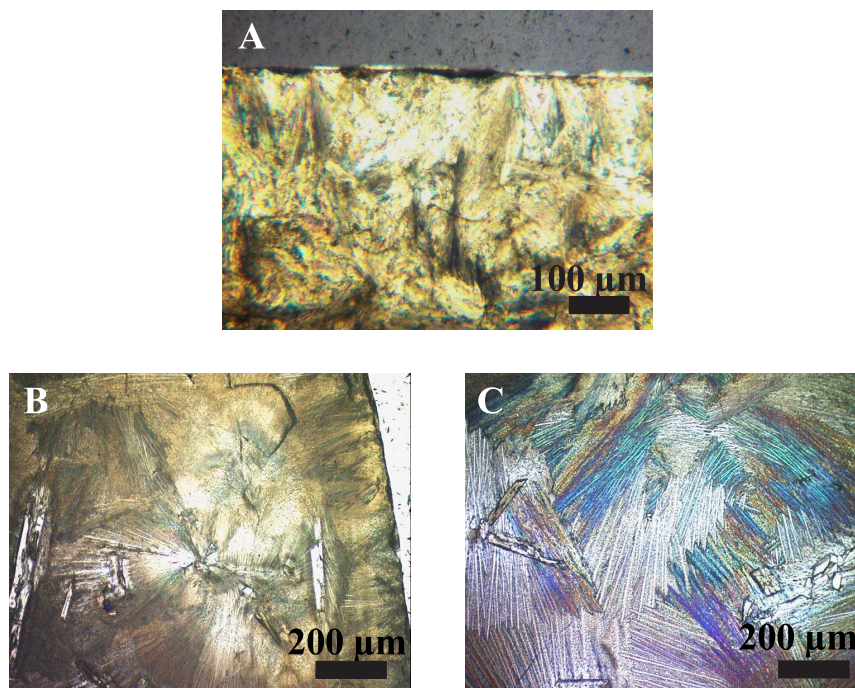


Figure 5.31: Optical micrographs of the glass-ceramics  $0.9\text{BaO} - 1.0\text{Al}_2\text{O}_3 - 1.1\text{B}_2\text{O}_3 + \text{Pt}$  (A), I-  $2.5\text{TiO}_2 + \text{Pt}$  (B) and II-  $2.5\text{TiO}_2 + \text{Pt}$  (C).

glass-ceramics subdivided into type I and II glasses and glass-ceramics. The base glass  $0.90\text{BaO} - 1.00\text{Al}_2\text{O}_3 - 1.10\text{B}_2\text{O}_3$  is also shown to allow a comparison with the glasses derived hereof.

The plotted bands can be associated to the known structural groups in analogy to the previous band assignment (see Table 5.3 at page 37). The spectra of the glasses type I and II are similar and no significant changes are detectable with increasing  $\text{TiO}_2$  concentration. The glass-ceramics type I exhibit no difference in the spectra in comparison to the base glass-ceramics, however, no band is observed around  $880\text{ cm}^{-1}$  in comparison to the respective glasses. This behaviour is related to the decreased  $\text{BaO}$  concentration, which results in the disappearance of this  $\text{BO}_4$  group band. Furthermore, new bands are not observed through the addition of  $\text{TiO}_2$ , which could result from the low  $\text{TiO}_2$  concentration or the overlapping with other bands. As it can be seen in Fig. 5.32, the glass-ceramics type II, beside sample II-  $12.5\text{TiO}_2$ , have spectra similar to the glass-ceramics type I. Sample II-  $12.5\text{TiO}_2$  exhibits a different IR-reflectance spectrum, which could be caused by insufficient crystallisation or the formation of another crystalline phase. XRD patterns of this sample show a high amount of glassy phase and low intensities of an unknown crystalline phase and  $\text{BaAl}_2\text{B}_2\text{O}_7$  (JCPDS 86-2168), which proves the previous assumptions.

In conclusion, the addition of  $\text{TiO}_2$  increases the hydrolytic durability of the glasses.

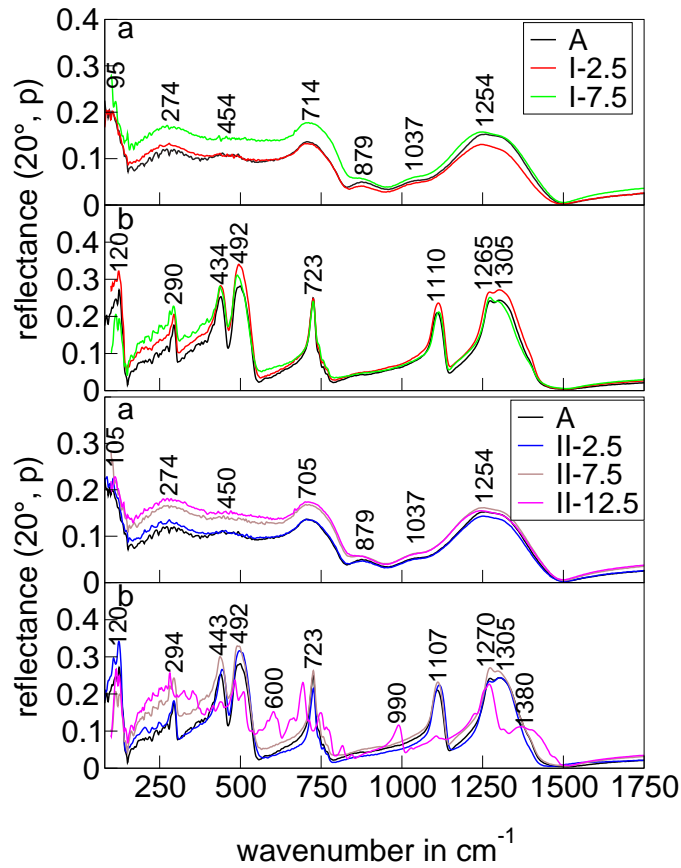


Figure 5.32: IR-reflectance spectra of the glasses (a) and glass-ceramics (b) with the addition of TiO<sub>2</sub> (incidence angle 20°, parallel polarised radiation; A = 0.9 BaO - 1.0 Al<sub>2</sub>O<sub>3</sub> - 1.1 B<sub>2</sub>O<sub>3</sub>, Ti = TiO<sub>2</sub>, I = type I, II = type II).

The tendency to crystallisation of the glasses decreases with increasing TiO<sub>2</sub> concentration. Even the addition of platinum as heterogeneous nucleation agent only results in a slight improvement of the crystallisation of BaAl<sub>2</sub>B<sub>2</sub>O<sub>7</sub> (JCPDS 86-2168). Therefore, the thermal expansion coefficient of the glass-ceramics increases with increasing TiO<sub>2</sub> concentration. While the glass-ceramics with 2.5 mol% TiO<sub>2</sub> and platinum show a smaller thermal expansion than the base glass-ceramics, the thermal expansion increases for the glass-ceramics with higher TiO<sub>2</sub> concentration. Furthermore, a decrease in the hydrolytic durability of the glass-ceramics (except II-2.5 TiO<sub>2</sub>+Pt) in comparison to the respective glasses was observed.

In summary, the addition of TiO<sub>2</sub> leads to a slight improvement of the hydrolytic durability of the glass-ceramics compared to the base glass-ceramics. On the other hand, an increase of the thermal expansion coefficient is observed. Due to these results, the next chapter illustrates the addition of a 1:1 mixture of TiO<sub>2</sub>/ZrO<sub>2</sub> to increase the degree of crystallisation of the glass accompanied by an increase in the hydrolytic durability.

## 5.5 Addition of $\text{TiO}_2 / \text{ZrO}_2$

Glasses with the addition of  $\text{TiO}_2 / \text{ZrO}_2$  were melted, starting from the base glass  $0.9 \text{BaO} - 1.0 \text{Al}_2\text{O}_3 - 1.1 \text{B}_2\text{O}_3$ . The mixture of  $\text{TiO}_2 / \text{ZrO}_2$  with a molar ratio of 1:1 was added as potential nucleation agent [61–63] and furthermore, to improve the hydrolytic durability [64]. In Table 5.7, the compositions, glass transformation temperatures,  $T_g$ , and softening temperatures,  $T_D$  are presented.

Table 5.7: Chemical composition, glass transformation and softening temperature of the glasses with the addition of  $\text{TiO}_2 / \text{ZrO}_2$ .

Glass name	BaO in mol%	$\text{Al}_2\text{O}_3$ in mol%	$\text{B}_2\text{O}_3$ in mol%	$\text{TiO}_2$ in mol%	$\text{ZrO}_2$ in mol%	$T_g$ in °C	$T_D$ in °C
base glass	30.0	33.3	36.7	-	-	585	644
2.5 $\text{TiO}_2 / \text{ZrO}_2$	29.3	32.5	35.8	1.2	1.2	602	671
5.0 $\text{TiO}_2 / \text{ZrO}_2$	28.6	31.7	35.0	2.4	2.4	607	657
7.5 $\text{TiO}_2 / \text{ZrO}_2$	27.9	31.0	34.1	3.5	3.5	601	642
10.0 $\text{TiO}_2 / \text{ZrO}_2$	27.3	30.3	33.4	4.5	4.5	608	664
12.5 $\text{TiO}_2 / \text{ZrO}_2$	26.7	29.6	32.6	5.6	5.6	607	664

The  $\text{TiO}_2 / \text{ZrO}_2$  mixture was added to the base glass  $0.90 \text{BaO} - 1.00 \text{Al}_2\text{O}_3 - 1.10 \text{B}_2\text{O}_3$  while the ratio of the molar concentrations of the other oxides was kept constant. All melted glasses, except  $12.5 \text{TiO}_2 / \text{ZrO}_2$ , were glassy and transparent samples; crystals and bubbles were not observed. The sample  $12.5 \text{TiO}_2 / \text{ZrO}_2$  was glassy at the surface and opaque to white in the bulk. This sample was studied by TEM to clarify the phenomenon. However, micrographs taken from samples prepared by replica technique, did not show any indication of phase separation or crystallisation.

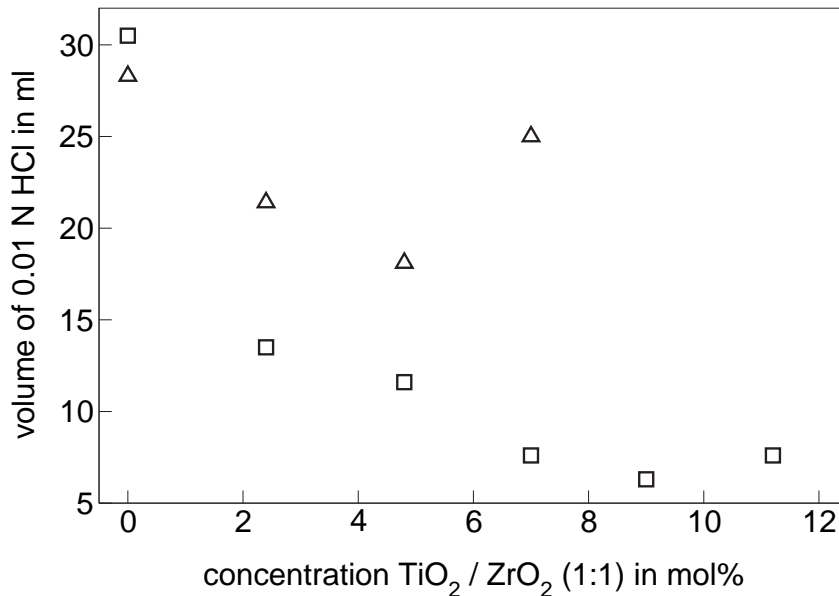
The addition of  $\text{TiO}_2 / \text{ZrO}_2$  influences  $T_g$  and  $T_D$  as shown in Table 5.7. The addition of 2.5 mol%  $\text{TiO}_2 / \text{ZrO}_2$  results in an increase in  $T_g$  and  $T_D$  of about 17 and 27 K, respectively. Further additions of  $\text{TiO}_2 / \text{ZrO}_2$  lead, within the limits of error ( $\pm 5$  K), to a constant  $T_g$ . On the other hand, the softening temperature decreases until 7.5 mol%  $\text{TiO}_2 / \text{ZrO}_2$  and increases again with further addition of  $\text{TiO}_2 / \text{ZrO}_2$ . The densities of the glasses increase with increasing  $\text{TiO}_2 / \text{ZrO}_2$  concentration in the range of 3.29 and 3.41  $\text{g/cm}^3$  (see Table 5.8).

Figure 5.33 shows results from studies on the chemical durability, illustrated by the volume of 0.01 N HCl versus the  $\text{TiO}_2 / \text{ZrO}_2$  concentration. The volume of acid indicates the hydrolytic durability and is used to classify the glasses (see section 4.4.4). The higher

Table 5.8: Densities and thermal expansion coefficients of the glasses and glass-ceramics with the addition of  $\text{TiO}_2 / \text{ZrO}_2$ .

Glass name	$\rho_{\text{glass}}$ in $\text{g}/\text{cm}^3$	$\rho_{\text{glass-ceramics}}$ in $\text{g}/\text{cm}^3$	$\alpha_{\text{min.neg.}}$ in $10^{-7} \text{K}^{-1}$	$\alpha_{100-300^\circ\text{C}}$ in $10^{-7} \text{K}^{-1}$
base glass	3.25	3.06	0 (100 °C)	24
2.5 $\text{TiO}_2 / \text{ZrO}_2$	3.29	3.16	0 (100 °C)	27
5.0 $\text{TiO}_2 / \text{ZrO}_2$	3.34	3.19	0 (100 °C)	33
7.5 $\text{TiO}_2 / \text{ZrO}_2$	3.35	3.24	-	33
10.0 $\text{TiO}_2 / \text{ZrO}_2$	3.37	3.34	-	37
12.5 $\text{TiO}_2 / \text{ZrO}_2$	3.41	3.53	-	38

the volume of 0.01 N HCl, the lower is the hydrolytic durability. For the base glass 0.90 BaO - 1.00  $\text{Al}_2\text{O}_3$  - 1.10  $\text{B}_2\text{O}_3$ , an addition of 30.5 ml 0.01 N HCl was necessary and the glass started to dissolve during heat treatment in water. The addition of 2.5 mol% of  $\text{TiO}_2 / \text{ZrO}_2$  decreased the volume of HCl to 13.5 ml, a strong improvement of the hydrolytic durability. Further addition of  $\text{TiO}_2 / \text{ZrO}_2$  resulted in a further increase of the hydrolytic durability. The smallest value, 6.3 ml 0.01 N HCl, was reached with the glass 10.0  $\text{TiO}_2 / \text{ZrO}_2$ , while the glass 12.5  $\text{TiO}_2 / \text{ZrO}_2$  had again a smaller durability (7.6 ml 0.01 N HCl).

Figure 5.33: Hydrolytic durability of the glasses ( $\square$ ) and glass-ceramics ( $\triangle$ ) with  $\text{TiO}_2 / \text{ZrO}_2$  addition.

After the characterisation of the glasses, the standard thermal treatment was carried

out (see section 4.2). The obtained glass-ceramics were white, completely crystallised and the samples were slightly deformed during crystallisation. In Table 5.8, the densities and the thermal expansion coefficients of the glass-ceramics are presented. The densities of the glass-ceramics 2.5 TiO<sub>2</sub>/ZrO<sub>2</sub>, 5.0 TiO<sub>2</sub>/ZrO<sub>2</sub> and 7.5 TiO<sub>2</sub>/ZrO<sub>2</sub> are smaller than those of the respective glasses, and clearly larger than the (X-ray) density of the crystalline phase BaAl<sub>2</sub>B<sub>2</sub>O<sub>7</sub> (JCPDS 86-2168) (3.09 g/cm<sup>3</sup>). A reason for the difference could be the formation of other crystalline phases or a higher amount of glassy phase in the glass-ceramics. In Fig. 5.34, the XRD patterns of the glass-ceramics with TiO<sub>2</sub>/ZrO<sub>2</sub> addition are shown. The XRD patterns of the samples 2.5 TiO<sub>2</sub>/ZrO<sub>2</sub>, 5.0 TiO<sub>2</sub>/ZrO<sub>2</sub> and 7.5 TiO<sub>2</sub>/ZrO<sub>2</sub> show only peaks attributed to the BaAl<sub>2</sub>B<sub>2</sub>O<sub>7</sub> crystalline phase (JCPDS 86-2168). The glass-ceramics 10.0 TiO<sub>2</sub>/ZrO<sub>2</sub> exhibit, beside BaAl<sub>2</sub>B<sub>2</sub>O<sub>7</sub> (JCPDS 86-2168), lines of the crystalline phase BaZr(BO<sub>3</sub>)<sub>2</sub> (JCPDS 24-0129). The density of this sample is only slightly smaller than that of the glass it was prepared from. Sample 12.5 TiO<sub>2</sub>/ZrO<sub>2</sub> shows an even higher density than the respective glass and the XRD lines are of low intensity indicating a high amount of glassy phase. The only crystalline phase detected was BaZr(BO<sub>3</sub>)<sub>2</sub> (JCPDS 24-0129).

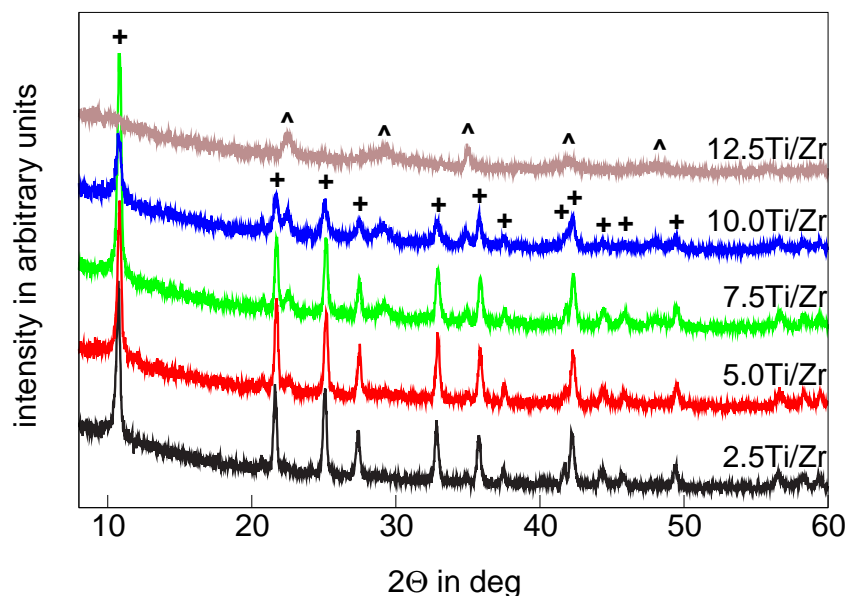


Figure 5.34: XRD patterns of the glass-ceramics with TiO<sub>2</sub>/ZrO<sub>2</sub> addition (crystalline phases: + - BaAl<sub>2</sub>B<sub>2</sub>O<sub>7</sub> (JCPDS 86-2168), ^ - BaZr(BO<sub>3</sub>)<sub>2</sub> (JCPDS 24-0129); Ti/Zr = TiO<sub>2</sub>/ZrO<sub>2</sub>).

Figure 5.35 illustrates the thermal expansion coefficients of the glasses and glass-ceramics as a function of the TiO<sub>2</sub>/ZrO<sub>2</sub> concentration. The thermal expansion coefficients of the glasses decrease up to a concentration of 5.0 mol% TiO<sub>2</sub>/ZrO<sub>2</sub> and increase again for larger TiO<sub>2</sub>/ZrO<sub>2</sub> concentrations. Glass 12.5 TiO<sub>2</sub>/ZrO<sub>2</sub> has almost

the same expansion coefficient ( $70 \cdot 10^{-7} \text{ K}^{-1}$ ) as the base glass ( $72 \cdot 10^{-7} \text{ K}^{-1}$ ). Furthermore, the thermal expansion coefficient of the glass-ceramics increases linearly within the  $\text{TiO}_2 / \text{ZrO}_2$  concentration in the investigated range. A zero expansion is only observed for the base glass-ceramics and the glass-ceramics 2.5  $\text{TiO}_2 / \text{ZrO}_2$  and 5.0  $\text{TiO}_2 / \text{ZrO}_2$  in the temperature range from 25 to 100 °C.

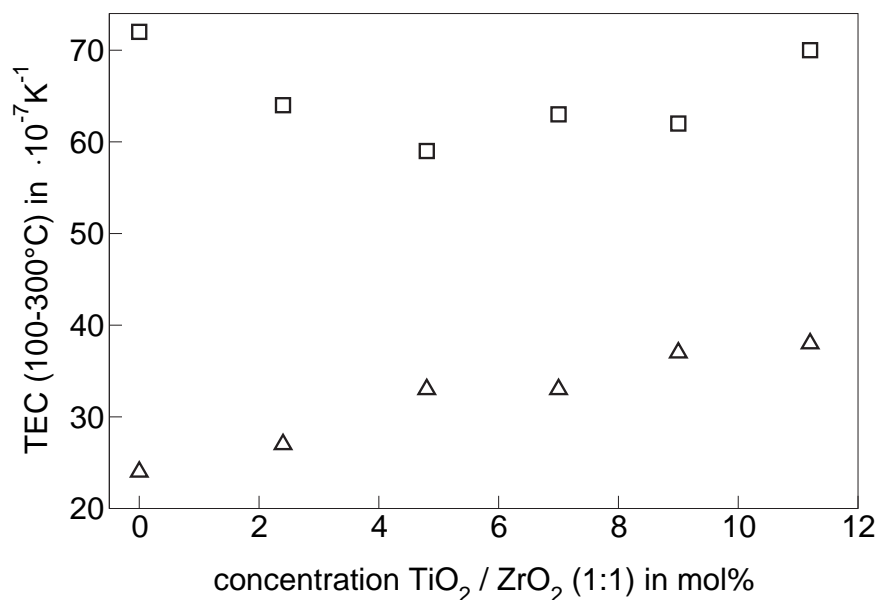


Figure 5.35: Thermal expansion coefficient from 100 to 300 °C of the glasses ( $\square$ ) and glass-ceramics ( $\triangle$ ) with  $\text{TiO}_2 / \text{ZrO}_2$  addition.

The results of the hydrolytic durability determination are shown in Fig. 5.33 at page 59. Through the addition of 2.5 and 5.0 mol%  $\text{TiO}_2 / \text{ZrO}_2$ , the hydrolytic durability of the glass-ceramics increases, i.e. the volume of 0.01 N HCl decreases. A further addition of  $\text{TiO}_2 / \text{ZrO}_2$ , in sample 7.5  $\text{TiO}_2 / \text{ZrO}_2$ , results in a decrease of the hydrolytic durability, but the volume of 25 ml 0.01 N HCl is still less than that of 28 ml 0.01 N HCl attributed to the base glass-ceramics. The glass-ceramics 10.0  $\text{TiO}_2 / \text{ZrO}_2$  and 12.5  $\text{TiO}_2 / \text{ZrO}_2$  were not analysed due to the insufficient crystallisation and a much higher thermal expansion coefficient compared to the base glass.

In Fig. 5.36, the optical micrographs of the glass-ceramics with the addition of  $\text{TiO}_2 / \text{ZrO}_2$  are presented. The micrographs give informations on the morphology of the glass-ceramics and the type of crystallisation (volume or surface crystallisation). The base glass, 0.90 BaO - 1.00  $\text{Al}_2\text{O}_3$  - 1.10  $\text{B}_2\text{O}_3$ , has a surface crystallisation layer of 200 to 300  $\mu\text{m}$  thickness. In the volume, the crystals are randomly grown, but a more detailed characterisation of the shape is not possible caused by the high thickness of the thin section. Sample 2.5  $\text{TiO}_2 / \text{ZrO}_2$  is also crystallised at the surface, while the crystals in the volume are smaller but randomly oriented. The increase of the  $\text{TiO}_2 / \text{ZrO}_2$  concentration results in



a thinner surface crystallisation layer and a constant appearance in the volume, see glass-ceramics 5.0 TiO<sub>2</sub>/ZrO<sub>2</sub>. The sample 7.5 TiO<sub>2</sub>/ZrO<sub>2</sub> shows again a thicker crystallised layer at the surface and also longer crystals in the volume. Finally, the glass-ceramics 10.0 TiO<sub>2</sub>/ZrO<sub>2</sub> and 12.5 TiO<sub>2</sub>/ZrO<sub>2</sub> are crystallised at the surface, but the crystals in the volume look different compared to the other samples. These crystals did not show birefringence like the other samples. Reasons for this behaviour is the occurrence of another crystalline phase, as proved by the XRD patterns (see Fig. 5.34 at page 60).

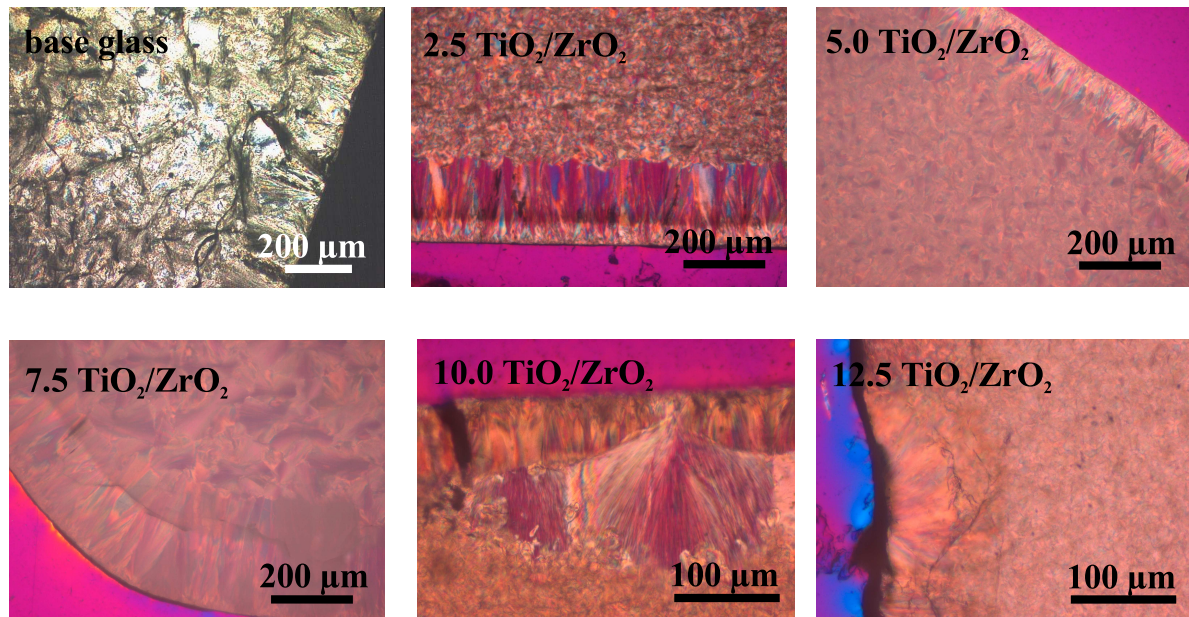


Figure 5.36: Optical micrographs of the glass-ceramics with the addition of TiO<sub>2</sub>/ZrO<sub>2</sub>.

In Fig. 5.37, the IR-reflectance spectra of the glasses and glass-ceramics with the addition of TiO<sub>2</sub>/ZrO<sub>2</sub> are plotted. The band assignment is the same as listed in Table 5.3 at page 37 and is not changed through the addition of TiO<sub>2</sub>/ZrO<sub>2</sub>. Furthermore, the base glass and the respective glass-ceramics 0.90 BaO - 1.00 Al<sub>2</sub>O<sub>3</sub> - 1.10 B<sub>2</sub>O<sub>3</sub> are also included in the graph to facilitate the detection of possible structural changes. The IR-spectra of the glasses are similar to the base glass. In the range from 100 to 400 cm<sup>-1</sup>, the spectra of the glasses 7.5 TiO<sub>2</sub>/ZrO<sub>2</sub> and 12.5 TiO<sub>2</sub>/ZrO<sub>2</sub> exhibit many small peaks due to spectral noise. On the other hand, the glass-ceramics with TiO<sub>2</sub>/ZrO<sub>2</sub> show changes in the spectra with respect to the base glass-ceramics. At around 317 cm<sup>-1</sup>, a new band of low intensity occurs, caused by the addition of TiO<sub>2</sub>/ZrO<sub>2</sub>. As this band can not be observed in the base glass-ceramics as well as in the glass-ceramics with TiO<sub>2</sub> addition (see Fig. 5.32 at page 57), it can be assigned to ZrO<sub>2</sub> groups or TiO<sub>2</sub> groups in another coordination sphere than in the glass-ceramics with sole TiO<sub>2</sub> addition. Furthermore, with increasing TiO<sub>2</sub>/ZrO<sub>2</sub> concentration a shoulder can be seen at 1200 cm<sup>-1</sup>, which results

in a new band at  $1221\text{ cm}^{-1}$  in the glass-ceramics  $7.5\text{ TiO}_2/\text{ZrO}_2$  and  $12.5\text{ TiO}_2/\text{ZrO}_2$ . The IR-reflectance spectrum of sample  $12.5\text{ TiO}_2/\text{ZrO}_2$  shows less pronounced bands in comparison to the other glass-ceramics, which could be caused by a higher concentration of the residual glass phase or the formation of another crystalline phase. Smaller quantities of this crystalline phase are also present in the other glass-ceramics. XRD patterns are shown in Fig. 5.34 at page 60. They prove these assumptions: the XRD lines of sample  $12.5\text{ TiO}_2/\text{ZrO}_2$  are of low intensity indicating a high amount of glassy phase and only the crystalline phase  $\text{BaZr}(\text{BO}_3)_2$  (JCPDS 24-0129) was detected. In the other glass-ceramics, XRD patterns show the crystalline phase  $\text{BaAl}_2\text{B}_2\text{O}_7$  (JCPDS 86-2168) as main phase and only very small peaks of the phase  $\text{BaZr}(\text{BO}_3)_2$  (JCPDS 24-0129).

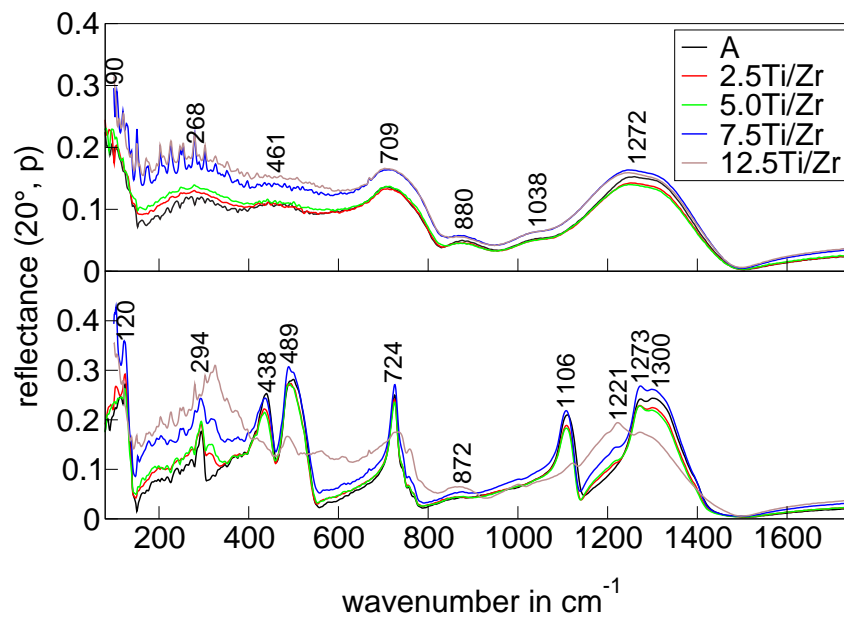


Figure 5.37: IR-reflectance spectra of the glasses (upper part) and glass-ceramics (lower part) with the addition of  $\text{TiO}_2/\text{ZrO}_2$  (incidence angle  $20^\circ$ , parallel polarised radiation;  $\text{A} = 0.9\text{ BaO} - 1.0\text{ Al}_2\text{O}_3 - 1.1\text{ B}_2\text{O}_3$ ,  $\text{Ti}/\text{Zr} = \text{TiO}_2/\text{ZrO}_2$ ).

In conclusion, the addition of  $\text{TiO}_2/\text{ZrO}_2$  results in an improvement of the hydrolytic durability of the glasses and glass-ceramics, but also increases the thermal expansion coefficient. Only the samples  $2.5\text{ TiO}_2/\text{ZrO}_2$  and  $5.0\text{ TiO}_2/\text{ZrO}_2$  have a zero expansion in the range from  $25$  to  $100^\circ\text{ C}$ , which is still acceptable.

In the next step, a mixture of  $\text{TiO}_2/\text{ZrO}_2$  was added to the stoichiometric glass  $\text{BaO} - \text{Al}_2\text{O}_3 - \text{B}_2\text{O}_3$ , which shows the lowest thermal expansion coefficient of all evaluated glass-ceramics. The influence of the  $\text{TiO}_2/\text{ZrO}_2$  addition is examined to confirm the previous results. The stoichiometric glass  $\text{BaO} - \text{Al}_2\text{O}_3 - \text{B}_2\text{O}_3$  was melted with an addition of  $2.5\text{ mol}\%$   $\text{TiO}_2$  and  $2.5\text{ mol}\%$   $\text{ZrO}_2$ , furthermore platinum was added to one part of



the glass. Afterwards the glasses with and without platinum were crystallised in order to prepare glass-ceramics using the standard crystallisation procedure. The densities of the glasses were  $3.42 \text{ g/cm}^3$  and  $3.25$  and  $3.19 \text{ g/cm}^3$  for crystallised samples without and with platinum, respectively. A decrease in density was observed here, but also in this case, the low (X-ray) density of the crystalline phase  $\text{BaAl}_2\text{B}_2\text{O}_7$  (JCPDS 86-2168) was not reached. The XRD patterns of the glass-ceramics show lines attributed to the crystalline phase  $\text{BaAl}_2\text{B}_2\text{O}_7$  (JCPDS 86-2168) and additional low intensity lines of an unknown crystalline phase. Both glass-ceramics were crystallised in the volume.

Glass  $\text{BaO} - \text{Al}_2\text{O}_3 - \text{B}_2\text{O}_3$  with  $2.5 \text{ mol}\%$   $\text{TiO}_2$  and  $2.5 \text{ mol}\%$   $\text{ZrO}_2$  shows a thermal expansion coefficient of  $70 \cdot 10^{-7} \text{ K}^{-1}$  in the temperature range from  $100$  to  $300 \text{ }^\circ\text{C}$ . In the same temperature range, the respective glass-ceramics have a coefficient of thermal expansion of  $51 \cdot 10^{-7} \text{ K}^{-1}$ , while the glass-ceramics with platinum have a lower coefficient of  $24 \cdot 10^{-7} \text{ K}^{-1}$ . On the other hand, the glass-ceramics with platinum show a zero expansion in the temperature range from  $25$  to  $100 \text{ }^\circ\text{C}$ . Furthermore, the hydrolytic durability of the glass and glass-ceramics without platinum was determined. The volume of  $0.01 \text{ N}$   $\text{HCl}$  was  $19.6 \text{ ml}$  for the glass and  $20.1 \text{ ml}$  for the respective glass-ceramics, which is a slight improvement with regard to the glass without  $\text{TiO}_2 / \text{ZrO}_2$  ( $23 \text{ ml}$   $0.01 \text{ N}$   $\text{HCl}$ ), but a strong one compared to the glass-ceramics without  $\text{TiO}_2 / \text{ZrO}_2$  ( $36.5 \text{ ml}$   $0.01 \text{ N}$   $\text{HCl}$ ).

The previous results with respect to the addition of  $\text{TiO}_2 / \text{ZrO}_2$  could be confirmed for the stoichiometric glass  $\text{BaO} - \text{Al}_2\text{O}_3 - \text{B}_2\text{O}_3$ . The addition of a  $1:1$  mixture of  $\text{TiO}_2 / \text{ZrO}_2$  results in an improvement of the hydrolytic durability, but increases the thermal expansion coefficient of the glass-ceramics.

# Chapter 6

## Conductivity measurements

Glasses in the system BaO - Al<sub>2</sub>O<sub>3</sub> - B<sub>2</sub>O<sub>3</sub> can be transformed into glass-ceramics due to volume crystallisation. The crystallisation temperature, however, is difficult to determine by DTA measurements. The idea was to detect the phase transitions by conductivity measurements, because phase transition means change of the phase composition of the sample and hence, also of the conductivity. Furthermore, the conductivity measurements should be used to determine all types of phase transitions, e.g. crystallisation and melting of the crystalline phases.

### 6.1 General analysis and errors of the measurements

#### 6.1.1 Analysis of the impedance measurements

The setup and experimental procedure of the impedance measurements are described in section 4.6. During the measurement, the impedance and phase angle of the sample are recorded. Figure 6.1 shows the graphs of the impedance and phase angle versus the measurement time.

In the next step, the resistivity of the sample is calculated from the impedance and the phase angle using the simulation program Thales. An equivalent circuit is necessary to carry out the conversion. For that purpose, the impedance measurements were carried out at various frequencies and constant temperature. The obtained spectra were simulated with the equivalent circuit shown in Fig. 6.2 [16–18]. The inductivity L represents the inductive effects of the connecting wires to the sample. The inductivity influences the impedance spectra only at frequencies > 500 kHz. The impedance elements W, R1 and C1 are caused by the electron transfer from an electron conductor to an ionic conductor with W represents the Warburg impedance, R1 the electron transfer resistance and C1

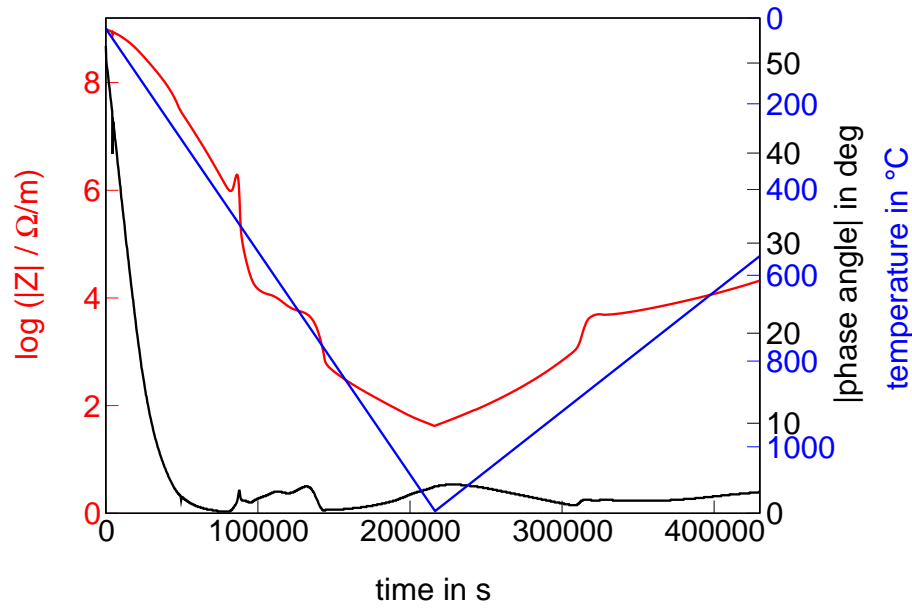


Figure 6.1: Impedance  $|Z|$  and  $|\text{phase angle}|$  versus measurement time (thermal treatment: the temperature is increased from  $550\text{ }^{\circ}\text{C}$  to  $1150\text{ }^{\circ}\text{C}$ , kept for 6 min and subsequently cooled to  $550\text{ }^{\circ}\text{C}$  with  $0.167\text{ K/min}$ ).

the double layer capacitance. These elements dominate the lower frequency part of the impedance spectra and are only observed at high temperatures.  $R_2$  and  $C_2$  represent the ionic conductivity and the dielectric properties of the volume, respectively. The spectra are dominated by  $R_2$  in a wide temperature range. In the case of lower temperatures ( $T < 700\text{ }^{\circ}\text{C}$ ),  $R_2$  is so large (M $\Omega$ m range), that  $C_2$  dominates at medium frequencies.

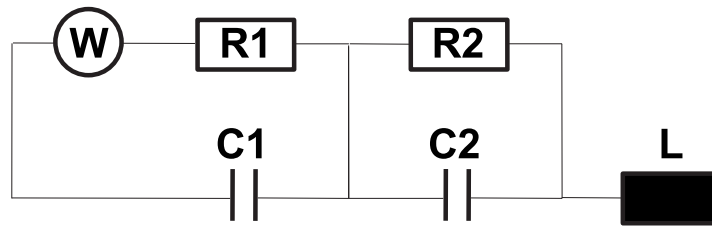


Figure 6.2: Equivalent circuit.

The evaluation and simulation of the measured impedances show, that  $R_2$  dominates or at least provides a significant contribution to the impedance of a parallel circuit of  $R_2$  and  $C_2$  in the frequency range from 0.1 to 5 Hz in the entire temperature range. This frequency range lies out of the frequencies at which  $L$ ,  $W$ ,  $R_1$  and  $C_1$  significantly contribute to the impedance. As a result, fixed frequency measurements were carried out with all samples using a frequency of 3.7 Hz. These measurements were evaluated under the assumption of a R-C parallel circuit. The frequency of 3.7 Hz was selected because the measured phase angle was approximately zero in the interesting temperature range.

The specific conductivity ( $\sigma$ ) of a sample was calculated from the parallel resistor (R2) and the sample geometry, while the corresponding temperatures were calculated from the measuring time, heating rate and starting temperature. Figure 6.3 shows a plot of the specific conductivity versus temperature.

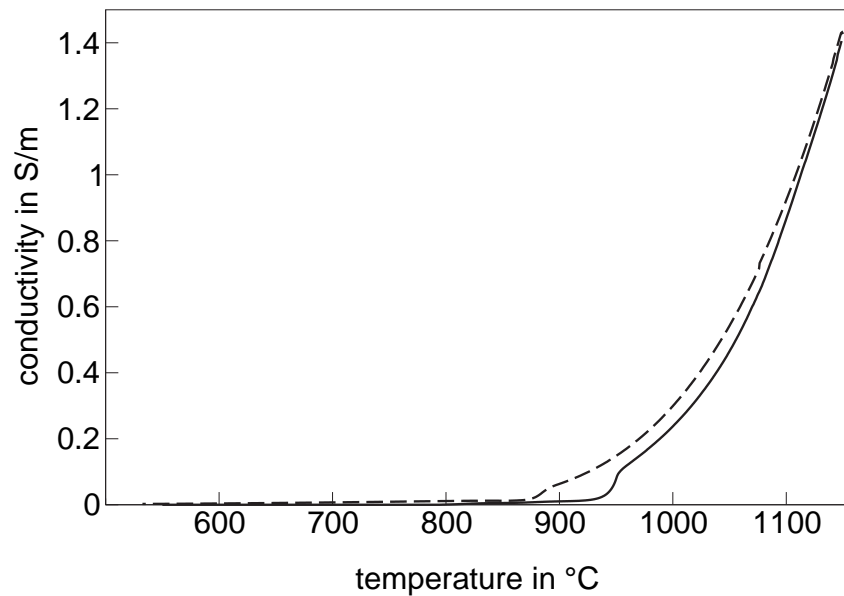


Figure 6.3: Plots of the specific conductivities versus temperature during heating (solid line) and subsequent cooling (dashed line).

In the next step the logarithm of the specific conductivity was calculated and illustrated versus  $1/\text{temperature}$ , i.e. as Arrhenius plot, as shown in Fig. 6.4.

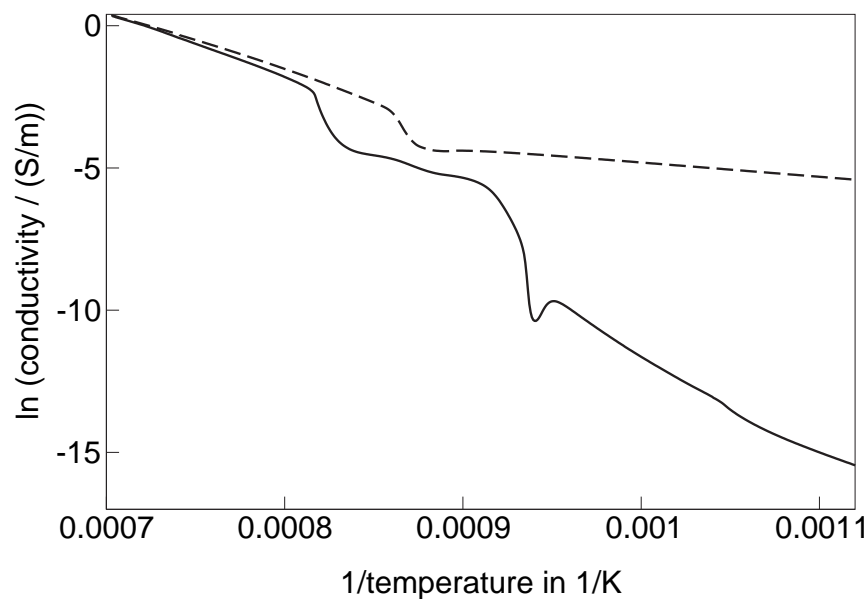


Figure 6.4: Arrhenius plots of the specific conductivities versus  $1/\text{temperature}$  during heating (solid line) and subsequent cooling (dashed line).

All arithmetical operations were done using the program `xmgrace` [65]. The Arrhenius plot was smoothed by running average using five points and subsequently numerical differentiated. Finally, the first derivative of the conductivity ( $-\ln\sigma/d(1/kT)$ ) was plotted as function of the temperature in  $^{\circ}\text{C}$ , as shown in Fig. 6.5.

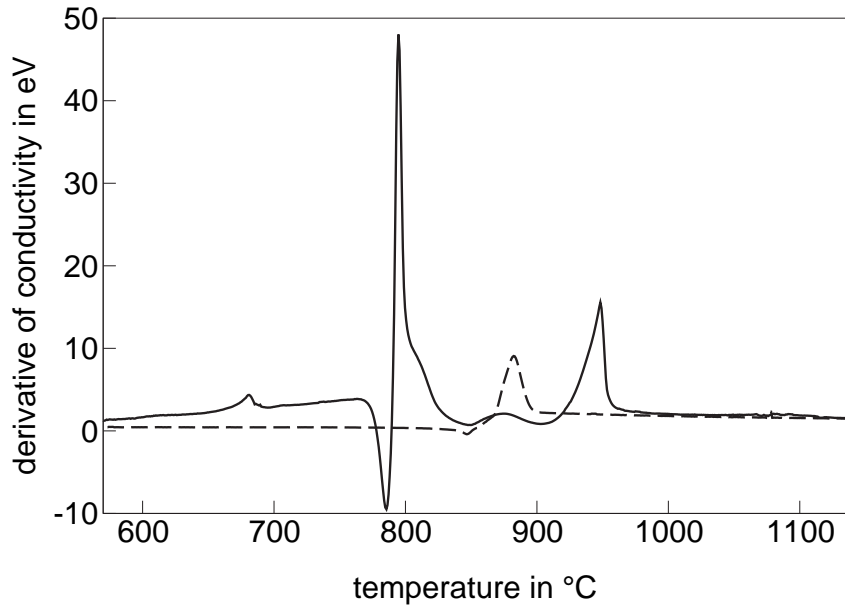


Figure 6.5: Plots of the derivative of the specific conductivities ( $-\ln\sigma/d(1/kT)$ ) versus temperature during heating (solid line) and subsequent cooling (dashed line).

If this derivative is constant within a certain temperature range (e.g. Fig. 6.5 from  $1100^{\circ}\text{C}$  to  $950^{\circ}\text{C}$  during cooling), it has the physical meaning of an activation energy. The occurrence of a well pronounced peak illustrates the dynamic changes of the conductivity during phase transition. In the following ( $-\ln\sigma/d(1/kT)$ ) ( $\sigma$  in  $\text{S/m}$ ) is denoted as derivative.

### 6.1.2 Discussion of the measurement errors

The error of the temperature is  $\pm 2\text{ K}$  and impedances  $< 100\text{ M}\Omega$  are measured with an accuracy of  $\pm 0.5\%$ . The experimental setup withstands differences of the thermal expansion coefficient, TEC, during heating and cooling until  $T_g$  is reached. During heating, the expansion of the glass will be tolerated by the gap between the sample and the spacer (see section 4.6) and at temperatures  $> T_g$  the sample will relax by viscous flow. During cooling, the viscous flow will adapt the differences in TEC until the sample crystallises. After crystallisation the sample is solid and hence, the geometry is stable. The possible breaking of the spacer does not influence the sample geometry, as the platinum electrode tolerates the differences in TEC due to its ductility. Furthermore, the geometry changes

due to thermal expansion are negligible, because these changes are in the range of 1%. Hence, the errors caused by calculating the conductivity assuming a constant geometry are smaller than those due to the error of the temperature measurement.

## 6.2 BaO - Al<sub>2</sub>O<sub>3</sub> - B<sub>2</sub>O<sub>3</sub>

The DTA profiles do not exhibit exothermic peaks, which leads to the primary motivation for the conductivity measurements. The crystallisation temperature should be approximately equal to the temperature at which the derivative of the conductivity changes, if the glass and the crystallised sample have different specific conductivities.

Figure 6.6 shows an Arrhenius plot of sample BaO - Al<sub>2</sub>O<sub>3</sub> - B<sub>2</sub>O<sub>3</sub> during heating and subsequent cooling using different rates (2, 1, 0.5 and 0.167 K/min). Each heating and cooling cycle represents a single measurement of a single sample.

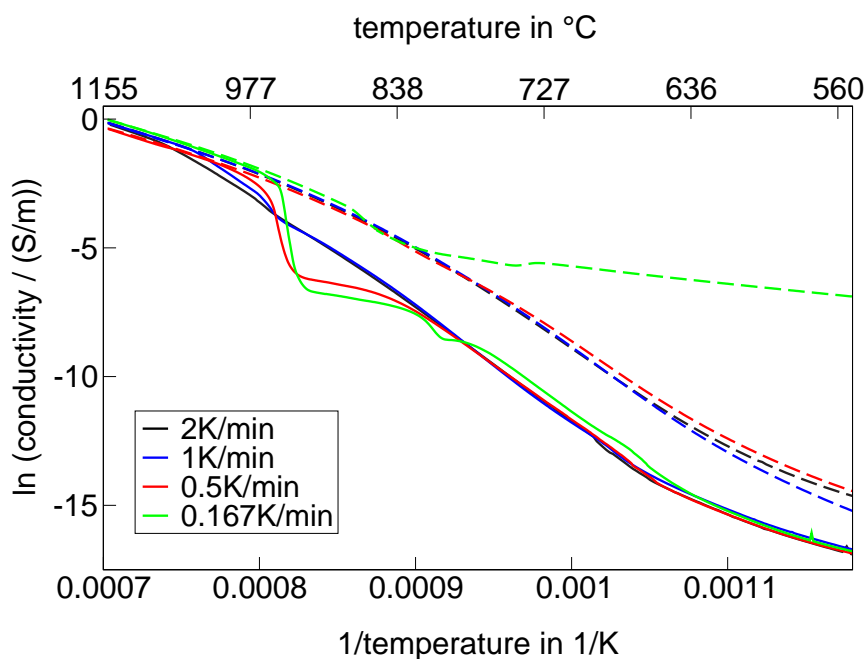


Figure 6.6: Arrhenius plots of the specific conductivities (different rates) of the sample BaO - Al<sub>2</sub>O<sub>3</sub> - B<sub>2</sub>O<sub>3</sub> during heating (solid line) and subsequent cooling (dash dotted line).

During heating, the conductivity is nearly the same at all supplied rates up to a temperature of 670 °C. Above 670 °C the conductivity attributed to a heating rate of 0.167 K/min increases. Above 800 °C the conductivities at heating rates of 0.167 0.5 K/min increase strongly. At temperatures above 1050 °C the conductivities during heating and cooling are the same for different rates. At temperatures below 1050 °C, the conductivities measured during cooling are notably larger than during heating in the entire temperature range studied. During cooling, the samples with cooling rates of 2, 1

and 0.5 K/min behave similar. By contrast, the sample cooled with 0.167 K/min has a different behaviour below 830 °C. Below this temperature, the slope of the plot decreases notably and  $\ln$  conductivity (-7.4 to -5.3) is larger than supplying larger rates ( $< -8.5$ ).

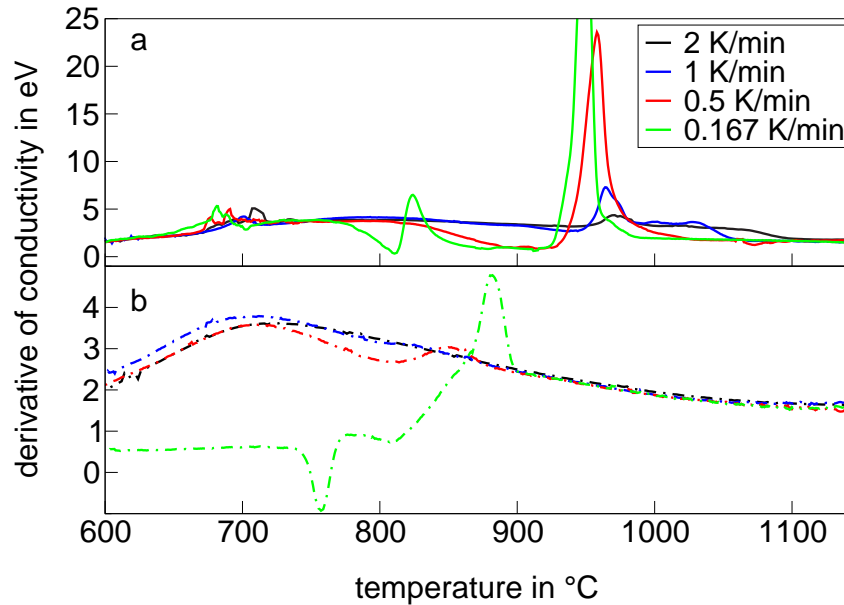


Figure 6.7: Derivatives of the specific conductivities ( $-\text{dln}\sigma/\text{d}(1/kT)$ ) of the sample BaO- $\text{Al}_2\text{O}_3$ - $\text{B}_2\text{O}_3$  during a: heating and b: cooling.

In Fig. 6.7, the derivatives ( $-\text{dln}\sigma/\text{d}(1/kT)$ ) of the sample BaO- $\text{Al}_2\text{O}_3$ - $\text{B}_2\text{O}_3$  are shown for different heating and cooling rates. First, the changes during cooling will be described. The activation energy increases significantly from 1.60 to 2.40 eV for all cooling rates in the temperature range from 1150 to 900 °C. At lower temperatures the derivative is affected by the cooling rate. Supplying a cooling rate of 0.167 K/min, a maximum of the derivative is observed at 882 °C. With further decrease of the temperature, this derivative decreases and is approximately constant from 810 to 775 °C with a minimum at 755 °C. Below 740 °C, the derivative at 0.167 K/min remains nearly constant. At a cooling rate of 0.5 K/min, the maximum of the derivative is shifted to a lower temperature (855 °C) and is less pronounced compared to a cooling rate of 0.167 K/min. During further cooling, a small minimum at around 810 °C and a broad maximum at 715 °C is observed. At cooling rates of 1 and 2 K/min, the shapes of the curves are similar, except of the minimum which is not observed at these cooling rates. The derivatives are identical in the temperature range from 1150 to 750 °C. At lower temperatures, the derivative of 2 K/min is smaller and the maximum is observed at higher temperature (730 °C) than at a cooling rate of 1 K/min (710 °C). Below the temperature of the maximum, the derivatives of 0.5, 1 and 2 K/min decrease with decreasing temperature, but have a much higher derivative (2.30 eV) than the sample with 0.167 K/min (0.50 eV) at 600 °C.



During heating, the derivatives are the same for all heating rates up to a temperature of 645 °C. The first small and sharp peak is shifted to higher temperatures with increasing heating rate (680, 690, 700 and 708 °C for 0.167, 0.5, 1 and 2 K/min respectively). Within a temperature range from 720 to 760 °C, the derivative (around 3.80 eV) is again the same for all heating rates. At a heating rate of 2 K/min, the derivative remains nearly constant up to a temperature of 950 °C and has a small maximum at 970 °C. Above 1070 °C, the derivative decreases to 1.80 eV. At a heating rate of 1 K/min, a similar change is observed, however, the derivative decreases slightly at temperatures > 900 °C and the maximum is shifted to lower temperatures (965 °C) and is more pronounced. At temperatures higher than those attributed to the maximum, the derivative (around 3.40 eV) is constant up to 1035 °C and then also decreases to 1.80 eV. The derivative at a heating rate of 0.5 K/min is also constant after the first sharp maximum up to 810 °C, but then in the range from 890 to 930 °C decreases to around 0.90 eV. Above 930 °C, the derivative increases again and has a maximum at 960 °C which is much higher (23.00 eV) than at a heating rate of 1 (7.00 eV) or 2 K/min (4.00 eV). During further heating, the derivative decreases again and above 1020 °C also possesses a value of 1.80 eV. At a heating rate of 0.167 K/min, the derivative after the first maximum (680 °C) is nearly constant up to 760 °C, then shows a sharp minimum at 810 °C and a sharp maximum at 825 °C. After this maximum, the derivative has a value of around 0.90 eV up to a temperature of 920 °C and shows another sharp maximum at 950 °C that is even higher (33.00 eV) than that at a heating rate of 0.5 K/min. Above 990 °C, the derivative is almost constant attributed to an activation energy of 1.80 eV and is assigned to the liquid phase.

### 6.3 0.9 BaO - Al<sub>2</sub>O<sub>3</sub> - B<sub>2</sub>O<sub>3</sub>

The conductivity of the glass 0.9 BaO - Al<sub>2</sub>O<sub>3</sub> - B<sub>2</sub>O<sub>3</sub> was measured to verify the results of the measurements of glass BaO - Al<sub>2</sub>O<sub>3</sub> - B<sub>2</sub>O<sub>3</sub>. Also the influence of composition changes should be analysed. Figure 6.8 shows Arrhenius plots of sample 0.9 BaO - Al<sub>2</sub>O<sub>3</sub> - B<sub>2</sub>O<sub>3</sub> for different heating and cooling rates. In analogy to BaO - Al<sub>2</sub>O<sub>3</sub> - B<sub>2</sub>O<sub>3</sub>, the conductivities above 968 °C are the same during heating and cooling for all supplied heating rates. During heating, the conductivities for the different heating rates are almost the same up to the temperature of 778 °C. Above this temperature, the samples exhibit differences as a function of the heating rate. During cooling, the conductivities are the same for all cooling rates in the temperature range from 1150 to 886 °C. At a cooling rate of

0.167 K/min, the conductivity decreases stronger than for the other rates from 886 to 853 °C. Below 853 °C, the conductivity at a cooling rate of 0.167 K/min is almost constant and much higher than at other cooling rates. At cooling rates of 0.5, 1 and 2 K/min, the conductivities are the same down to a temperature of 805 °C. In the temperature range from 805 to 550 °C, the conductivities slightly increase with decreasing cooling rates.

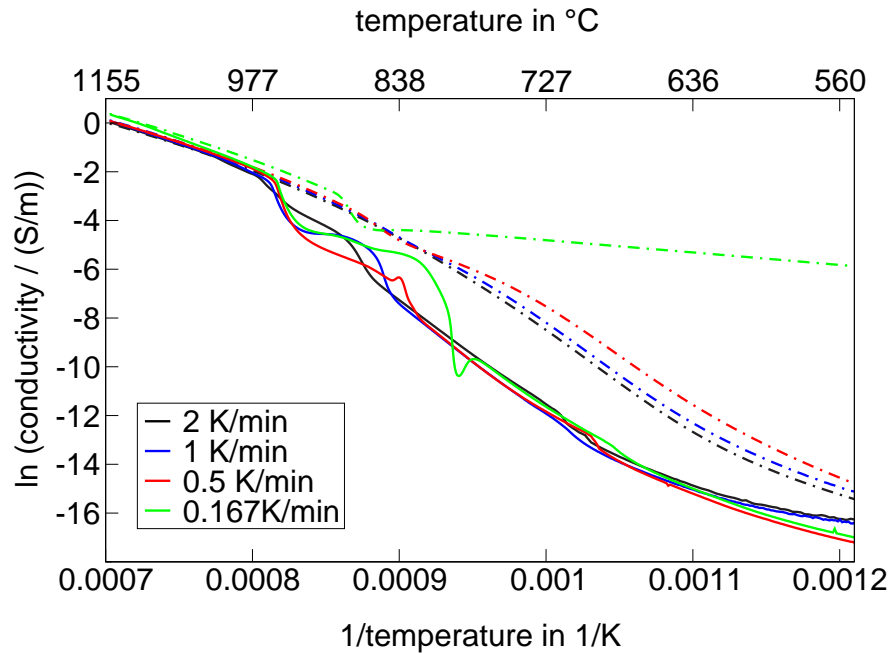


Figure 6.8: Arrhenius plots of the specific conductivities (different rates) of the sample  $0.9\text{BaO}-\text{Al}_2\text{O}_3-\text{B}_2\text{O}_3$  during heating (solid line) and subsequent cooling (dash dotted line).

In Fig. 6.9, the derivatives of sample  $0.9\text{BaO}-\text{Al}_2\text{O}_3-\text{B}_2\text{O}_3$  are presented for different heating and cooling rates, respectively. In analogy to  $\text{BaO}-\text{Al}_2\text{O}_3-\text{B}_2\text{O}_3$ , the derivatives increase during cooling and are equal for all rates within the temperature range from 1150 to 900 °C. Further decreasing the temperature results in maxima of the derivatives for cooling rates of 0.167, 0.5 and 1 K/min. At a cooling rate of 0.167 K/min, the maximum occurs at 883 °C. With increasing the cooling rate, the maximum is shifted to lower temperatures (0.5 K/min: 860 °C, 1 K/min: 844 °C) and decreases in amplitude. The derivative at a cooling rate of 0.167 K/min shows a small negative peak at 848 °C and then remains almost constant (0.45 eV) with decreasing temperature. Larger cooling rates (0.5 and 1 K/min) result in a minimum at around 820 °C and a maximum at 680 and 700 °C for 0.5 and 1 K/min, respectively. At a cooling rate of 2 K/min, only a broad maximum is observed at 700 °. After this maximum, the derivatives decrease for cooling rates of 0.5, 1 and 2 K/min, but possess a higher value at 550 °C (from 1.80 to 2.00 eV)

than at a cooling rate of 0.167 K/min.

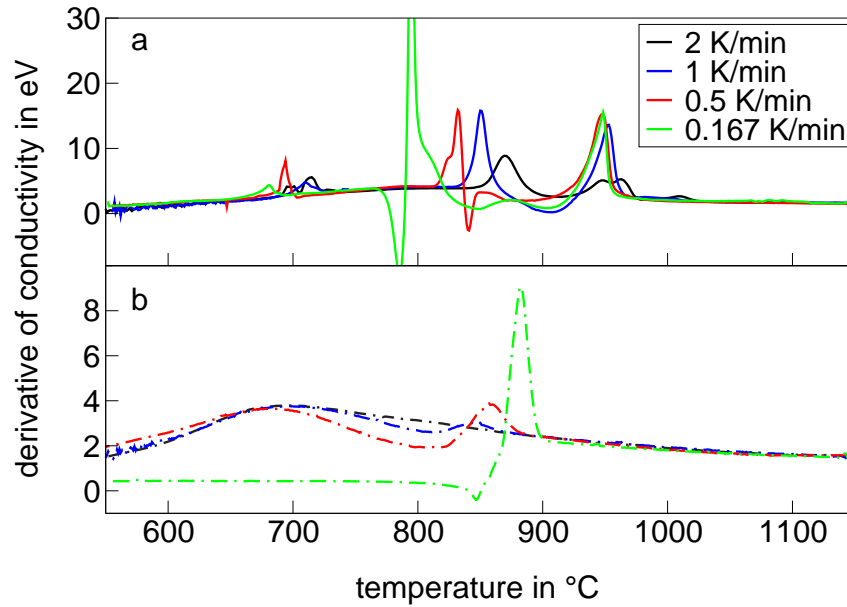


Figure 6.9: Derivatives of the specific conductivities ( $-\text{dln}\sigma/\text{d}(1/kT)$ ) of the sample 0.9 BaO - Al<sub>2</sub>O<sub>3</sub> - B<sub>2</sub>O<sub>3</sub> during a: heating and b: cooling.

During heating, the derivatives increase from 0.80 eV at 550 °C to 2.15 eV at 650 °C for all rates. Further heating results in a smaller maximum which, by analogy to BaO - Al<sub>2</sub>O<sub>3</sub> - B<sub>2</sub>O<sub>3</sub>, is shifted to higher temperatures with increasing heating rate (0.167 K/min: 680 °C, 0.5 K/min: 694 °C, 1 K/min: 710 °C and 2 K/min: 715 °C). In the temperature range from 725 to 765 °C, the derivatives are again equal for all studied heating rates. At higher temperatures, the effect of the heating rate is more pronounced and two maxima are observed at any heating rate. The first maximum occurs at 795 °C at a heating rate of 0.167 K/min and is shifted to higher temperatures (0.5 K/min: 832 °C, 1 K/min: 851 °C and 2 K/min: 870 °C) and decreases in amplitude with increasing heating rate. The second maximum is observed at around 950 °C for all heating rates, but at the largest heating rate (2 K/min) an additional maximum occurs at 965 °C. At all heating rates also minima are observed: at 0.167 K/min at 785, 850 and 905 °C. The derivative at 0.5 K/min has minima at 840 and 880 °C and at a heating rate of 1 K/min, a minimum occurs at 905 °C. At temperatures above 980 °C, the derivative and also the conductivity are the same for all used heating and cooling rates.

Figure 6.10 shows the DTA measurement and the derivative of the specific conductivity ( $-\text{dln}\sigma/\text{d}(1/kT)$ ) of sample 0.9 BaO - Al<sub>2</sub>O<sub>3</sub> - B<sub>2</sub>O<sub>3</sub> during heating. The comparison of these two different types of measurement helps to attribute the effects occurring during heating. From the DTA measurement a glass transition temperature of 637 °C is deter-

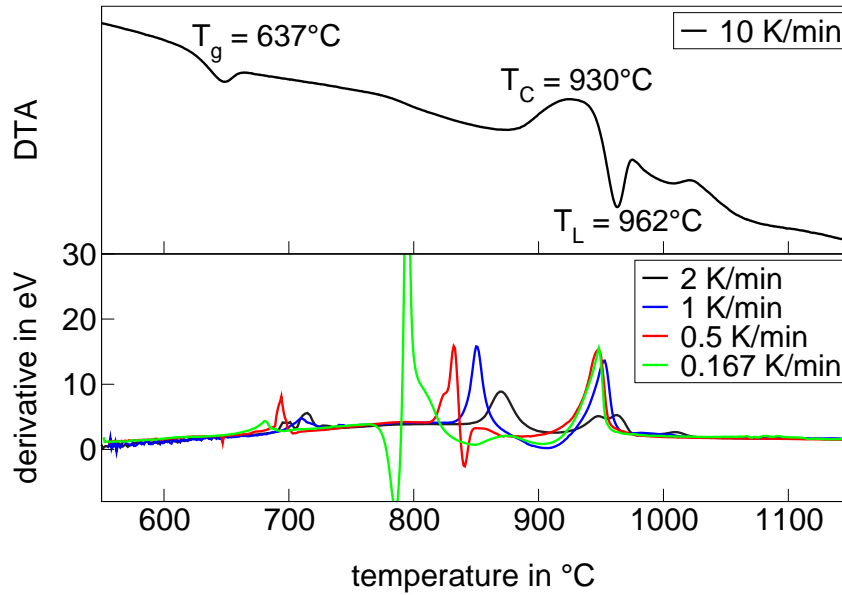


Figure 6.10: Comparison of DTA and conductivity measurement glass  $0.9\text{BaO}-\text{Al}_2\text{O}_3-\text{B}_2\text{O}_3$ .

mined, the crystallisation temperature is  $930^\circ\text{C}$  and the liquidus temperature  $962^\circ\text{C}$ . For comparison, the attributed temperatures of the conductivity measurement at a heating rate of  $2\text{ K/min}$  will be used. The glass transition temperature is not detected by the conductivity measurement since there is no detectable effect in this temperature range. At a heating rate of  $2\text{ K/min}$ , the conductivity measurement shows a first peak at  $715^\circ\text{C}$ . The peak can not be the transition temperature, because it should be  $637^\circ\text{C}$  or less. Since the glass transition temperature is shifted to lower values with smaller heating rates and the DTA was recorded using a rate of  $10\text{ K/min}$ , i.e. a five times higher rate. This explains also the  $60\text{ K}$  lower crystallisation temperature which in the conductivity measurement is observed at  $870^\circ\text{C}$ . Furthermore, the liquidus temperature is almost equal for DTA and conductivity measurement ( $962^\circ\text{C}$ ), because the melting temperature of the crystalline phase is thermodynamically defined.

## 6.4 Discussion - Conductivity measurements of $\text{BaO}-\text{Al}_2\text{O}_3-\text{B}_2\text{O}_3$ and $0.9\text{BaO}-\text{Al}_2\text{O}_3-\text{B}_2\text{O}_3$

Figure 6.11: Thermal expansion of the glass-ceramics with  $\text{TiO}_2$  addition.

The DTA profile was recorded from a powdered sample while the conductivity measurements were performed from a bulk sample. Hence, in the case of DTA, the surface/volume

ratio is larger which may increase the contribution of surface effects such as surface crystallisation. On the other hand, the conductivity measurements were carried out after the samples were heated up to the softening temperature to achieve an electrical contact to the electrodes. Therefore, the thermal histories of the samples for DTA and conductivity measurements are different. In addition, during the conductivity measurements, crystallisation may also be initiated at the interfaces platinum / sample and alumina / sample which also might contribute to the conductivity [66]. But, these surface effects could also occur between platinum crucible and sample during the DTA measurements. The DTA profiles and conductivity measurements of the samples BaO - Al<sub>2</sub>O<sub>3</sub> - B<sub>2</sub>O<sub>3</sub> and 0.9 BaO - Al<sub>2</sub>O<sub>3</sub> - B<sub>2</sub>O<sub>3</sub> will be discussed taking into account the different measurement parameters.

In the case of an ideal Arrhenian ion conductor,  $\ln(\sigma)$  will show a linear dependency upon  $1/T$  and hence, the derivative should be constant in the entire studied temperature range. Thus, the derivative is equal to the activation energy. If a phase transition would occur, the derivative changes with temperature and has no longer the physical meaning of an activation energy.

From the DTA measurements, glass transition temperatures,  $T_g$ , were determined in the range from 620 to 640 °C. In the Arrhenius plots of the conductivities and the derivatives, effects attributed to  $T_g$  could not be detected in the studied samples BaO - Al<sub>2</sub>O<sub>3</sub> - B<sub>2</sub>O<sub>3</sub> and 0.9 BaO - Al<sub>2</sub>O<sub>3</sub> - B<sub>2</sub>O<sub>3</sub>. In the  $T_g$  range, the resistance of the samples was too high to detect small changes in the conductivity. First, the changes during cooling should be discussed. At high temperatures, a homogeneous liquid occurs and the conductivity as well as the derivative do not depend on the cooling rate. For the studied samples and all applied cooling rates, the derivatives increase during cooling from 1150 °C and remain the same for all heating rates until approximately 900 °C, as shown in Figs. 6.7 and 6.9. In this temperature range, the derivative has the physical meaning of an activation energy. Further cooling of the sample, applying a cooling rate of 0.167 K/min, results in a maximum of the derivative. Here, a phase transition occurs. The XRD patterns of the samples show lines attributed to the crystalline phase BaAl<sub>2</sub>B<sub>2</sub>O<sub>7</sub> (JCPDS 86-2168). Therefore, the maximum in the derivative is attributed to the crystallisation of this phase. Figure 6.12 presents optical micrographs of the samples BaO - Al<sub>2</sub>O<sub>3</sub> - B<sub>2</sub>O<sub>3</sub> and 0.9 BaO - Al<sub>2</sub>O<sub>3</sub> - B<sub>2</sub>O<sub>3</sub> after the conductivity measurement. The micrographs show thin sections of the samples which were cut perpendicular to the platinum disks. Both samples are completely crystallised and the crystal growth is predominantly perpendicular to the platinum disks.

With increasing cooling rates (0.5 and 1 K/min), the maxima decrease in amplitude and

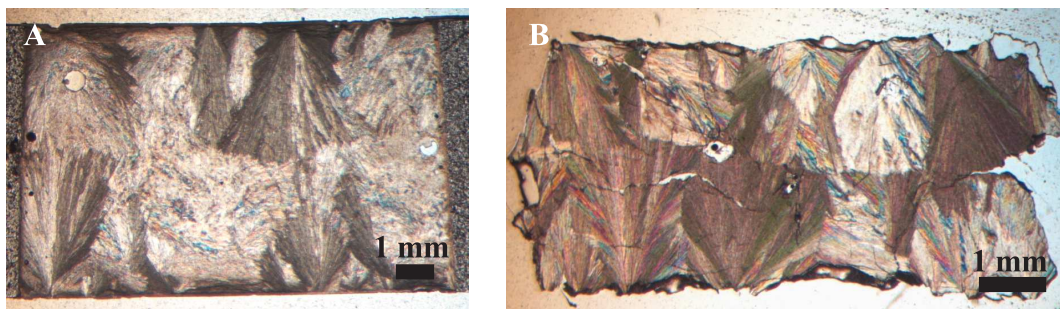


Figure 6.12: Optical micrographs of the samples  $\text{BaO}-\text{Al}_2\text{O}_3-\text{B}_2\text{O}_3$  (A) and  $0.9\text{BaO}-\text{Al}_2\text{O}_3-\text{B}_2\text{O}_3$  (B) after conductivity measurement with  $0.167\text{ K/min}$ .

are shifted to lower temperatures. At a cooling rate of  $2\text{ K/min}$ , the XRD patterns give no indication of crystallinity. Samples at lower cooling rates show the XRD patterns of  $\text{BaAl}_2\text{B}_2\text{O}_7$  (JCPDS 86-2168), i.e. the volume fraction of the crystalline phase increases with decreasing heating rate. The effect of the cooling rate on the maximum in the derivative as well as on the crystallinity of the sample can be explained by the nucleation and crystal growth kinetics, because the maximum during cooling only occurs, if there is sufficient time for nucleation and crystal growth. Furthermore, this result is supported by the DTA measurements of the samples which did not show any crystallisation peak because of the fast heating rate of  $10\text{ K/min}$ .

Differences in the volume fraction of the crystalline phase  $\text{BaAl}_2\text{B}_2\text{O}_7$  (JCPDS 86-2168) could also be observed between the studied samples  $\text{BaO}-\text{Al}_2\text{O}_3-\text{B}_2\text{O}_3$  and  $0.9\text{BaO}-\text{Al}_2\text{O}_3-\text{B}_2\text{O}_3$ . Figure 6.13 shows the XRD patterns and conductivity of these samples. The conductivity is higher for the sample  $0.9\text{BaO}-\text{Al}_2\text{O}_3-\text{B}_2\text{O}_3$  during cooling which indicates an increased volume fraction of the crystalline phase compared to sample  $\text{BaO}-\text{Al}_2\text{O}_3-\text{B}_2\text{O}_3$ . This behaviour is observed because the conductivity of the crystalline phase at this temperature is higher than the glassy phase, i.e. an increased volume fraction of the crystalline phase increases also the conductivity of the whole sample. The XRD patterns of these samples support the result: the intensity of the lines of sample  $0.9\text{BaO}-\text{Al}_2\text{O}_3-\text{B}_2\text{O}_3$  is increased in comparison to sample  $\text{BaO}-\text{Al}_2\text{O}_3-\text{B}_2\text{O}_3$ , i.e. the volume fraction of the crystalline phase is higher.

At temperatures less than approximately  $700\text{ }^\circ\text{C}$ , the crystal growth velocity is too small and the derivatives decrease again. While at cooling rates in the range of  $0.5$  to  $2\text{ K/min}$ , the derivatives at  $600\text{ }^\circ\text{C}$  are all in a range from  $2.00$  to  $2.80\text{ eV}$ , those at a cooling rate of  $0.167\text{ K/min}$  are smaller,  $0.40$  to  $0.50\text{ eV}$ . Obviously, the derivatives at higher cooling rates are predominantly attributed to the conductivity of the liquid phase, while those of the smallest cooling rate are attributed to the crystalline phase at



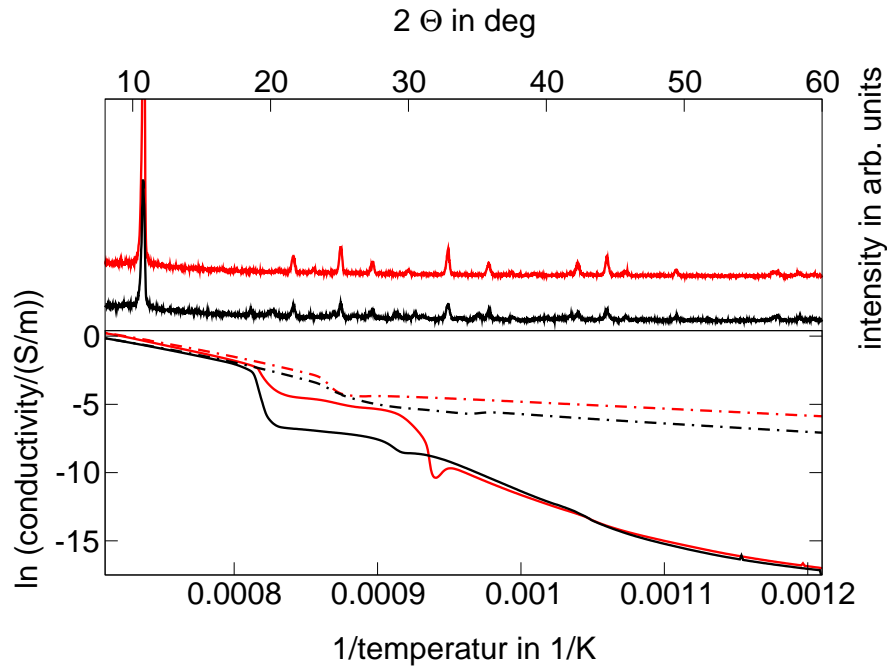


Figure 6.13: Comparison of the XRD patterns and the Arrhenius plots of the specific conductivities of the samples  $\text{BaO} - \text{Al}_2\text{O}_3 - \text{B}_2\text{O}_3$  (black) and  $0.9\text{BaO} - \text{Al}_2\text{O}_3 - \text{B}_2\text{O}_3$  (red); solid line: heating, dash dotted line: cooling.

temperatures below  $700^\circ\text{C}$ .

Minima in the derivative are only seen at a cooling rate of  $0.167\text{ K/min}$ . These minima are attributed to a fast phase transition, possibly between two allotropes of  $\text{BaAl}_2\text{B}_2\text{O}_7$ . In numerous thermal treatments it was tried to get the high temperature allotrope to determine its structure. At first, the glasses were crystallised starting at high temperature, cooling them down and removing them out of the furnace before the phase transition temperature, between  $800$  and  $860^\circ\text{C}$ , was reached. The sample was fast cooled to freeze the high temperature state. These experiments were not successful, the rhombohedral phase was always found after cooling. The cooling might not be fast enough to get the high temperature form of  $\text{BaAl}_2\text{B}_2\text{O}_7$ . Therefore, the experimental parameters were changed. At first, the glass was crystallised using the standard thermal treatment (see section 4.2) and according to the XRD analysis, the sample was heat treated again at  $900^\circ\text{C}$  for 24 h. This experiment was carried out with the sample  $0.9\text{BaO} - \text{Al}_2\text{O}_3 - \text{B}_2\text{O}_3$  which forms a high amount of crystalline phase using the standard thermal treatment. So the formation of other crystalline phases from the residual glassy phase would be minimised and phase transition should occur instead.

In Fig. 6.14, the XRD patterns of the glass-ceramics of  $0.9\text{BaO} - \text{Al}_2\text{O}_3 - \text{B}_2\text{O}_3$  with different thermal histories are shown. The glass-ceramics, treated with the standard

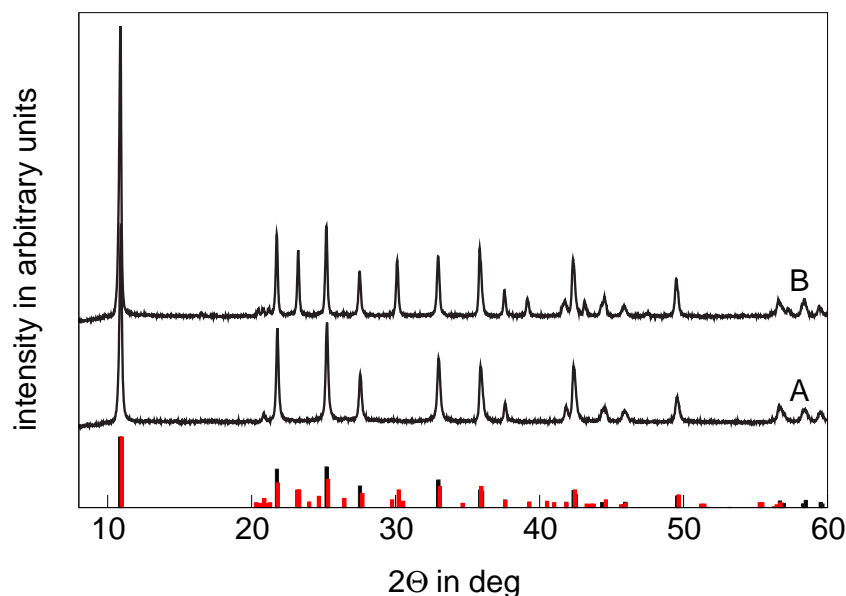


Figure 6.14: XRD patterns of the glass-ceramics  $0.9 \text{ BaO} - \text{Al}_2\text{O}_3 - \text{B}_2\text{O}_3$  with different thermal histories (A:  $720^\circ \text{C}$ , 24 h and  $780^\circ \text{C}$ , 8 h, B: sample A again at  $900^\circ \text{C}$ , 24 h) and the line pattern of the  $\text{BaAl}_2\text{B}_2\text{O}_7$  crystalline phases (black: rhombohedral (JCPDS 86-2168), red: monoclinic (JCPDS 29-0144)).

thermal treatment, show the peaks of the rhombohedral crystalline phase  $\text{BaAl}_2\text{B}_2\text{O}_7$  (JCPDS 86-2168). A further thermal treatment at  $900^\circ \text{C}$  for 24 h results in a glass-ceramics crystallised with the monoclinic phase of  $\text{BaAl}_2\text{B}_2\text{O}_7$  (JCPDS 29-0144). These experiments show the monoclinic phase as the high temperature modification, while the rhombohedral phase of  $\text{BaAl}_2\text{B}_2\text{O}_7$  (JCPDS 86-2168) is the low temperature modification.

The changes during heating are more complex. In the initially amorphous samples, first maxima in the derivatives are observed at temperatures between  $670$  and  $730^\circ \text{C}$ . In all studied samples, these maxima are shifted to higher temperatures while increasing the heating rate. The derivatives observed at temperatures below  $670^\circ \text{C}$  are in the same range as those observed during cooling, except at a cooling rate of  $0.167 \text{ K/min}$ , and are attributed to the glassy state. At both compositions, the derivatives are independent from the heating rate within a small temperature range from  $730$  to  $770^\circ \text{C}$  and hence, should be related to the same state. In sample  $0.9 \text{ BaO} - \text{Al}_2\text{O}_3 - \text{B}_2\text{O}_3$ , a second peak is observed at temperatures between  $770$  and  $900^\circ \text{C}$ , while this peak only occurs at a heating rate of  $0.167 \text{ K/min}$  in sample  $\text{BaO} - \text{Al}_2\text{O}_3 - \text{B}_2\text{O}_3$ . This second maximum could be assigned to crystallisation, as shown by the comparison with the DTA measurement of sample  $0.9 \text{ BaO} - \text{Al}_2\text{O}_3 - \text{B}_2\text{O}_3$  (see Fig. 6.10). At temperatures of around  $950^\circ \text{C}$ , the third maximum is observed. Since the derivatives and conductivities are independent from the heating rates at temperatures larger than  $1100^\circ \text{C}$ , the third peak can be attributed

to the melting of the crystalline phase. These melting peaks get more resolved with smaller heating rates, indicating that the volume fraction of crystalline phase is larger supplying smaller heating rates. This is also correlated to the minimum observed in the range from 800 to 900 °C, which indicates the activation energy of the conductivity of the crystalline phase. The maxima as well as the minima are both indications for the crystallisation process as will be explained later. The minimum is shifted to higher temperatures with increasing heating rate. Obviously, the crystallisation kinetics are decisive because the minimum is attributed to a given volume fraction of crystalline phase. At infinitely fast crystallisation kinetics, the occurrence of the minimum should be heating rate independent. Furthermore, the less resolved melting peak at larger heating rates, e.g. sample 0.9 BaO - Al<sub>2</sub>O<sub>3</sub> - B<sub>2</sub>O<sub>3</sub> with 2 K/min, occurs because of a temperature gap between the inner region of the sample and the thermocouple. The sample starts to melt at the alumina spacer and at the platinum disks which gives the first peak. But inside the sample, the crystalline phase still remains, because a temperature gradient occurs. Further heating results in the melting of the whole sample and the formation of the second peak at higher temperatures.

The effect of the sample composition on the conductivity can be summarised as follows: sample 0.9 BaO - Al<sub>2</sub>O<sub>3</sub> - B<sub>2</sub>O<sub>3</sub> crystallises more rapidly during heating and cooling. This is illustrated by the larger amplitudes of the maxima and minima in the derivatives during heating and cooling as shown in Fig. 6.9.

The activation energy of the conductivity of the glassy state is affected by the temperature. For sample BaO - Al<sub>2</sub>O<sub>3</sub> - B<sub>2</sub>O<sub>3</sub>, it changes from 3.80 to 1.70 eV during cooling from 700 to 550 °C. This effect may be caused by a change of the glass structure. A possible explanation might be the change in coordination of boron and aluminum. Such changes cannot be proved by impedance measurements. Another reason might be the occurrence of a phase separation, which should be detectable by TEM or AFM measurements. These possibilities are discussed in the next sections. The activation energy of the conductivity of the crystalline phase is 0.45 eV. This leads to larger conductivities of the crystallised samples at lower temperatures. At temperatures larger than 850 °C ( $T_x$ ), the specific conductivity of the glassy sample should be larger than that of the fully crystallised one. Depending on the heating rate, crystallisation of the glassy sample occurs at temperatures in the range from 780 to 870 °C. This means that the crystallisation may occur at temperatures at which the specific conductivity of the crystalline phase is larger or smaller than of the glassy phase.

In the next part of the section, the schematic evaluation of the conductivity measure-

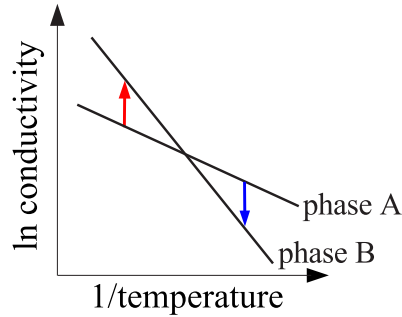


Figure 6.15: Schematic explanation of the derivative of phase transitions phase A into phase B (blue and red line).

ments is illustrated. The derivative of a phase transition may result in a positive (red) or negative peak (blue) as shown in Fig. 6.15. Whether a positive or negative peak is observed depends on the temperature at which the phase transition occurs (blue or red line) and the conductivity of the respective phases. The phase transition at lower temperatures (in the scheme blue line) would result in a negative peak in the derivative.

In Fig. 6.16, schematic plots of the specific conductivities and the respective derivatives are illustrated. At temperatures  $> 950$  °C, the sample is thermodynamically stable (range I in Fig. 6.16). Crystallisation during cooling occurs at temperatures  $\leq 900$  °C (range III). Here, the conductivity of the glassy state is larger than that of the crystalline one. Hence, the conductivity decreases more strongly than it would be the case without crystallisation and the derivative is larger than that of the activation energy of the glassy phase. This condition results in a maximum of the derivative. If the sample crystallises completely, the conductivity matches that of the crystalline phase and the activation energy decreases to 0.45 eV attributed to the crystalline phase. The crystalline phase has an Arrhenius activated conductivity mechanism which temperature dependence is described by an activation energy. At further decreasing temperature, a phase transition occurs. The new crystalline phase has a larger specific conductivity. Hence, the conductivity increases and the derivative has a minimum. If the cooling rate is larger, the crystallisation occurs at lower temperatures. If crystallisation occurs below  $T_x$  (see Fig. 6.16, part (a)), the conductivity would increase during crystallisation and the derivative would be negative. However, this is not observed. As schematically shown in Fig. 6.16, the following is observed at a larger cooling rate: the conductivity deviates from that of the glassy sample at lower temperatures, reaches a maximum in the derivative at temperatures  $> T_x$ , but continues to crystallise below  $T_x$  which results in a minimum of the derivative. The conductivity is somewhat larger than that of the glassy phase, due to a small contribution of the crystalline phase; a phase transition cannot be observed in the conductivity

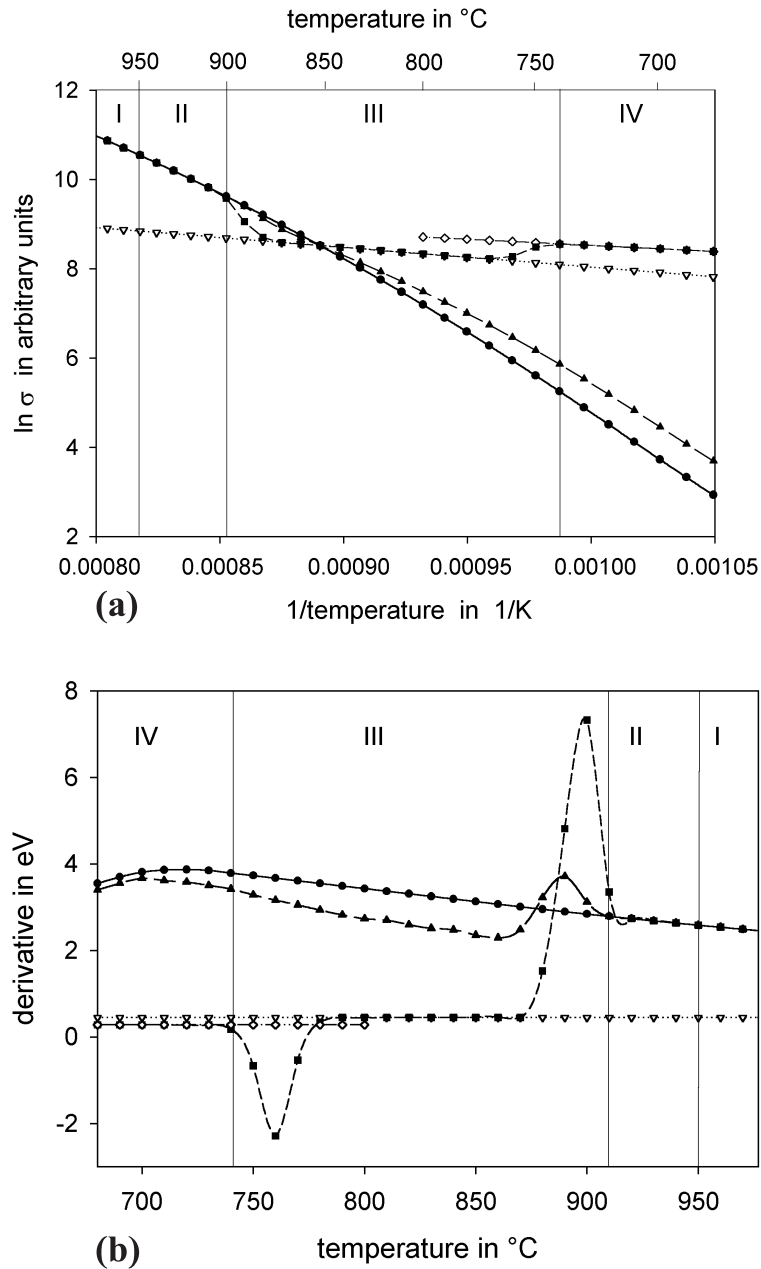


Figure 6.16: (a) Schematic plot of the specific conductivity during cooling. (b) Schematic plot of the derivative ( $-\text{d} \ln \sigma / \text{d}(1/kT)$ ) during cooling; (●): glass melt, (▽): crystalline phase I, (◇): crystalline phase II, (▲): fast cooling and (■): slow cooling.

measurements.

The changes during heating are schematically shown in Fig. 6.17. Below 740 °C, the conductivity and the activation energy are attributed to the liquid state at temperatures  $> T_g$  (range IV). At a smaller heating rate, the crystallisation occurs in the temperature range III and starts below  $T_x$  (850 °C). Here, the conductivity increases at a higher rate than that of the glassy phase. Hence, the derivative has a maximum and then decreases to the activation energy of the crystalline phase. At larger heating rates, the

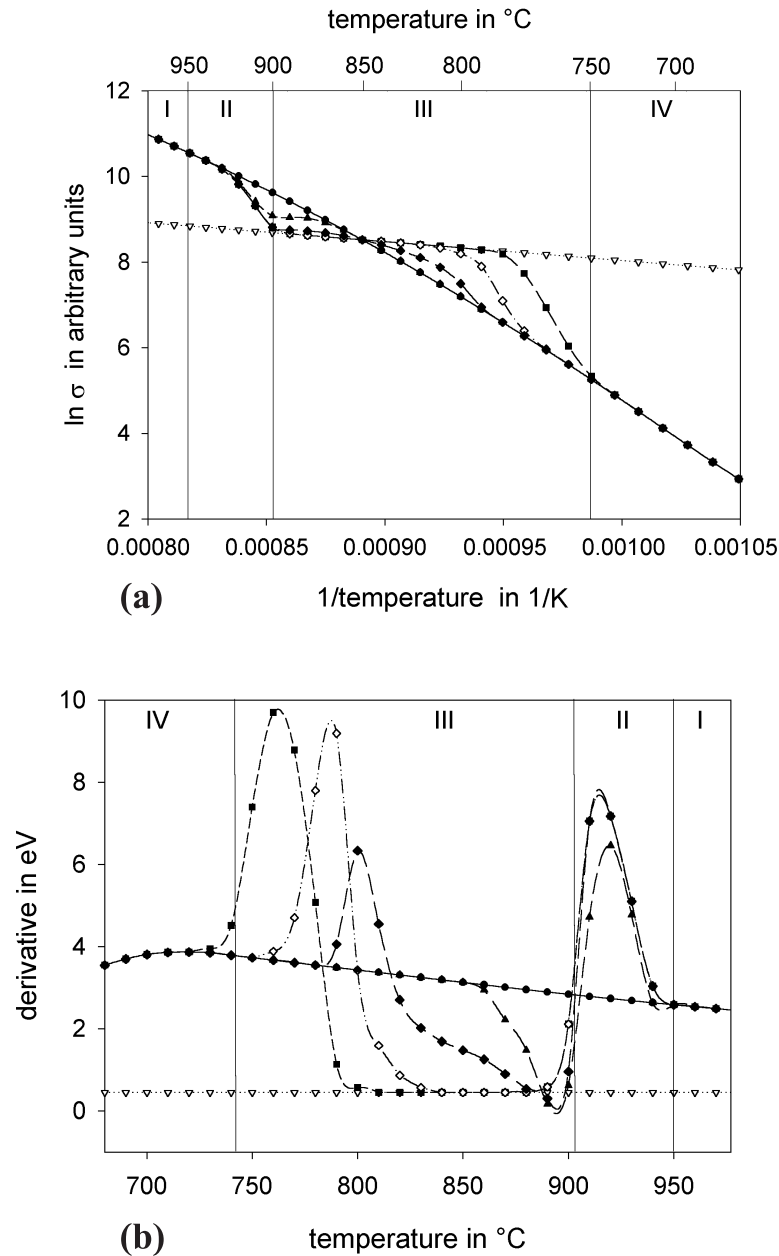


Figure 6.17: (a) Schematic plot of the specific conductivity during heating. (b) Schematic plot of the derivative  $(-d\ln\sigma/d(1/kT))$  during cooling; (●): glass melt, (▽): crystalline phase II, (▲): very fast heating, (◆): fast heating, (◇): moderate heating and (■): slow heating.

crystallisation starts at a higher temperature, therefore the increase in the derivative is not as large as in the case of smaller heating rates. Above  $T_x$ , the crystallisation process continues and a minimum is observed; here the derivative might be smaller than that of the crystalline sample and even negative. As shown in Fig. 6.17, part (b), at large enough heating rates, a maximum is not observed, however, the minimum still occurs. Using smaller heating rates, the crystallisation is completed at temperatures between 800 and



900 °C; the conductivity and the derivative are equal to those of the crystalline phase. At higher temperature (> 900 °C), the melting process starts (range II) and hence, the conductivity increases again more strongly than that of the glassy sample, i.e. another maximum is seen in the derivative. In the experiment, this temperature should be slightly shifted to higher temperatures due to the limited thermal conductivity of the sample and the experimental setup. With increasing heating rates only partial crystallisation occurs. Then, also the maximum, due to the melting process, is not as evident as in the case of smaller heating rates. If the melting process is completed, the derivative is again equal to that of the glassy sample; the sample is in a thermodynamic equilibrium (range I).

## 6.5 Influence of MgO and Li<sub>2</sub>O additions on the miscibility gap and the conductivity of the melt

The following sections present the conductivity measurements of glasses which were melted with the additives MgO or Li<sub>2</sub>O to change a possible miscibility gap. If a phase separation occurs before crystallisation, it can be detected by conductivity measurements [17, 18]. The tendency to phase separation can be changed by small concentration of additives. MgO should open the miscibility gap, while Li<sub>2</sub>O should close it [67, 68]. In previous investigations, it was assumed that Ba<sup>2+</sup> is the charge carrier responsible for the conductivity. In Li<sub>2</sub>O containing glasses, however, Li<sup>+</sup> should dominate Ba<sup>2+</sup> according to its higher mobility; therefore it should be possible to assign the phenomena which are caused by the Ba<sup>2+</sup> ions.

Table 6.1 gives an overview on the chemical compositions of the base glasses BaO-Al<sub>2</sub>O<sub>3</sub>-B<sub>2</sub>O<sub>3</sub> and 0.9BaO-Al<sub>2</sub>O<sub>3</sub>-B<sub>2</sub>O<sub>3</sub> as well as the derived glasses with MgO and Li<sub>2</sub>O additions, which were used for the conductivity measurements.

Table 6.1: Chemical composition of the base glasses BaO-Al<sub>2</sub>O<sub>3</sub>-B<sub>2</sub>O<sub>3</sub> and 0.9BaO-Al<sub>2</sub>O<sub>3</sub>-B<sub>2</sub>O<sub>3</sub> as well as the glasses with MgO and Li<sub>2</sub>O addition.

Sample name	BaO in mol%	Al <sub>2</sub> O <sub>3</sub> in mol%	B <sub>2</sub> O <sub>3</sub> in mol%	MgO in mol%	Li <sub>2</sub> O in mol%
0.9 BaO - Al <sub>2</sub> O <sub>3</sub> - B <sub>2</sub> O <sub>3</sub>	31.0	34.5	34.5	-	-
0.1 MgO - 0.8 BaO - Al <sub>2</sub> O <sub>3</sub> - B <sub>2</sub> O <sub>3</sub>	27.6	34.5	34.5	3.4	-
1.0 BaO - Al <sub>2</sub> O <sub>3</sub> - B <sub>2</sub> O <sub>3</sub>	33.3	33.3	33.3	-	-
0.1 Li <sub>2</sub> O - 0.9 BaO - Al <sub>2</sub> O <sub>3</sub> - B <sub>2</sub> O <sub>3</sub>	30.0	33.3	33.3	-	3.3
0.2 Li <sub>2</sub> O - 0.8 BaO - Al <sub>2</sub> O <sub>3</sub> - B <sub>2</sub> O <sub>3</sub>	26.7	33.3	33.3	-	6.7

### 6.5.1 0.1 MgO - 0.8 BaO - Al<sub>2</sub>O<sub>3</sub> - B<sub>2</sub>O<sub>3</sub>

Magnesium oxide was added to the glass 0.9 BaO - Al<sub>2</sub>O<sub>3</sub> - B<sub>2</sub>O<sub>3</sub> in order to increase a possible miscibility gap.

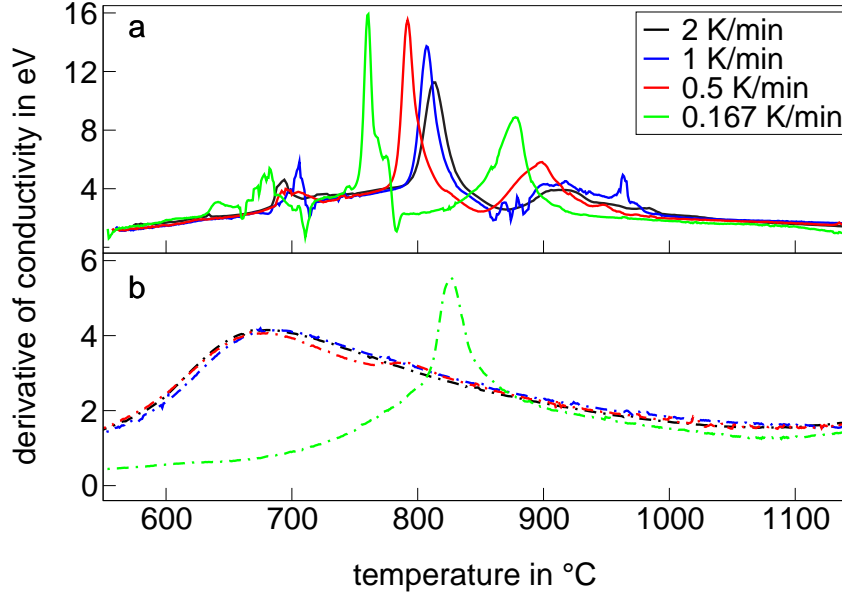


Figure 6.18: Derivatives of the specific conductivities ( $-\text{dln}\sigma/\text{d}(1/kT)$ ) of the sample 0.1 MgO - 0.8 BaO - Al<sub>2</sub>O<sub>3</sub> - B<sub>2</sub>O<sub>3</sub> during a: heating and b: cooling.

In Fig. 6.18, the derivatives ( $-\text{dln}\sigma/\text{d}(1/kT)$ ) of sample 0.1 MgO - 0.8 BaO - Al<sub>2</sub>O<sub>3</sub> - B<sub>2</sub>O<sub>3</sub> are shown for different heating and cooling rates. First, the changes during cooling will be described. In analogy to the base samples, the derivatives slightly increase and are approximately similar for all supplied cooling rates in the temperature range from 1150 to 880 °C. The derivative of the sample with a cooling rate of 0.167 K/min is slightly smaller than the other cooling rates, but the difference is within the limits of error. While further decreasing the temperatures, a positive peak at 828 °C is observed in the derivative at a cooling rate of 0.167 K/min. At a cooling rate of 0.5 K/min, this peak is shifted to lower temperatures (790 °C) with a strong decrease in amplitude. With further increasing the cooling rate (1 and 2 K/min), the positive peak completely disappears. At a cooling rate of 0.167 K/min, the derivative slowly decreases up to 650 °C and remains almost constant in the range of 0.60 to 0.46 eV while further decreasing the temperature. Larger cooling rates of 0.5, 1 and 2 K/min result in a broad maximum (4.00 eV) at 670, 690 and 680 °C, respectively.

During heating, for all heating rates, the derivatives increase from 1.20 eV at 550 °C to 2.00 eV at 625 °C. Further heating results in a peak, which is shifted to higher temperatures with increasing heating rate, except 2 K/min (0.167 K/min: 680 °C, 0.5 K/min:

695 °C, 1 K/min: 706 °C, 2 K/min: 695 °C). However, this peak is not well resolved and the amplitude is independent of the heating rate. At larger heating rates (0.5 to 2 K/min), the derivatives are again equal in the temperature range from 725 to 770 °C. The sample with a heating rate of 0.167 K/min shows, after the first peak, a small negative peak at 710 °C and a maximum at 760 °C. This maximum is shifted to higher temperatures and declines in amplitude with increasing heating rate (0.5 K/min: 793 °C, 1 K/min: 808 °C, 2 K/min: 814 °C). Further increase of the temperature results in another peak. While the peak is well resolved for a heating rate of 0.167 K/min (at 878 °C), it is spreaded over a wider temperature range with increasing heating rate. At temperatures above 1030 °C, the derivatives and also the conductivities are the same within the limits of error for all heating and cooling rates supplied.

XRD patterns were used to identify crystalline phases as well as to gain an approximate idea on the amount of crystalline phases. At a cooling rate of 2 K/min, the crystalline phase BaMgAl<sub>10</sub>O<sub>17</sub> (JCPDS 26-0163) is detected with very low intensities, i.e. the major part of the sample is still amorphous. With decreasing cooling rate (1 K/min), the crystalline phase BaAl<sub>2</sub>B<sub>2</sub>O<sub>7</sub> (JCPDS 86-2168) starts to become detectable (beside BaMgAl<sub>10</sub>O<sub>17</sub> (JCPDS 26-0163)). The smaller the cooling rate (0.5 and 0.167 K/min), the more resolved are the XRD patterns and the larger are the intensities of the crystalline phase BaAl<sub>2</sub>B<sub>2</sub>O<sub>7</sub> (JCPDS 86-2168). According to the XRD patterns, the amount of the crystalline phase BaMgAl<sub>10</sub>O<sub>17</sub> (JCPDS 26-0163) is cooling rate independent and is negligible in comparison to the main crystalline phase BaAl<sub>2</sub>B<sub>2</sub>O<sub>7</sub> (JCPDS 86-2168).

### 6.5.2 0.1 Li<sub>2</sub>O - 0.9 BaO - Al<sub>2</sub>O<sub>3</sub> - B<sub>2</sub>O<sub>3</sub>

BaO - Al<sub>2</sub>O<sub>3</sub> - B<sub>2</sub>O<sub>3</sub> was the initial composition for the following investigations. Now, BaO was partially replaced by Li<sub>2</sub>O, which was added to the batch as lithium carbonate. The exact chemical composition of the glass 0.1 Li<sub>2</sub>O - 0.9 BaO - Al<sub>2</sub>O<sub>3</sub> - B<sub>2</sub>O<sub>3</sub> is listed in Table 6.1 at page 83. According to the high mobility of Li<sup>+</sup> in comparison to Ba<sup>2+</sup> ions [69], the charge is assumed to be carried by Li<sup>+</sup> ions. Therefore it might be possible to separate the phenomena which might occur through the Ba<sup>2+</sup> ions. Figure 6.19 presents a scheme of a possible conduction mechanism in presence of both Ba<sup>2+</sup> and Li<sup>+</sup>. The measurements can be evaluated under the assumption of a Ba<sup>2+</sup>-Li<sup>+</sup> parallel circuit. Indeed, the Li<sup>+</sup> ions move faster than the Ba<sup>2+</sup> ions, because of the lower charge and smaller size. Hence, if the Ba<sup>2+</sup> ions are the charge carriers in the melt BaO - Al<sub>2</sub>O<sub>3</sub> - B<sub>2</sub>O<sub>3</sub>, then the Li<sup>+</sup> would at least partially carry the charge in the melt 0.1 Li<sub>2</sub>O - 0.9 BaO - Al<sub>2</sub>O<sub>3</sub> - B<sub>2</sub>O<sub>3</sub>. Another aspect of Li<sub>2</sub>O as additive is the diminution of a possible miscibility gap in the investigated

system.

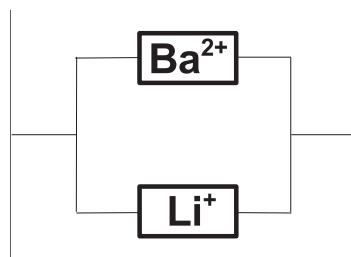


Figure 6.19: Scheme of the parallel circuit  $\text{Ba}^{2+} / \text{Li}^{+}$  ions.

In Fig. 6.20, the derivatives of the sample  $0.1 \text{Li}_2\text{O} - 0.9 \text{BaO} - \text{Al}_2\text{O}_3 - \text{B}_2\text{O}_3$  are plotted for different heating and cooling rates. In contrast to sample  $\text{BaO} - \text{Al}_2\text{O}_3 - \text{B}_2\text{O}_3$ , during cooling, an increase in the derivatives at 1 and 2 K/min from 1.40 to 2.50 eV is observed within the temperature range from 1150 to 690 °C. Further decreasing the temperature down to 550 °C results in a decrease of the derivative to 2.30 eV. At cooling rates of 0.5 and 0.167 K/min, the derivatives have approximately the same shape as the curves at cooling rates of 1 and 2 K/min down to 850 °C. Below 850 °C, the derivatives at cooling rates of 0.5 and 0.167 K/min show a maximum, which is shifted to lower temperatures and it diminishes in amplitude with increasing cooling rates (0.5 K/min: 820 °C, 0.167 K/min: 832 °C). At a cooling rate of 0.167 K/min, a minimum occurs at 790 °C. While further decreasing the temperature, the derivative remains almost constant (0.65 eV), except for a small peak at 625 °C. On the other hand, at a cooling rate of 0.5 K/min, the minimum is shifted to 780 °C and is less pronounced. Further decreasing the temperature (< 780 °C) results in an increase of the derivative at a cooling rate of 0.5 K/min to 2.50 eV. Below 635 °C, the derivative has the same shape and position as the derivatives at cooling rates of 1 and 2 K/min.

During heating, the derivatives possess a constant value of 2.00 eV for all applied rates up to a temperature of 670 °C. Further heating results in a positive peak, which is shifted to higher temperatures and it declines strongly in amplitude with increasing heating rates (0.167 K/min: 697 °C, 0.5 K/min: 745 °C). At a heating rate of 1 K/min, only a low intensity peak can be observed at 765 °C and does not appear at a rate of 2 K/min. The derivative at a heating rate of 0.167 K/min shows after the first peak a small negative peak at 740 °C, a high maximum at 775 °C and in the temperature range from 790 to 850 °C, a broad minimum ( $\approx 0.40$  eV). Above 850 °C, the derivative increases again and another positive peak at 909 °C with two shoulders at 880 and 895 °C is observed. The maximum at 775 °C (0.167 K/min) is strongly shifted to higher temperatures with increasing heating rates (0.5 K/min: double peak at 831 and 848 °C, 1 K/min: 877 °C,

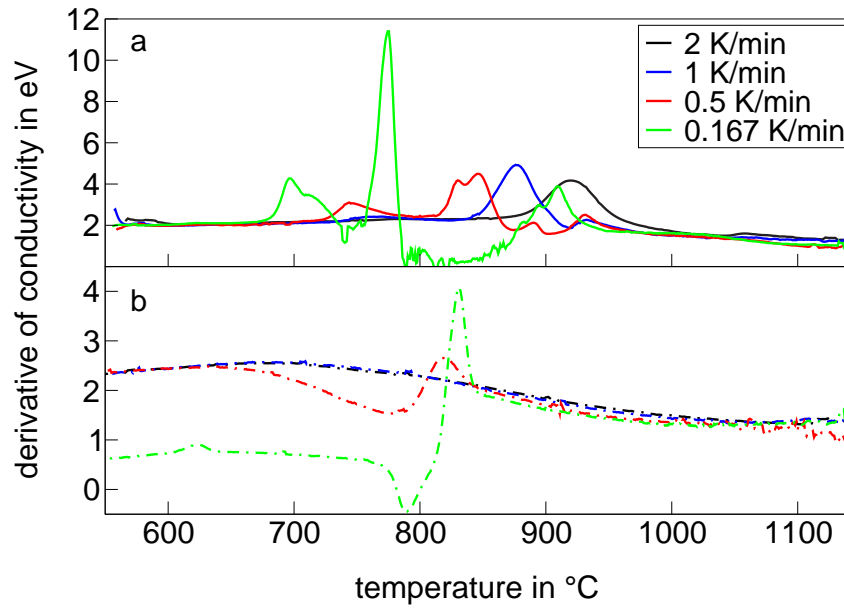


Figure 6.20: Derivatives of the specific conductivities ( $-\ln\sigma/d(1/kT)$ ) of the sample  $0.1 \text{ Li}_2\text{O} - 0.9 \text{ BaO} - \text{Al}_2\text{O}_3 - \text{B}_2\text{O}_3$  during a: heating and b: cooling.

2 K/min: 922 °C). At a heating rate of 2 K/min only this peak at 922 °C was observed, while the derivatives at heating rates of 0.5 and 1 K/min show small positive peaks (0.5 K/min: 890 °C, 930 °C; 1 K/min: 935 °C). At temperatures above 1000 °C, the derivative and also the conductivity are in good agreement (within the limits of error) for all heating and cooling rates supplied.

The XRD patterns should give informations about the type of crystalline phase in the samples after completing the measurement as well as an approximate amount of the crystalline phase. At cooling rates of 1 and 2 K/min the samples are amorphous. The smaller the cooling rates (0.5 and 0.167 K/min) the more resolved are the XRD patterns; the lines observed could be attributed to the crystalline phase  $\text{BaAl}_2\text{B}_2\text{O}_7$  (JCPDS 86-2168).

### 6.5.3 0.2 Li<sub>2</sub>O - 0.8 BaO - Al<sub>2</sub>O<sub>3</sub> - B<sub>2</sub>O<sub>3</sub>

The glass  $0.2 \text{ Li}_2\text{O} - 0.8 \text{ BaO} - \text{Al}_2\text{O}_3 - \text{B}_2\text{O}_3$  was obtained through further substitution of BaO by Li<sub>2</sub>O in the composition  $\text{BaO} - \text{Al}_2\text{O}_3 - \text{B}_2\text{O}_3$ . In this way, the effects assigned to the charge carrier  $\text{Ba}^{2+}$  should be further diminished.

The derivatives of sample  $0.2 \text{ Li}_2\text{O} - 0.8 \text{ BaO} - \text{Al}_2\text{O}_3 - \text{B}_2\text{O}_3$  for different heating and cooling rates are plotted as a function of the temperature in Fig. 6.21. At first, the behaviour of the samples during cooling will be described. In analogy to glass  $0.1 \text{ Li}_2\text{O} - 0.9 \text{ BaO} - \text{Al}_2\text{O}_3 - \text{B}_2\text{O}_3$ , the derivatives slightly increase and are approximately equal within

the limits of error for cooling rates of 1 and 2 K/min in the temperature range from 1150 to 630 °C. Below 630 °C, the derivatives at cooling rates of 1 and 2 K/min remain almost constant (2.35 eV). At a cooling rate of 0.5 K/min, the derivative has the same shape as those at 1 and 2 K/min, but small positive and negative peaks were observed at 770 and 734 °C, respectively. With decreasing the cooling rate (0.167 K/min), the derivative in the temperature range from 1150 to 800 °C is slightly shifted to a smaller activation energy, but shows a similar shape as at the other cooling rates. At 770 °C, a positive peak is also observed in the sample cooled with 0.167 K/min, however, the amplitude is much larger than using a cooling rate of 0.5 K/min. Further decreasing the temperature at a cooling rate of 0.167 K/min results, within the limits of error, in almost constant derivative (1.10 eV).

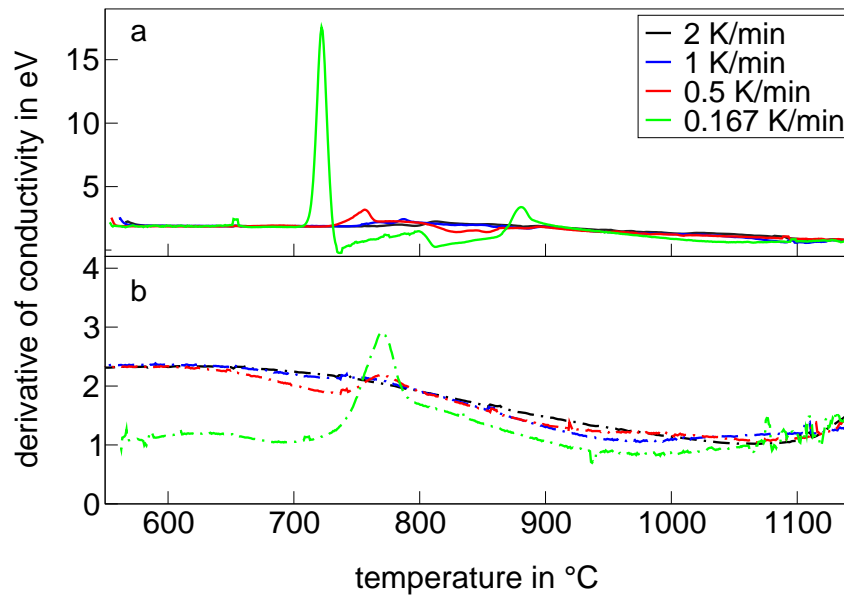


Figure 6.21: Derivatives of the specific conductivities ( $-\text{dln}\sigma/\text{d}(1/kT)$ ) of the sample  $0.2\text{Li}_2\text{O}-0.8\text{BaO}-\text{Al}_2\text{O}_3-\text{B}_2\text{O}_3$  during a: heating and b: cooling.

During heating, the shape of the derivatives are much simpler in comparison to the samples previously described. At heating rates of 1 and 2 K/min, the derivative is approximately constant ( $\approx 1.80$  eV) in the temperature range from 550 to 900 °C and declines slowly at higher temperatures (0.72 eV). In the temperature range from 550 to 705 °C, the derivatives at heating rates of 0.167 and 0.5 K/min are also equal to the other heating rates. At a heating rate of 0.167 K/min, a maximum occurs at 723 °C, which is shifted to a higher temperature and declines strongly in amplitude for a heating rate of 0.5 K/min (758 °C). In the temperature range from 730 to 870 °C, the derivative at a heating rate of 0.167 K/min is significantly below the curves attributed to larger heating rates and show a small positive peak at 800 °C, which, however, remains still below the activation

energies at other heating rates. Further heating with a rate of 0.167 K/min results in another small positive peak at 880 °C. At a heating rate of 0.5 K/min, the derivative decreases slightly below the derivatives at heating rates of 1 and 2 K/min and has the same value above 865 °C. At temperatures above 900 °C, the derivative and the conductivity are almost the same for all heating and cooling rates supplied.

The XRD patterns were also used for this sample to identify crystalline phases as well as to have an approximate idea about the quantity of crystalline phases in the heat treated samples. At cooling rates of 1 and 2 K/min, the samples are mainly amorphous and the lines of the crystalline phases  $\text{BaAl}_2\text{B}_2\text{O}_7$  (JCPDS 86-2168) and  $\text{LiAl}_5\text{O}_8$  (JCPDS 38-1425) have very low intensities. The smaller the cooling rate, the more resolved are the XRD patterns, i.e., the crystallinity of the sample after cooling with a rate of 0.167 K/min is larger than that of the sample with 0.5 K/min. Both samples contain the same crystalline phases:  $\text{BaAl}_2\text{B}_2\text{O}_7$  (JCPDS 86-2168) and  $\text{BaAl}_{12}\text{O}_{19}$  (JCPDS 14-0107) which shows lines of very low intensity in the XRD patterns.

#### 6.5.4 Summary of the conductivity measurements

The results of the conductivity measurements are summarised to compare the base glasses and glasses with  $\text{Li}_2\text{O}$  or  $\text{MgO}$  addition. In section 6.4, the achieved peaks were assigned to the processes of crystallisation or, however, to the melting of a crystalline phase. By analogy to these results, the liquidus and crystallisation temperature during heating as well as during cooling using a rate of 0.167 K/min are presented in Table 6.2 for all investigated samples.

Table 6.2: Crystallisation ( $T_C$ ) and liquidus temperatures ( $T_L$ ) as well as the crystalline phases formed during the conductivity measurements for all investigated samples.

Sample name	$T_L$ in °C up 0.167 K/min	$T_C$ in °C up 0.167 K/min	$T_C$ in °C down 0.167 K/min	XRD
0.9BaO- $\text{Al}_2\text{O}_3$ - $\text{B}_2\text{O}_3$	949	795	884	$\text{BaAl}_2\text{B}_2\text{O}_7$
0.1MgO-0.8BaO- $\text{Al}_2\text{O}_3$ - $\text{B}_2\text{O}_3$	879	761	827	$\text{BaAl}_2\text{B}_2\text{O}_7$ , $\text{BaMgAl}_{10}\text{O}_{17}$
BaO- $\text{Al}_2\text{O}_3$ - $\text{B}_2\text{O}_3$	951	825	883	$\text{BaAl}_2\text{B}_2\text{O}_7$
0.1 $\text{Li}_2\text{O}$ -0.9BaO- $\text{Al}_2\text{O}_3$ - $\text{B}_2\text{O}_3$	910	775	832	$\text{BaAl}_2\text{B}_2\text{O}_7$
0.2 $\text{Li}_2\text{O}$ -0.8BaO- $\text{Al}_2\text{O}_3$ - $\text{B}_2\text{O}_3$	880	723	770	$\text{BaAl}_2\text{B}_2\text{O}_7$ , $\text{BaAl}_{12}\text{O}_{19}$



Overall, the liquidus as well as the crystallisation temperatures are shifted to lower temperatures through the addition of  $\text{Li}_2\text{O}$  or  $\text{MgO}$ . On the other hand, the main crystalline phase which crystallises during cooling of the samples is still  $\text{BaAl}_2\text{B}_2\text{O}_7$  (JCPDS 86-2168). Other crystalline phases which are also listed in Table 6.2 appear only with very low intensity in the XRD patterns. In the next section, the results of all investigated samples will be compared more deeply and discussed with respect to the still unknown effect in the derivatives of the conductivity measurement.

### 6.5.5 Discussion - Conductivity measurements of glasses with the additions of $\text{Li}_2\text{O}$ or $\text{MgO}$

In this section the results of the conductivity measurements of the base glasses and of the glasses with the additions of  $\text{Li}_2\text{O}$  or  $\text{MgO}$  will be compared and discussed. At first, the proposed changes of a possible miscibility gap due to the additives  $\text{MgO}$  and  $\text{Li}_2\text{O}$  should be explained in more detail. The base glasses consist of the oxides  $\text{BaO}$ ,  $\text{Al}_2\text{O}_3$  and  $\text{B}_2\text{O}_3$  in which  $\text{BaO}$  acts as typical network-modifier,  $\text{B}_2\text{O}_3$  as network-former and  $\text{Al}_2\text{O}_3$  as intermediate [70] which has also the function of a network-former in the present glass system. If two or more network-formers are present in one glass system, the tendency to phase separation increases [39]. The addition of  $\text{MgO}$  as well as  $\text{Li}_2\text{O}$  changes the proportion network-former / network-modifier and should simultaneously influence the tendency to immiscibility.  $\text{Li}_2\text{O}$  as network-modifier should close the miscibility gap and decrease the crystallisation temperature [67,68]. On the other hand,  $\text{MgO}$  as intermediate could react as network-former or network-modifier, but it is assumed that  $\text{MgO}$  acts as network-former beside  $\text{B}_2\text{O}_3$  and  $\text{Al}_2\text{O}_3$ , i.e., the miscibility gap will increase with the addition of  $\text{MgO}$  [71,72].

From this point of view, the comparison of the impedance measurements of the different glasses will be discussed. In Fig. 6.22, the derivatives of the base glasses and the derived glasses with  $\text{MgO}$  and  $\text{Li}_2\text{O}$  are plotted as a function of the temperature for all supplied heating rates. The patterns of the derivatives are subdivided into three zones marked with I, II and III on top of the figure. In analogy to the former results (see Table 6.2), the zone II is related to the crystallisation and zone III to the melting of a crystalline phase, while the origin of the peaks in zone I will be discussed in this section. The borders of these zones are only schematically fixed, because these zones are shifted to lower temperatures with decreasing heating rates especially in the case of the crystallisation peak.

At first, the known effects of crystallisation and melting will be discussed for the investigated samples and heating rates. At a heating rate of 2 K/min, crystallisation peaks

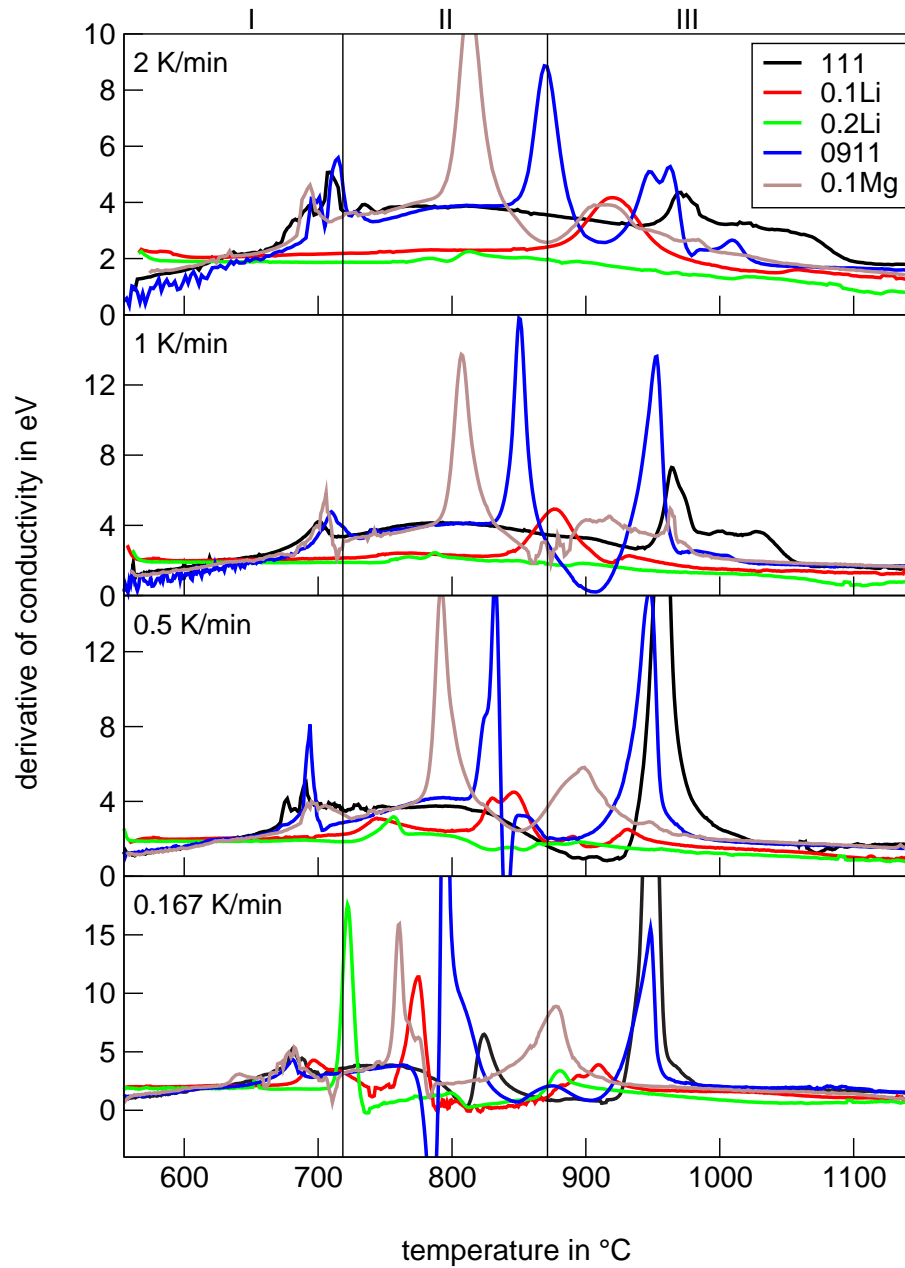


Figure 6.22: Derivatives of the specific conductivities ( $-\ln\sigma/d(1/kT)$ ) of the samples (111):  $\text{BaO}-\text{Al}_2\text{O}_3-\text{B}_2\text{O}_3$ , (0.1Li):  $0.1\text{Li}_2\text{O}-0.9\text{BaO}-\text{Al}_2\text{O}_3-\text{B}_2\text{O}_3$ , (0.2Li):  $0.2\text{Li}_2\text{O}-0.8\text{BaO}-\text{Al}_2\text{O}_3-\text{B}_2\text{O}_3$ , (0911):  $0.9\text{BaO}-\text{Al}_2\text{O}_3-\text{B}_2\text{O}_3$  and (0.1Mg):  $0.1\text{MgO}-0.8\text{BaO}-\text{Al}_2\text{O}_3-\text{B}_2\text{O}_3$  with different heating rates.

can be seen in the derivatives of the base glass  $0.9\text{BaO}-\text{Al}_2\text{O}_3-\text{B}_2\text{O}_3$  at  $870^\circ\text{C}$  and of the MgO containing glass at  $814^\circ\text{C}$ , whereas the other investigated samples do not show crystallisation peaks. It should be noted, that the tendency to crystallisation increases in the glass with the additive MgO, because the crystallisation peak is shifted around  $56\text{K}$  to lower temperature. Further heating of the samples leads to the melting of the crystalline phase, however, not only the samples  $0.9\text{BaO}-\text{Al}_2\text{O}_3-\text{B}_2\text{O}_3$  and

0.1 MgO-0.8 BaO-Al<sub>2</sub>O<sub>3</sub>-B<sub>2</sub>O<sub>3</sub> show a peak, but also the samples BaO-Al<sub>2</sub>O<sub>3</sub>-B<sub>2</sub>O<sub>3</sub> and 0.1 Li<sub>2</sub>O-0.9 BaO-Al<sub>2</sub>O<sub>3</sub>-B<sub>2</sub>O<sub>3</sub>. The derivative of the sample 0.1 Li<sub>2</sub>O-0.9 BaO-Al<sub>2</sub>O<sub>3</sub>-B<sub>2</sub>O<sub>3</sub> shows a well pronounced peak at around 920 °C, while the peaks of the other samples are less resolved, which is due to the formerly discussed temperature gap between the inner region and the borders of the sample (see section 6.4). Due to the absence of a crystallisation peak of sample 0.1 Li<sub>2</sub>O-0.9 BaO-Al<sub>2</sub>O<sub>3</sub>-B<sub>2</sub>O<sub>3</sub>, the peak could be caused by a possible overlapping of crystallisation and melting process. Decreasing the heating rate to 1 K/min, the samples 0.9 BaO-Al<sub>2</sub>O<sub>3</sub>-B<sub>2</sub>O<sub>3</sub> and 0.1 MgO-0.8 BaO-Al<sub>2</sub>O<sub>3</sub>-B<sub>2</sub>O<sub>3</sub> show still a distinct crystallisation peak, whereas the crystallisation temperature is again shifted to lower temperatures for the derivative of the sample with MgO. For the other samples, no peaks were recorded in zone II referring to the crystallisation of a crystalline phase. Further heating results in a decrease of the derivative of the 0.9 BaO-Al<sub>2</sub>O<sub>3</sub>-B<sub>2</sub>O<sub>3</sub> sample to 0.22 eV, while the sample 0.1 MgO-0.8 BaO-Al<sub>2</sub>O<sub>3</sub>-B<sub>2</sub>O<sub>3</sub> shows a value of approximately 1.90 eV. According to former results (see section 6.4), the value of 0.22 eV can be assigned to the activation energy of the crystalline phase BaAl<sub>2</sub>B<sub>2</sub>O<sub>7</sub> (JCPDS 86-2168), i.e., sample 0.9 BaO-Al<sub>2</sub>O<sub>3</sub>-B<sub>2</sub>O<sub>3</sub> consists of a higher amount of the crystalline phase BaAl<sub>2</sub>B<sub>2</sub>O<sub>7</sub> (JCPDS 86-2168) than sample 0.1 MgO-0.8 BaO-Al<sub>2</sub>O<sub>3</sub>-B<sub>2</sub>O<sub>3</sub>. Another difference between these two samples is observed during melting. The sample 0.9 BaO-Al<sub>2</sub>O<sub>3</sub>-B<sub>2</sub>O<sub>3</sub> shows a well resolved melting peak at 953 °C, whereas the addition of MgO results in a decrease of the melting temperature and a less resolved peak shape. In the derivative of sample 0.1 Li<sub>2</sub>O-0.9 BaO-Al<sub>2</sub>O<sub>3</sub>-B<sub>2</sub>O<sub>3</sub>, two positive peaks are visible in zone III at a heating rate of 1 K/min, a well defined one at 878 °C and a much smaller and less resolved one at around 935 °C. These two peaks are assigned to the crystallisation and melting of a crystalline phase as already suggested for a heating rate of 2 K/min. Furthermore, the derivative of sample 0.2 Li<sub>2</sub>O-0.8 BaO-Al<sub>2</sub>O<sub>3</sub>-B<sub>2</sub>O<sub>3</sub> does not show any indication of crystallisation or melting at heating rates of 1 and 2 K/min. In analogy to impedance measurements at heating rates of 1 and 2 K/min, the derivatives of the samples BaO-Al<sub>2</sub>O<sub>3</sub>-B<sub>2</sub>O<sub>3</sub>, 0.9 BaO-Al<sub>2</sub>O<sub>3</sub>-B<sub>2</sub>O<sub>3</sub> and 0.1 MgO-0.8 BaO-Al<sub>2</sub>O<sub>3</sub>-B<sub>2</sub>O<sub>3</sub> show similar shapes. Two peaks could be observed in zone II for sample 0.1 Li<sub>2</sub>O-0.9 BaO-Al<sub>2</sub>O<sub>3</sub>-B<sub>2</sub>O<sub>3</sub>, which could be assigned to the formation of a crystalline phase. On the other hand, sample 0.2 Li<sub>2</sub>O-0.8 BaO-Al<sub>2</sub>O<sub>3</sub>-B<sub>2</sub>O<sub>3</sub> with an even higher concentration of Li<sub>2</sub>O exhibits a very small peak at 760 °C indicating a possible crystallisation as well. Both derivatives of the samples containing Li<sub>2</sub>O also show very small melting peaks in zone III, which results from an incomplete crystallisation. Finally, at a heating rate of 0.167 K/min, all investigated samples show a crystallisation peak in the assigned

zone II and a melting peak in zone III. The crystallisation temperature is shifted to lower temperatures with the addition of MgO or Li<sub>2</sub>O in the order 0.2 Li<sub>2</sub>O - 0.8 BaO - Al<sub>2</sub>O<sub>3</sub> - B<sub>2</sub>O<sub>3</sub> < 0.1 MgO - 0.8 BaO - Al<sub>2</sub>O<sub>3</sub> - B<sub>2</sub>O<sub>3</sub> < 0.1 Li<sub>2</sub>O - 0.9 BaO - Al<sub>2</sub>O<sub>3</sub> - B<sub>2</sub>O<sub>3</sub>, while the sample 0.9 BaO - Al<sub>2</sub>O<sub>3</sub> - B<sub>2</sub>O<sub>3</sub> has a slightly lower crystallisation temperature than sample BaO - Al<sub>2</sub>O<sub>3</sub> - B<sub>2</sub>O<sub>3</sub>. Furthermore, the melting temperature is also lower than in the base glasses, but has approximately the same value as for the glasses with 0.2 Li<sub>2</sub>O or 0.1 MgO and a 30 K higher melting temperature than for 0.1 Li<sub>2</sub>O. At temperatures above 990 °C, the derivatives during heating are the same for the base glasses, however, a slight shift to lower values is observed of adding MgO or Li<sub>2</sub>O in the order 0.1 MgO - 0.8 BaO - Al<sub>2</sub>O<sub>3</sub> - B<sub>2</sub>O<sub>3</sub> > 0.1 Li<sub>2</sub>O - 0.9 BaO - Al<sub>2</sub>O<sub>3</sub> - B<sub>2</sub>O<sub>3</sub> > 0.2 Li<sub>2</sub>O - 0.8 BaO - Al<sub>2</sub>O<sub>3</sub> - B<sub>2</sub>O<sub>3</sub>. This phenomenon is also observed for other heating rates, whereas the temperature, at which the derivatives are almost equal, is shifted to higher values with increasing heating rate.

All investigated samples, except 0.2 Li<sub>2</sub>O - 0.8 BaO - Al<sub>2</sub>O<sub>3</sub> - B<sub>2</sub>O<sub>3</sub> at a heating rate of 0.167 K/min, which show a crystallisation peak in zone II form a small peak in zone I. During heating with a rate of 2 K/min, the derivatives of the base glasses BaO - Al<sub>2</sub>O<sub>3</sub> - B<sub>2</sub>O<sub>3</sub> and 0.9 BaO - Al<sub>2</sub>O<sub>3</sub> - B<sub>2</sub>O<sub>3</sub> as well as the glass with MgO, 0.1 MgO - 0.8 BaO - Al<sub>2</sub>O<sub>3</sub> - B<sub>2</sub>O<sub>3</sub> show peaks in the temperature range from 670 to 730 °C (zone I) and, as already mentioned before, a crystallisation peak in zone II. The glasses with Li<sub>2</sub>O, 0.1 Li<sub>2</sub>O - 0.9 BaO - Al<sub>2</sub>O<sub>3</sub> - B<sub>2</sub>O<sub>3</sub> and 0.2 Li<sub>2</sub>O - 0.8 BaO - Al<sub>2</sub>O<sub>3</sub> - B<sub>2</sub>O<sub>3</sub>, do not exhibit any peaks in the lower as well as the middle temperature range. Another effect is the increase of the curve up to a temperature of 785 °C in case of the glasses BaO - Al<sub>2</sub>O<sub>3</sub> - B<sub>2</sub>O<sub>3</sub>, 0.9 BaO - Al<sub>2</sub>O<sub>3</sub> - B<sub>2</sub>O<sub>3</sub> and 0.1 MgO - 0.8 BaO - Al<sub>2</sub>O<sub>3</sub> - B<sub>2</sub>O<sub>3</sub>. In analogy to the measurements with 2 K/min, the derivatives, at heating rates of 0.5 and 1 K/min, of the base glasses and the glass with MgO increase up to a temperature of 785 °C and show also small peaks in the low temperature range (zone I), while the Li<sub>2</sub>O containing glasses exhibit a constant derivative in zone I. Finally, the derivatives using a heating rate of 0.167 K/min, except sample 0.2 Li<sub>2</sub>O - 0.8 BaO - Al<sub>2</sub>O<sub>3</sub> - B<sub>2</sub>O<sub>3</sub>, show a small peak around 680 °C, which is shifted to a temperature of 700 °C for the sample 0.1 Li<sub>2</sub>O - 0.9 BaO - Al<sub>2</sub>O<sub>3</sub> - B<sub>2</sub>O<sub>3</sub>.

The occurrence of peaks in zone I (always previous to a crystallisation peak in zone II) leads to the conclusion that these peaks can be assigned to the process of phase separation. In analogy to the base glasses, the addition of MgO results in an increased phase separation which is shown in a decreased crystallisation temperature and the tendency to crystallise even at higher heating rates (1 and 2 K/min). On the other hand, the glass 0.1 Li<sub>2</sub>O - 0.9 BaO - Al<sub>2</sub>O<sub>3</sub> - B<sub>2</sub>O<sub>3</sub> exhibits a peak in zone I only at a very low heating rate (0.167 K/min) and the temperature shift indicates the lower tendency of the

sample to phase separation. The effect is more pronounced in sample  $0.2\text{Li}_2\text{O}-0.8\text{BaO}-\text{Al}_2\text{O}_3-\text{B}_2\text{O}_3$ , which does not show any peaks in the derivative at temperatures below the crystallisation peak. A reason could be the shift of the crystallisation to lower temperatures that causes the crystallisation of the glasses before phase separation occurs. These results support the proposed immiscibility of the system.  $\text{Li}_2\text{O}$  closes the miscibility gap, therefore the crystallisation ability of the glass decreases, while  $\text{MgO}$  increases the tendency to phase separation caused by the opening of the miscibility gap. Another difference is the increase of the derivative up to  $800^\circ\text{C}$  and further decrease of the curve for the samples without  $\text{Li}_2\text{O}$ , while the curve of the samples with  $\text{Li}_2\text{O}$  is at one level without much change. These phenomena will be discussed in the next section with the results of the cooling of the samples.

Figure 6.23 presents the derivatives of the base glasses and the derived glasses with  $\text{MgO}$  and  $\text{Li}_2\text{O}$  as a function of the temperature for all supplied cooling rates. During cooling, the derivatives of the different samples are not so complex in comparison to the behaviour during heating, however, the graphs can also be divided into three zones: (I) phase separation, (II) crystallisation and (III) melt.

In zone III, no peaks are observed with any supplied cooling rate, because the samples remain in the state of melt down to  $900^\circ\text{C}$ . On the other hand, the derivative is almost constant in the temperature range from  $1150$  to  $1000^\circ\text{C}$ .

The peaks in zone II can be assigned to the crystallisation during cooling. At a cooling rate of  $2\text{K}/\text{min}$ , crystallisation peaks can not be observed in the derivatives of all investigated samples. The cooling rate of  $2\text{K}/\text{min}$  is too fast for crystallisation of these melts without previous immiscibility, which never occurs at high temperatures. During cooling with  $1\text{K}/\text{min}$ , notable deviations of the derivatives in comparison to the cooling rate of  $2\text{K}/\text{min}$  are not noted. The only difference can be observed in the derivatives of  $0.9\text{BaO}-\text{Al}_2\text{O}_3-\text{B}_2\text{O}_3$  and  $\text{BaO}-\text{Al}_2\text{O}_3-\text{B}_2\text{O}_3$ , which show a slight peak at  $850$  and  $830^\circ\text{C}$ , respectively. These peaks indicate that both samples start to crystallise during cooling in contrast to the other samples. Lowering the cooling rate to  $0.5\text{K}/\text{min}$  results in more complex derivatives of the different samples. Below  $890^\circ\text{C}$ , the samples start to crystallise, which is indicated by positive peaks. Good agreement (within the limits of error) of the crystallisation temperatures have been obtained for the base glasses  $0.9\text{BaO}-\text{Al}_2\text{O}_3-\text{B}_2\text{O}_3$  and  $\text{BaO}-\text{Al}_2\text{O}_3-\text{B}_2\text{O}_3$ , whereas the temperature is shifted to lower values in the order  $0.1\text{Li}_2\text{O}-0.9\text{BaO}-\text{Al}_2\text{O}_3-\text{B}_2\text{O}_3 > 0.1\text{MgO}-0.8\text{BaO}-\text{Al}_2\text{O}_3-\text{B}_2\text{O}_3 > 0.2\text{Li}_2\text{O}-0.8\text{BaO}-\text{Al}_2\text{O}_3-\text{B}_2\text{O}_3$ . Furthermore, at a cooling rate of  $0.167\text{K}/\text{min}$ , the base samples exhibit a positive peak below  $905^\circ\text{C}$ , which can be assigned to the

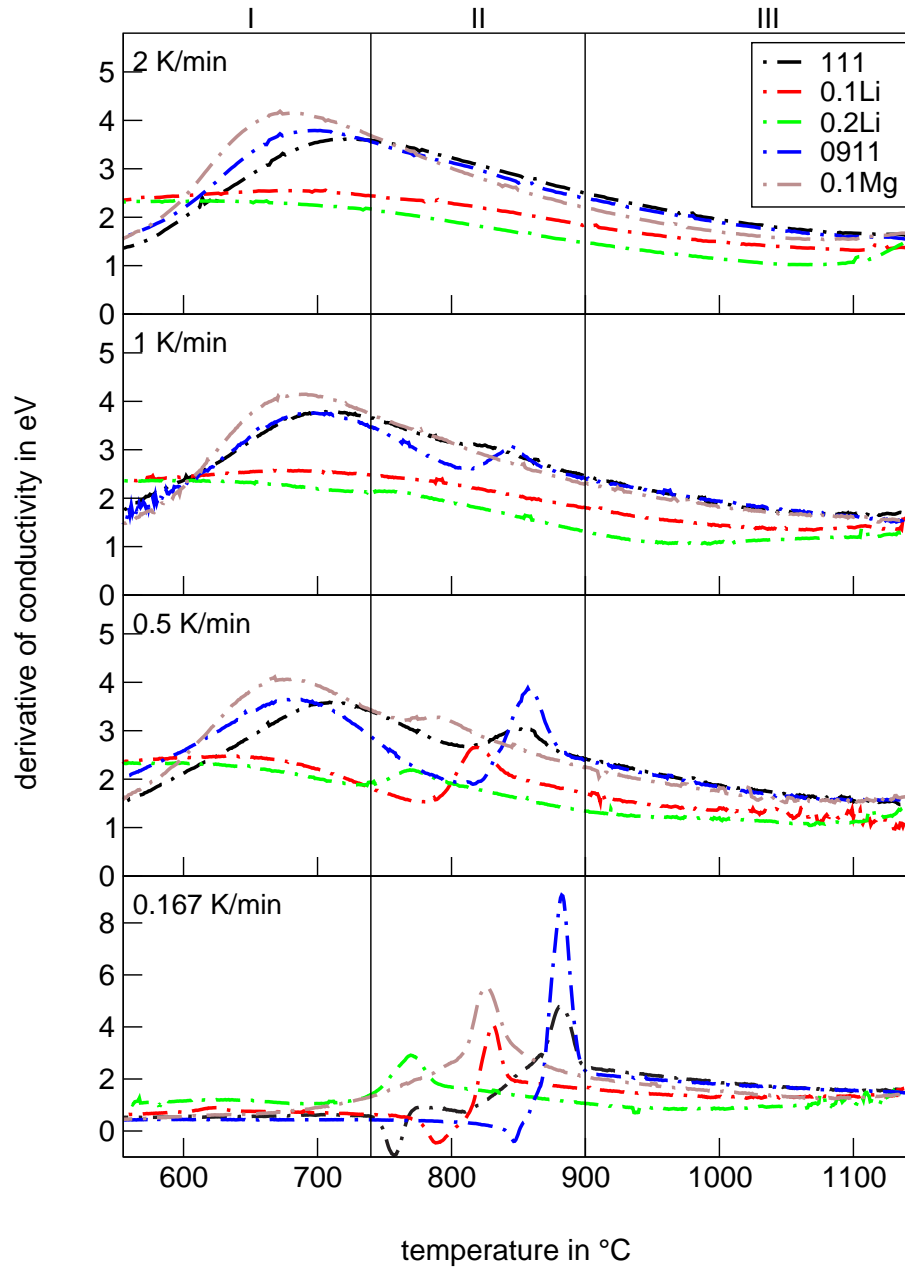


Figure 6.23: Derivatives of the specific conductivities ( $-\ln\sigma/d(1/kT)$ ) of the samples (111):  $\text{BaO}-\text{Al}_2\text{O}_3-\text{B}_2\text{O}_3$ , (0.1Li):  $0.1\text{Li}_2\text{O}-0.9\text{BaO}-\text{Al}_2\text{O}_3-\text{B}_2\text{O}_3$ , (0.2Li):  $0.2\text{Li}_2\text{O}-0.8\text{BaO}-\text{Al}_2\text{O}_3-\text{B}_2\text{O}_3$ , (0911):  $0.9\text{BaO}-\text{Al}_2\text{O}_3-\text{B}_2\text{O}_3$  and (0.1Mg):  $0.1\text{MgO}-0.8\text{BaO}-\text{Al}_2\text{O}_3-\text{B}_2\text{O}_3$  with different cooling rates.

crystallisation of the liquid phase. Similar to heating, the crystallisation process during cooling is also shifted to lower temperatures through the addition of  $\text{Li}_2\text{O}$  and  $\text{MgO}$  in the order  $0.1\text{Li}_2\text{O}-0.9\text{BaO}-\text{Al}_2\text{O}_3-\text{B}_2\text{O}_3 > 0.1\text{MgO}-0.8\text{BaO}-\text{Al}_2\text{O}_3-\text{B}_2\text{O}_3 > 0.2\text{Li}_2\text{O}-0.8\text{BaO}-\text{Al}_2\text{O}_3-\text{B}_2\text{O}_3$ . Further cooling results in a negative peak signalling a phase transition between two allotrops of the  $\text{BaAl}_2\text{B}_2\text{O}_7$  crystalline phase. The negative peak is only observed for the base glasses and the glass  $0.1\text{Li}_2\text{O}-0.9\text{BaO}-\text{Al}_2\text{O}_3-\text{B}_2\text{O}_3$  with

3.3 mol%  $\text{Li}_2\text{O}$ . On the other hand, the samples  $0.1 \text{ MgO} - 0.8 \text{ BaO} - \text{Al}_2\text{O}_3 - \text{B}_2\text{O}_3$  as well as  $0.2 \text{ Li}_2\text{O} - 0.8 \text{ BaO} - \text{Al}_2\text{O}_3 - \text{B}_2\text{O}_3$  do not show a negative peak, which indicates the immediate formation of the low temperature modification of the crystalline phase  $\text{BaAl}_2\text{B}_2\text{O}_7$  (JCPDS 86-2168). This assumption is proved by the XRD patterns of these samples.

Finally, the curves in zone I exhibit the same shape at cooling rates of 2, 1 and 0.5 K/min, i.e. the processes, which occur in this temperature range are cooling rate independent. The derivatives of the base samples and the sample with MgO rise to a maximum at approximately 670 °C, however, a shift to lower temperatures and higher amplitudes can be observed in the order  $\text{BaO} - \text{Al}_2\text{O}_3 - \text{B}_2\text{O}_3 / 0.9 \text{ BaO} - \text{Al}_2\text{O}_3 - \text{B}_2\text{O}_3 / 0.1 \text{ MgO} - 0.8 \text{ BaO} - \text{Al}_2\text{O}_3 - \text{B}_2\text{O}_3$ . The derivative of the samples with  $\text{Li}_2\text{O}$  addition remain nearly constant over the whole temperature range in zone I. At a cooling rate of 0.167 K/min, the derivatives of all investigated samples are constant in zone I, due to a previous formation (in zone II) of the crystalline phase  $\text{BaAl}_2\text{B}_2\text{O}_7$  (JCPDS 86-2168) in all samples. These constant derivatives are equal to the activation energy of the crystalline phase, which is slightly higher through the addition of  $\text{Li}_2\text{O}$ .

Changes during cooling, in principle, might be caused by four phenomena: crystallisation, phase separation and boric acid anomaly as well as aluminum coordination change. In analogy to the heating process, the samples crystallise during cooling in zone II, which is seen in the peaks of the activation energy. Furthermore, phase separation of the samples can be recognised by the broad peak that is observed in zone I for non-crystallised samples. The temperatures of the peak maxima correspond to the peaks of phase separation during heating, which supports this assumption. However, other processes overlap the phase separation and these are the boric acid anomaly and the change of the aluminum coordination in the melt. According to Dietzel [39], the boric acid anomaly should not exist in glass at high temperatures, because the  $[\text{BO}_4^-]$  tetrahedron formation occurs only below 1000 °C. The conductivity measurements show that the activation energies of the samples are constant at temperatures above 1000 °C proving that the boric acid anomaly does not exist, i.e. the melt consists of  $[\text{BO}_3]$  planar triangles. Decreasing the temperature, some  $[\text{BO}_3]$  groups are transformed to  $[\text{BO}_4^-]$  tetrahedra which is shown through the increase of the derivative during cooling. These processes can be observed with the base glasses and the glasses that contain MgO or  $\text{Li}_2\text{O}$ . However, the maximum in zone I occurs only in the derivative of the base glasses and the glass with MgO, which might be explained through the non occurrence of phase separation in the  $\text{Li}_2\text{O}$  containing glasses.

Another interesting property is the activation energy, which changes through the addition of  $\text{Li}_2\text{O}$ . In the glass, i.e. below  $T_g$ , the activation energy of the samples  $\text{BaO} - \text{Al}_2\text{O}_3 -$



$B_2O_3$ ,  $0.9 BaO - Al_2O_3 - B_2O_3$  and  $0.1 MgO - 0.8 BaO - Al_2O_3 - B_2O_3$  is almost similar and has a value of approximately 1.30 eV. The addition of  $Li_2O$  results in an increase of the activation energy to 2.15 eV. Furthermore, the activation energy of the liquid phase declines with increasing  $Li_2O$  concentration (0.68 eV), while the other glasses show approximately the similar values of 1.69 eV. The most outstanding result is the activation energy of the crystalline phase, which is formed in the base glasses and has the very low value of 0.45 eV. Adding  $Li_2O$ , the value increases to 0.67 and 1.06 eV for  $0.1 Li_2O - 0.9 BaO - Al_2O_3 - B_2O_3$  and  $0.2 Li_2O - 0.8 BaO - Al_2O_3 - B_2O_3$ , respectively. However, the activation energy of the crystallised samples with  $Li_2O$  addition is still similar to the activation energy of the crystalline phase  $BaAl_2B_2O_7$  (JCPDS 86-2168) indicating that the  $Ba^{2+}$  ions in the crystalline phase dominate the  $Li^+$  ions in the residual glassy phase, which is an unusual behaviour. In literature, only one compound was found to have a lower activation energy than the crystalline phase  $BaAl_2B_2O_7$  (JCPDS 86-2168), which is  $Ag_2SeO_4$  with 0.28 eV [73]. Other silver containing compositions show also low activation energies around 0.50 eV [74, 75]. Alkaline silicates exhibit activation energies of approximately 0.70 eV [76–78], which increase if  $SiO_2$  is substituted by  $B_2O_3$  [79, 80]. The highest activation energies show alkaline earth borate glasses [81]; Gough [82] published a value of 1.64 eV for the glass  $32 BaO - 28 Al_2O_3 - 40 B_2O_3$ . The base glasses exhibit a slightly lower activation energy, however, the agreement with the literature is good.

Arrhenius plots of the investigated samples are presented in Fig. 6.24 showing the changes of the conductivity caused by the variation of the chemical composition, i.e., the addition of  $MgO$  or  $Li_2O$  to the base glasses. During heating, the conductivities of the glassy as well as of the liquid phase have approximately the same value for the base glasses  $0.9 BaO - Al_2O_3 - B_2O_3$ ,  $BaO - Al_2O_3 - B_2O_3$  and the  $MgO$  containing glass  $0.1 MgO - 0.8 BaO - Al_2O_3 - B_2O_3$ . An addition of 3.3 mol%  $Li_2O$  results in an increase of the conductivity of about the factor six. Furthermore, the doubling of the  $Li_2O$  concentration in the glass  $0.2 Li_2O - 0.8 BaO - Al_2O_3 - B_2O_3$  shows also a doubling of the conductivity. At high temperatures, the differences in the conductivity are not so large for the different liquid phases. At low temperatures, the mobility of the charge carriers is responsible for the conductivity, i.e. the  $Li^+$  ions move much faster than the  $Ba^{2+}$  ions which results in a higher conductivity of the  $Li_2O$  containing glasses. On the other hand, at high temperatures, other effects are more significant than the mobility of the ions. Due to the low viscosity at these temperatures the size of the ions is not decisive. The  $Ba^{2+}$  ions dominate because of their high concentration, which can be seen in a nearly equal conductivity of the liquid phases.

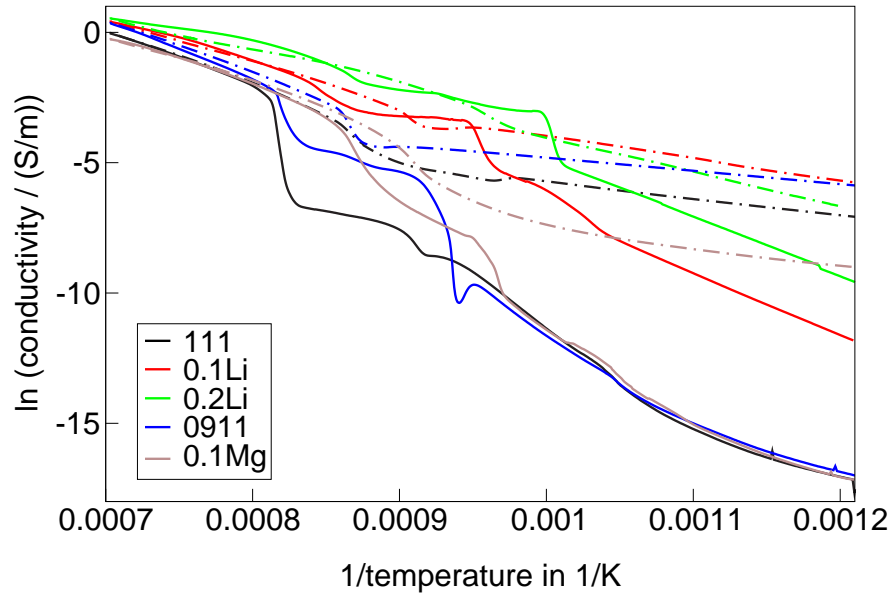


Figure 6.24: Arrhenius plots of the specific conductivities of the samples (111): BaO - Al<sub>2</sub>O<sub>3</sub> - B<sub>2</sub>O<sub>3</sub>, (0.1Li): 0.1 Li<sub>2</sub>O - 0.9 BaO - Al<sub>2</sub>O<sub>3</sub> - B<sub>2</sub>O<sub>3</sub>, (0.2Li): 0.2 Li<sub>2</sub>O - 0.8 BaO - Al<sub>2</sub>O<sub>3</sub> - B<sub>2</sub>O<sub>3</sub>, (0911): 0.9 BaO - Al<sub>2</sub>O<sub>3</sub> - B<sub>2</sub>O<sub>3</sub> and (0.1Mg): 0.1 MgO - 0.8 BaO - Al<sub>2</sub>O<sub>3</sub> - B<sub>2</sub>O<sub>3</sub> during heating (solid line) and subsequent cooling (dash dotted line) with 0.167 K/min.

During cooling with a rate of 0.167 K/min, the samples start to crystallise, which gives the possibility to compare the conductivity of the crystallised samples. The sample 0.2 Li<sub>2</sub>O - 0.8 BaO - Al<sub>2</sub>O<sub>3</sub> - B<sub>2</sub>O<sub>3</sub> will not be included in the discussion, because the slope of the curve differs strongly from the other samples. The conductivity of the crystallised samples increases in the following order: 0.1 MgO - 0.8 BaO - Al<sub>2</sub>O<sub>3</sub> - B<sub>2</sub>O<sub>3</sub> / BaO - Al<sub>2</sub>O<sub>3</sub> - B<sub>2</sub>O<sub>3</sub> / 0.9 BaO - Al<sub>2</sub>O<sub>3</sub> - B<sub>2</sub>O<sub>3</sub> / 0.1 Li<sub>2</sub>O - 0.9 BaO - Al<sub>2</sub>O<sub>3</sub> - B<sub>2</sub>O<sub>3</sub>. As mentioned in section 6.4, the conductivity of the crystallised samples depend on the amount of crystalline phase. Another aspect, which influences the conductivity, is the charge carrier, i.e., as already shown for the glassy phase, Li<sup>+</sup> ions cause a higher conductivity than the Ba<sup>2+</sup> ions. This result explains that the Li<sub>2</sub>O containing sample shows the highest conductivity, while the other samples differ in their amount of crystalline phase.

In conclusion, the additives MgO and Li<sub>2</sub>O influence the conductivities. The reason for the formation of the first peak in the derivative of the conductivity during heating and the broad peak during cooling (both around 700 °C) could be realised. MgO increases the immiscibility of the investigated glass system, which could be seen in the appearance of the first peak in the derivative and the shift of the crystallisation peak to lower temperatures in comparison to the base glass 0.9 BaO - Al<sub>2</sub>O<sub>3</sub> - B<sub>2</sub>O<sub>3</sub>. Furthermore, the glass 0.1 MgO - 0.8 BaO - Al<sub>2</sub>O<sub>3</sub> - B<sub>2</sub>O<sub>3</sub> crystallises also at higher heating rates (1 and 2 K/min)

which is possible through a previous phase separation of the system. On the other hand, during cooling, the crystallisation tendency decreases with the addition of MgO. At high temperatures, phase separation does not occur, therefore a slight crystallisation peak could not be observed until a cooling rate of 0.5 K/min.

The second additive was  $\text{Li}_2\text{O}$ , which should close the miscibility gap of the glass system  $\text{BaO} - \text{Al}_2\text{O}_3 - \text{B}_2\text{O}_3$ . An addition of 3.3 mol%  $\text{Li}_2\text{O}$  results in small changes in the derivative of the conductivity. Peaks attributed to the immiscibility of the glass could only be observed at a heating rate of 0.5 and 0.167 K/min. Further increase of the  $\text{Li}_2\text{O}$  concentration to 6.7 mol% in the glass  $0.2 \text{Li}_2\text{O} - 0.8 \text{BaO} - \text{Al}_2\text{O}_3 - \text{B}_2\text{O}_3$  leads to stronger effects in the conductivity of the system. The derivative is nearly constant in the entire temperature range down to heating and cooling rates of 0.5 K/min showing the prevention of the immiscibility through the addition of  $\text{Li}_2\text{O}$ . Without the occurrence of immiscibility, the samples crystallise only at very low heating rates, e.g. 0.167 K/min. Another explanation of the decreased tendency to crystallisation was described by Avramov [83]. The addition of  $\text{Li}^+$  causes the formation of boron and aluminum in fourfold coordination, which decreases the tendency of crystallisation. On the other hand, the doubling of the  $\text{Li}_2\text{O}$  concentration results also in a doubling of the conductivity of the glassy phase, which can be explained through the faster movement of  $\text{Li}^+$  ions in comparison to  $\text{Ba}^{2+}$ .

Furthermore, the melting temperature decreases in course of the addition of  $\text{Li}_2\text{O}$  and MgO which can be explained by a melting-point depression. The comparison of the derivatives of the different samples proves also a dependency already described under section 5.2. The lower the BaO concentration in the glasses, the higher is the tendency to crystallisation, as shown in samples  $\text{BaO} - \text{Al}_2\text{O}_3 - \text{B}_2\text{O}_3$  and  $0.9 \text{BaO} - \text{Al}_2\text{O}_3 - \text{B}_2\text{O}_3$ .

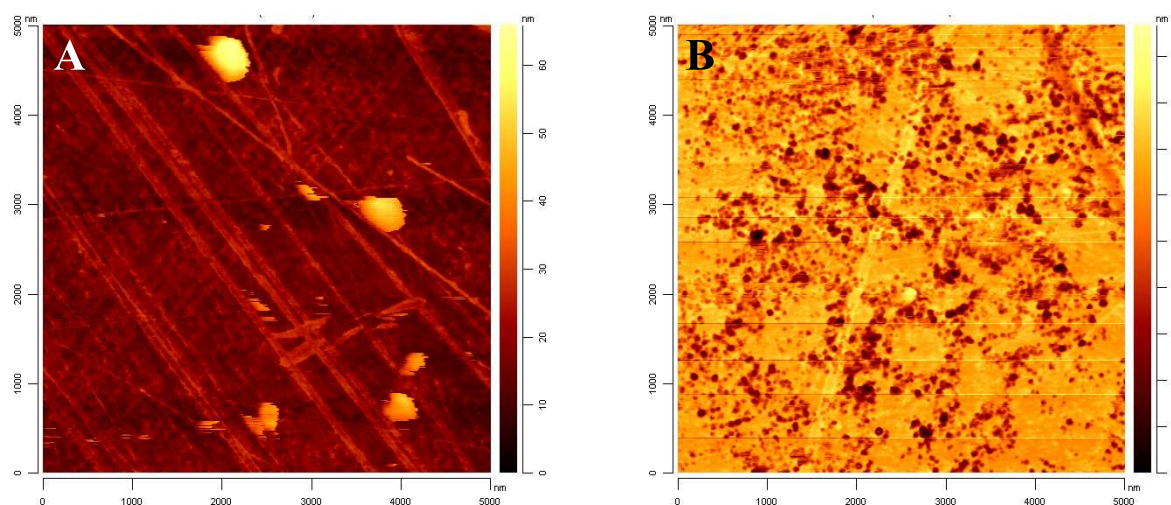


Figure 6.25: AFM micrographs of sample  $0.9 \text{BaO} - \text{Al}_2\text{O}_3 - \text{B}_2\text{O}_3$ ; (A): glass, (B): heat treated at  $680^\circ\text{C}$ , 48 h.

The final proof of the proposed immiscibility could be reported by AFM measurements of a heat treated sample of glass  $0.9 \text{ BaO} - \text{Al}_2\text{O}_3 - \text{B}_2\text{O}_3$ . Figure 6.25 presents the AFM micrographs of the base glass  $0.9 \text{ BaO} - \text{Al}_2\text{O}_3 - \text{B}_2\text{O}_3$  and the heat treated sample. The heat treatment of the glass was carried out at  $680^\circ \text{C}$  for 48 h, while the temperature was chosen from the results of the conductivity measurement with a heating rate of  $0.167 \text{ K/min}$ . Both polished samples were etched with 3%  $\text{HNO}_3$  for 5 s, rinsed with water and further cleaned for 10 to 20 min in an ultrasonic bath before the AFM measurements were carried out. The micrograph of the base glass shows a smooth surface, which has some scratches caused by the polishing of the sample. According to the micrograph B, the heat treatment causes a droplet-shaped immiscibility in the glass  $0.9 \text{ BaO} - \text{Al}_2\text{O}_3 - \text{B}_2\text{O}_3$  with droplet sizes of only a few nanometres.

# Chapter 7

## Discussion

Glasses in the system BaO-Al<sub>2</sub>O<sub>3</sub>-B<sub>2</sub>O<sub>3</sub>, starting from the stoichiometric composition, show a strong tendency to surface crystallisation as already reported in previous studies [4, 15]. The decrease of the BaO concentration results in an increased volume crystallisation accompanied by a small surface crystallisation layer. The stoichiometric glass BaO-Al<sub>2</sub>O<sub>3</sub>-B<sub>2</sub>O<sub>3</sub> tends towards surface crystallisation. According to Zanotto [36], enhanced nucleation rates at the external surfaces are the result of the catalytic effect of some solid impurity particles. In the volume of the stoichiometric glass less nuclei are formed, which results in the growth of long spheroidal crystals. On the other hand, the glasses with decreased BaO concentration (0.80 BaO-Al<sub>2</sub>O<sub>3</sub>-B<sub>2</sub>O<sub>3</sub>, 0.90 BaO-Al<sub>2</sub>O<sub>3</sub>-B<sub>2</sub>O<sub>3</sub>) exhibit volume crystallisation, however, these glasses contain Al<sub>2</sub>O<sub>3</sub> crystals after the melting process. These results lead to the conclusion, that the stoichiometric glass contains a lack of B<sub>2</sub>O<sub>3</sub> caused by B<sub>2</sub>O<sub>3</sub> evaporation during the melting process, which decreases the formation of the crystalline phase BaAl<sub>2</sub>B<sub>2</sub>O<sub>7</sub> (JCPDS 86-2168). In the glasses with decreased BaO concentration, the ratio BaO / Al<sub>2</sub>O<sub>3</sub> / B<sub>2</sub>O<sub>3</sub> should be identical to that of the crystalline phase assuming a similar evaporation of B<sub>2</sub>O<sub>3</sub> during the melting process. On the other hand, the excess of Al<sub>2</sub>O<sub>3</sub> remains as crystals in the glass after melting. If the composition of the glass is similar to the crystalline phase, the glass crystallises easier in the volume. Chemical analysis of the boron concentration was not possible caused by the high alumina concentration, therefore, these assumptions can not be proved. Further increase of the boron oxide concentration, glass 0.90 BaO-1.00 Al<sub>2</sub>O<sub>3</sub>-1.10 B<sub>2</sub>O<sub>3</sub>, resulted in a transparent glass without crystals, which could be transformed in glass-ceramics by volume crystallisation. The excess of B<sub>2</sub>O<sub>3</sub> might be evaporated during the melting process and the remaining oxides form a glass. Crystals of Al<sub>2</sub>O<sub>3</sub> in the glass are not observed; obviously the excess in B<sub>2</sub>O<sub>3</sub> facilitates the glass formation and hence the incorporation of Al<sub>2</sub>O<sub>3</sub> in the glass structure. As mentioned above, the stoichiometric

ratio of the oxides in the glass leads to the crystallisation of  $\text{BaAl}_2\text{B}_2\text{O}_7$  (JCPDS 86-2168).

The additives  $\text{TiO}_2$  and the mixture  $\text{TiO}_2/\text{ZrO}_2$  showed different results in the crystallisation behaviour as well as in the properties of the glasses and respective glass-ceramics. As shown in section 5.4, the tendency to volume crystallisation decreases with the addition of  $\text{TiO}_2$ . Whereas, the mixture  $\text{TiO}_2/\text{ZrO}_2$  increases the nucleation tendency of the glass followed by volume crystallisation up to 7.5 mol%  $\text{TiO}_2/\text{ZrO}_2$  in comparison to the base glass 0.90 BaO - 1.00  $\text{Al}_2\text{O}_3$  - 1.10  $\text{B}_2\text{O}_3$ . A further addition of  $\text{TiO}_2/\text{ZrO}_2$  decreases the crystallisation tendency, which might result from a too high concentration of the nucleation agent. In conclusion,  $\text{TiO}_2$  does not act as nucleation agent in the system BaO -  $\text{Al}_2\text{O}_3$  -  $\text{B}_2\text{O}_3$ , while the mixture  $\text{TiO}_2/\text{ZrO}_2$  up to 7.5 mol% can be used as nucleation agent.

Platinum was added as nucleation agent to those glasses, which exhibit surface crystallisation. This results in volume crystallised glass-ceramics. In the case of all glasses doped with platinum, it may be assumed that heterogeneous nucleation occurred by the precipitation of platinum crystals which act as nucleating agents. A similar behaviour is reported in the literature for many other systems [84, 85].

Furthermore, the properties of the glasses and glass-ceramics are also influenced by the chemical composition of the glasses. In Table 7.1, the glass-ceramics with the lowest thermal expansion coefficients and the highest hydrolytic durabilities are listed for the base glasses as well as for the glasses with the addition of  $\text{TiO}_2$  or  $\text{TiO}_2/\text{ZrO}_2$ . All glass-ceramics shown in Table 7.1 (except samples II-12.5  $\text{TiO}_2$  and 10.0  $\text{TiO}_2/\text{ZrO}_2$ ) contain  $\text{BaAl}_2\text{B}_2\text{O}_7$  (JCPDS 86-2168) as the main crystalline phase. The XRD patterns of the glass-ceramics II-12.5  $\text{TiO}_2$  and 10.0  $\text{TiO}_2/\text{ZrO}_2$  show other crystalline phases and a glassy phase.

As shown in Table 7.1, the thermal expansion coefficients increase through the addition of  $\text{TiO}_2$  as well as of  $\text{TiO}_2/\text{ZrO}_2$  in comparison to the stoichiometric glass BaO- $\text{Al}_2\text{O}_3$ - $\text{B}_2\text{O}_3$ . However, it is still possible to achieve zero thermal expansion with low concentrations of the used additives, as shown for the glass-ceramics I-2.5  $\text{TiO}_2$ , II-2.5  $\text{TiO}_2$  and 5.0  $\text{TiO}_2/\text{ZrO}_2$ . The real reason for the different thermal expansion coefficients of the investigated glass-ceramics could not be figured out, as all consist of the crystalline phase  $\text{BaAl}_2\text{B}_2\text{O}_7$  (JCPDS 86-2168). Obviously, the microstructure is widely responsible for the thermal expansion of the resulting glass-ceramics. For a quantitative interpretation of the effect of microstructure on the thermal expansion, a three dimensional model of the microstructure including the orientation of each grain would be necessary. Additionally elastic constants as well as Young's moduli for the respective crystallographic axis

Table 7.1: Hydrolytic durability and thermal expansion coefficient of selected glasses and glass-ceramics with and without the addition of TiO<sub>2</sub> or TiO<sub>2</sub>/ZrO<sub>2</sub>

Sample name	Additive	Glass $V_{HCl}$ in ml	Glass-ceramics $V_{HCl}$ in ml	$\alpha_{min.neg.}$ in $10^{-7} K^{-1}$
BaO-Al <sub>2</sub> O <sub>3</sub> -B <sub>2</sub> O <sub>3</sub>	-	23.1	36.5	<b>-16 (307 ° C)</b>
0.9BaO-Al <sub>2</sub> O <sub>3</sub> -B <sub>2</sub> O <sub>3</sub>	Pt	25.9	24.5	<b>-7 (374 ° C)</b>
0.9BaO-1.0Al <sub>2</sub> O <sub>3</sub> -1.1B <sub>2</sub> O <sub>3</sub>	Pt	30.5	23.4	-2 (130 ° C)
I- 2.5 TiO <sub>2</sub>	TiO <sub>2</sub> , Pt	17.6	24.5	<b>0 (200 ° C)</b>
I- 7.5 TiO <sub>2</sub>	TiO <sub>2</sub> , Pt	<b>12.8</b>	<b>21.5</b>	-
II- 2.5 TiO <sub>2</sub>	TiO <sub>2</sub> , Pt	24.2	22.3	<b>0 (200 ° C)</b>
II- 12.5 TiO <sub>2</sub>	TiO <sub>2</sub>	<b>12.1</b>	-	-
5.0 TiO <sub>2</sub> /ZrO <sub>2</sub>	TiO <sub>2</sub> /ZrO <sub>2</sub>	<b>11.6</b>	<b>18.1</b>	<b>0 (100 ° C)</b>
10.0 TiO <sub>2</sub> /ZrO <sub>2</sub>	TiO <sub>2</sub> /ZrO <sub>2</sub>	<b>6.3</b>	-	-

should be taken into account. So a quantitative description of the effect of microstructure on the thermal expansion seems to be far too complicated. Furthermore, a reason for the negative thermal expansion of this particular crystalline phase might be the strong displacement effects between aluminum and oxygen connecting two layers of the crystal structure (shown in section 3.4). HT-XRD measurements showed the dependency of the thermal expansion coefficient on the crystallographic orientation of the phase BaAl<sub>2</sub>B<sub>2</sub>O<sub>7</sub> (JCPDS 86-2168). The thermal expansion coefficient is negative in the direction of the c-axis and positive in that of the a-axis. Furthermore, the displaced Al-O bonds are oriented parallel to the c-axis; with increasing temperature they might exhibit decreasing Al-O bond lengths.

With respect to the classification of the hydrolytic durability (shown in Table 4.3 at page 17), the hydrolytic durabilities of the glasses and glass-ceramics are poor. Reasons for this behaviour are associated with the types of used oxides and their coordination number. During boiling of the glasses in water, cations, which act as network-modifier, are dissolved, i.e. a high concentration of monovalent or bivalent cations in the glass leads to a low hydrolytic durability [86, 87]. On the other hand, the coordination of boron is a decisive property for the hydrolytic durability of borate glasses. Previous reports [88] showed, that the occurrence of [BO<sub>3</sub>] leads to a strong decrease of the hydrolytic durability in comparison to [BO<sub>4</sub>] units. The glasses in the system BaO-Al<sub>2</sub>O<sub>3</sub>-B<sub>2</sub>O<sub>3</sub> consist of a high concentration of barium oxide, i.e. a high concentration of Ba<sup>2+</sup> can be dissolved during boiling in water. Furthermore, IR-reflectance spectra showed that



the boron oxide is mainly threefold coordinated in the glass, while the bands indicating fourfold coordinated boron have very low intensities. In the glass-ceramics, the boron oxide is in threefold coordination as seen from the crystal structure of  $\text{BaAl}_2\text{B}_2\text{O}_7$  (JCPDS 86-2168) [21], which was further proved by IR-reflectance spectroscopy. As listed in Table 7.1, the hydrolytic durability of the base glasses and the respective glass-ceramics is very poor. Through the addition of  $\text{TiO}_2$  as well as  $\text{TiO}_2/\text{ZrO}_2$ , the hydrolytic durability of the glass could be improved. Furthermore, the results show, that the improvement is stronger if adding the mixture  $\text{TiO}_2/\text{ZrO}_2$  whereas adding only  $\text{TiO}_2$  has a minor effect. In analogy to previous reports [64], these investigations show a mixing effect of  $\text{TiO}_2$  and  $\text{ZrO}_2$ , which leads to a clear improvement of the hydrolytic durability. The improvement of the durability of the glass-ceramics is much more difficult, as the crystallised phase  $\text{BaAl}_2\text{B}_2\text{O}_7$  (JCPDS 86-2168) always includes  $[\text{BO}_3]$  units. Therefore, an improvement of the glass-ceramics is only possible through the formation of another crystalline phase showing a higher hydrolytic durability or an increased durability of the residual glassy phase.

Investigations with the additives  $\text{TiO}_2$  (see section 5.4 at page 48) and the mixture  $\text{TiO}_2/\text{ZrO}_2$  (see section 5.5 at page 58) showed that it was not possible to crystallise another phase besides  $\text{BaAl}_2\text{B}_2\text{O}_7$  (JCPDS 86-2168). In sample 12.5  $\text{TiO}_2/\text{ZrO}_2$ , the crystalline phase  $\text{BaZr}(\text{BO}_3)_2$  was detected by XRD, however, the crystalline phase  $\text{BaAl}_2\text{B}_2\text{O}_7$  (JCPDS 86-2168) did not crystallise from this glass composition. On the other hand, it was not possible to crystallise the phase  $\text{Al}_2\text{O}_3 \cdot \text{TiO}_2$  in the glasses with  $\text{TiO}_2$  addition, because the crystallisation temperature of this phase might be higher than the melting temperature of the phase  $\text{BaAl}_2\text{B}_2\text{O}_7$  (JCPDS 86-2168) ( $950^\circ\text{C}$  determined by conductivity measurement), i.e. a parallel crystallisation of both phases was not achieved. In conclusion, the crystallisation of a more durable crystalline phase beside  $\text{BaAl}_2\text{B}_2\text{O}_7$  (JCPDS 86-2168) was not successful.

An overall assessment of the properties shows the glass-ceramics 5.0  $\text{TiO}_2/\text{ZrO}_2$  as the sample with the best properties. These glass-ceramics exhibit volume crystallisation and only a slight surface crystallisation layer. Furthermore, the hydrolytic durability of the glass as well as of the glass-ceramics is higher than those of the base samples. On the other hand, the thermal expansion coefficient is zero in the temperature range from  $25$  to  $100^\circ\text{C}$  due to the crystalline phase  $\text{BaAl}_2\text{B}_2\text{O}_7$  (JCPDS 86-2168). The improvement of the hydrolytic durability of the glass-ceramics might be achieved through an appropriate ratio of glassy to crystalline phase, i.e. the improved durability of the glass increases also the hydrolytic durability of the glass-ceramics.

The conductivity measurements, which were carried out in the second part of this thesis, prove some of the above assumptions. As already mentioned, the decrease of the BaO concentration increases the tendency of crystallisation. The stoichiometric glass BaO - Al<sub>2</sub>O<sub>3</sub> - B<sub>2</sub>O<sub>3</sub> shows a crystallisation peak in the derivative of the conductivity only at a heating rate of 0.167 K/min, while the glass 0.9 BaO - Al<sub>2</sub>O<sub>3</sub> - B<sub>2</sub>O<sub>3</sub> exhibits a peak even at heating rates of 1 or 2 K/min. This result also shows that the crystal growth velocity of the stoichiometric glass is very low in comparison to the glass 0.9 BaO - Al<sub>2</sub>O<sub>3</sub> - B<sub>2</sub>O<sub>3</sub>. Furthermore, the observation of phase separation by conductivity measurements supports the assumption that aluminum is fourfold coordinated in the glass. Fourfold coordinated aluminum acts as network-former, which should cause phase separation with another network-former like boron.

In future studies, the conductivity measurements could be used to optimise the crystallisation programs of the glass-ceramics. As the results show, a thermal treatment program including two steps is necessary to obtain well crystallised glass-ceramics. The first holding time should be in the temperature range of the phase separation and the second step in the crystallisation range of the system. In analogy to previous reports [33], the immiscibility leads to homogeneous nucleation and hence, influences the crystallisation of the glass. Therefore, it should be possible to achieve small crystals in the resulting glass-ceramics without the addition of heterogeneous nucleation agents.

# Chapter 8

## Summary

The relatively unknown glass system BaO - Al<sub>2</sub>O<sub>3</sub> - B<sub>2</sub>O<sub>3</sub> was in the focus of this thesis. In the first part of the thesis, the preparation of new glass-ceramics is described starting from the stoichiometric composition BaO - Al<sub>2</sub>O<sub>3</sub> - B<sub>2</sub>O<sub>3</sub>. The crystallisation behaviour of the glasses and the properties of the glasses as well as of the respective glass-ceramics have been investigated to achieve volume crystallised glass-ceramics with low thermal expansion coefficients. Beside the stoichiometric composition, glasses with slightly modified stoichiometries, with the additives TiO<sub>2</sub> or TiO<sub>2</sub> / ZrO<sub>2</sub> and platinum doped glasses have been surveyed. Properties such as density, thermal expansion coefficient and hydrolytic durability were measured from the glasses and respective glass-ceramics. For a better understanding of the effect of composition and the effects of the additives on the physical properties, optical microscopy, scanning electron microscopy and infrared spectroscopy were used. In the second part, electrical impedances of the stoichiometric glass, a glass with slightly modified stoichiometry and glasses with the additives MgO and Li<sub>2</sub>O have been studied as a function of the temperature. These measurements have been used to determine the crystallisation and melting temperature as well as the range of immiscibility of the selected glasses.

In order to provide at first an understanding of the properties of the stoichiometric glass and respective glass-ceramics, the BaO - Al<sub>2</sub>O<sub>3</sub> - B<sub>2</sub>O<sub>3</sub> glass has been transformed in different types of glass-ceramics (bulk glass-ceramics with and without platinum as well as sinter glass-ceramics). These investigations have shown, that glass-ceramics with zero or negative thermal expansion can be produced from the stoichiometric BaO - Al<sub>2</sub>O<sub>3</sub> - B<sub>2</sub>O<sub>3</sub> glass. Responsible for this behaviour is the rhombohedral crystalline phase BaAl<sub>2</sub>B<sub>2</sub>O<sub>7</sub> (JCPDS 86-2168), which causes a decrease of the density in comparison to the base glass. Furthermore, the thermal expansion coefficients strongly depend on the preparation procedure. In sinter glass-ceramics as well as in bulk glass-ceramics with platinum as

nucleation agent, the thermal expansion coefficient is close to that of the crystallographic *a*-axis as shown by high temperature X-ray diffraction. Up to a temperature of 300 °C, the thermal expansion of the bulk glass-ceramics without nucleating agent is close to the value expected from a statistical arrangement of crystals, i.e. the mean thermal expansion of the unit cell.

However, the stoichiometric glass BaO-Al<sub>2</sub>O<sub>3</sub>-B<sub>2</sub>O<sub>3</sub> has a strong tendency to surface crystallisation. Therefore, the composition of the glass was slightly varied by means of the BaO and B<sub>2</sub>O<sub>3</sub> concentrations. The decrease of the BaO concentration resulted in an increased tendency to volume crystallisation, while the surface crystallisation layer strongly decreased. On the other hand, these glasses included some crystals after the preparation, which were identified as Al<sub>2</sub>O<sub>3</sub> crystals. Further experiments showed, that the formation of Al<sub>2</sub>O<sub>3</sub> crystals was promoted by a too low B<sub>2</sub>O<sub>3</sub> concentration, thus, the boron oxide concentration was increased. Finally, in the glass 0.90 BaO-1.00 Al<sub>2</sub>O<sub>3</sub>-1.10 B<sub>2</sub>O<sub>3</sub>, alumina crystals were not observed after the melting process. Whereas, the respective glass-ceramics with and without platinum are volume crystallised and a low thermal expansion coefficient was measured. Hence, for all further variations in the glass composition this glass was used as base glass.

In order to increase the low hydrolytic durability of the glasses and glass-ceramics, TiO<sub>2</sub> was added to the base glass 0.9 BaO-1.0 Al<sub>2</sub>O<sub>3</sub>-1.1 B<sub>2</sub>O<sub>3</sub> using two strategies. In the glasses type I, the TiO<sub>2</sub> concentration was increased, while the concentrations of BaO and B<sub>2</sub>O<sub>3</sub> were decreased, realising an excess of Al<sub>2</sub>O<sub>3</sub>. In the glasses type II, TiO<sub>2</sub> was added to the base glass, while the ratio of the molar concentrations of the other oxides was kept constant. The addition of TiO<sub>2</sub> increases the hydrolytic durability of the glasses type I as well as type II. On the other hand, the tendency to crystallisation of the glasses decreases with increasing TiO<sub>2</sub> concentration. Platinum was added as heterogeneous nucleation agent, however, only a slight improvement of the tendency to crystallisation, especially of the crystalline phase BaAl<sub>2</sub>B<sub>2</sub>O<sub>7</sub> (JCPDS 86-2168) was observed. The thermal expansion coefficient of the glass-ceramics increased with increasing TiO<sub>2</sub> concentration. While the glass-ceramics with 2.5 mol% TiO<sub>2</sub> and platinum showed a smaller thermal expansion than the base glass-ceramics, the thermal expansion increased for the glass-ceramics with higher TiO<sub>2</sub> concentration. The hydrolytic durability of the glass-ceramics with TiO<sub>2</sub> slightly larger in comparison to the base glass-ceramics, but smaller than that of the respective glasses.

Furthermore, the mixture of TiO<sub>2</sub>/ZrO<sub>2</sub> with a molar ratio of 1:1 was added as nucleation agent in order to improve the hydrolytic durability. TiO<sub>2</sub>/ZrO<sub>2</sub> were added to the

base glass  $0.9 \text{ BaO} - 1.0 \text{ Al}_2\text{O}_3 - 1.1 \text{ B}_2\text{O}_3$  keeping the ratio of the molar concentrations of the other oxides constant. The addition caused a stronger improvement of the hydrolytic durability of the glasses than the sole addition of  $\text{TiO}_2$ . All respective glass-ceramics crystallised in the volume and showed only a thin surface crystallisation layer. Up to an addition of 7.5 mol%  $\text{TiO}_2/\text{ZrO}_2$ , the main crystalline phase is  $\text{BaAl}_2\text{B}_2\text{O}_7$  (JCPDS 86-2168), above 7.5 mol%, the tendency to crystallisation decreases and the crystalline phase  $\text{BaZr}(\text{BO}_3)_2$  is formed. The thermal expansion coefficients increase with the addition of  $\text{TiO}_2/\text{ZrO}_2$ , however, up to 7.5 mol%  $\text{TiO}_2/\text{ZrO}_2$ , it is still zero in the temperature range from 25 to 100 °C. A clear improvement of the hydrolytic durability of the glass-ceramics with 2.5 and 5.0 mol%  $\text{TiO}_2/\text{ZrO}_2$  has also been observed in comparison to the base glass-ceramics.

The glass-ceramics with the most negative thermal expansion coefficient are the samples  $\text{BaO}-\text{Al}_2\text{O}_3-\text{B}_2\text{O}_3$  and  $0.9 \text{ BaO}-\text{Al}_2\text{O}_3-\text{B}_2\text{O}_3$  with platinum, with  $-16 \cdot 10^{-7} \text{ K}^{-1}$  from 25 to 307 °C and  $-7 \cdot 10^{-7} \text{ K}^{-1}$  from 25 to 374 °C, respectively. However, the hydrolytic durability of these glass-ceramics is very low. The best hydrolytic durability of all investigated glass-ceramics has been obtained with the sample with 5.0 mol%  $\text{TiO}_2/\text{ZrO}_2$ . Simultaneously, these glass-ceramics showed a zero expansion in the temperature range from 25 to 100 °C.

IR-reflectance spectroscopy was carried out at all investigated glasses and glass-ceramics to obtain informations on the incorporation of the oxides in the glasses and glass-ceramics. In the glasses, the boron oxide is mainly threefold coordinated, while the bands assigned to tetrahedral  $\text{BO}_4$  groups have low intensities. The coordination of aluminum in the glass could not be clarified; further investigations by NMR spectroscopy are necessary. In analogy to Ref. [21], the IR spectra of the glass-ceramics showed that boron oxide is only threefold coordinated in the glass-ceramics. Furthermore, raman spectroscopy was carried out with the base glass and respective glass-ceramics show spectra of very low intensity, which might be due to the poor scattering behaviour of the system  $\text{BaO} - \text{Al}_2\text{O}_3 - \text{B}_2\text{O}_3$ .

In the second part of this thesis, a new method has been developed to determine crystallisation and melting temperatures of glasses by impedance measurements. Impedance measurements can detect phase transitions as already reported for the phase separation of sodiumborosilicate systems [16–20]. The impedance has been measured as a function of the temperature in the range from 550 to 1150 °C during heating and cooling with different rates and at a fixed frequency. The derivative ( $-\text{dln}\sigma/\text{d}(1/kT)$ ) is equal to the activation energy if phase transitions do not occur. Maxima and/or minima in the derivative illustrate phase transitions. In contrast to differential thermal analysis, impedance mea-

surements can also be carried out with any heating and cooling rates, i.e. also with rates much smaller than those which can be applied for differential thermal analysis. Therefore it was possible to determine the crystallisation and melting temperatures in the system BaO - Al<sub>2</sub>O<sub>3</sub> - B<sub>2</sub>O<sub>3</sub>, which shows only a small crystal growth velocity. Another remarkable property of the crystalline phase BaAl<sub>2</sub>B<sub>2</sub>O<sub>7</sub> (JCPDS 86-2168) has been detected: the activation energy of the ionic conductivity of the glass-ceramics is extremely low with 0.50 eV. A further peculiarity of the glass-ceramics is the higher conductivity in comparison with the respective glasses. Furthermore, phase separation has also been detected by impedance measurements, which could be proved through the addition of MgO or Li<sub>2</sub>O to the stoichiometric glass BaO - Al<sub>2</sub>O<sub>3</sub> - B<sub>2</sub>O<sub>3</sub> and the slightly varied glass 0.9 BaO - Al<sub>2</sub>O<sub>3</sub> - B<sub>2</sub>O<sub>3</sub>. Magnesium oxide opened the miscibility gap, which resulted in a shift of the crystallisation to lower temperatures. On the other hand, the addition of Li<sub>2</sub>O closed the immiscibility gap and decreased the tendency to crystallisation. The doubling of the Li<sub>2</sub>O concentration resulted also in a doubling of the conductivity of the glass, while such dependency was not detected in the glass-ceramics. The activation energy of the crystallised samples with Li<sub>2</sub>O addition is similar to the activation energy of the crystalline phase BaAl<sub>2</sub>B<sub>2</sub>O<sub>7</sub> (JCPDS 86-2168), indicating that the Ba<sup>2+</sup> ions in the crystalline phase dominate the Li<sup>+</sup> ions in the residual glassy phase, which is an unusual behaviour. A common property of the additions MgO and Li<sub>2</sub>O is the decrease of the melting temperature in comparison to the base samples which can be explained by a melting-point depression. Finally, AFM measurements visualised the immiscibility; the droplet sizes are only a few nanometres.

New glass-ceramics with low thermal expansion coefficients were produced in the system BaO - Al<sub>2</sub>O<sub>3</sub> - B<sub>2</sub>O<sub>3</sub>, which might be used in the micromechanics.

# Bibliography

- [1] G. H. Beall and L. R. Pinckney. Nanophase glass-ceramics. *J. Am. Ceram. Soc.*, 82:5–16, 1999.
- [2] W. Vogel and W. Höland. Nucleation and crystallization kinetics of magnesium oxide-aluminum oxide-silicon dioxide base glass with different dopants. *Z. Chem.*, 22:429–438, 1982.
- [3] P. Wange, T. Höche, C. Rüssel, and J.-D. Schnapp. Microstructure-property relationship in high-strength MgO-Al<sub>2</sub>O<sub>3</sub>-SiO<sub>2</sub>-TiO<sub>2</sub> glass-ceramics. *J. Non-Cryst. Solids*, 298:137–145, 2002.
- [4] J. F. MacDowell. Aluminoborate glass-ceramics with low thermal expansivity. *J. Am. Ceram. Soc.*, 73:2287–92, 1990.
- [5] T. Rudolph, D. V. Szabo, W. Pannhorst, K.-L. Weisskopf, and G. Petzow. Microstructural development of a diphosphorus pentoxide modified cordierite glass ceramic during sintering. Part 1. Microscopic characterization. *Glastech. Ber.*, 64:218, 1991.
- [6] G. H. Beall. Design of glass-ceramics. *Rev. Solid State Sci.*, 3:333–354, 1989.
- [7] S. Habelitz, G. Carl, and C. Rüssel. Processing, microstructure and mechanical properties of extruded mica glass-ceramics. *Mater. Sci. Eng.*, A 307:1–14, 2001.
- [8] J. Elsen, G. S. D. King, W. Höland, W. Vogel, and G. Carl. Crystal structure of a fluorphlogopite synthesized in a glass ceramic. *J. Chem. Res.*, 6:160–161, 1989.
- [9] W. Vogel and W. Höland. Development of bioglass ceramics for medicine. *Angew. Chem.*, 99:541–558, 1987.
- [10] C. Moisescu, C. Jana, and C. Rüssel. Crystallization of rod-shaped fluoroapatite from glass melts in the system SiO<sub>2</sub>-Al<sub>2</sub>O<sub>3</sub>-CaO-P<sub>2</sub>O<sub>5</sub>-Na<sub>2</sub>O-K<sub>2</sub>O-f-. *J. Non-Cryst. Solids*, 248:169–175, 1999.



- [11] J. Vogel, C. Jana, and P. Hartmann. Structural investigation of SiO<sub>2</sub>-containing phosphate glasses. *Glastech. Ber. Glass Sci. Technol.*, 71:97–101, 1998.
- [12] H. Bach, editor. *Low thermal expansion glass ceramics*. Springer Berlin, Heidelberg, New York, 1995.
- [13] E. J. Smoke. Ceramic compositions having negative linear thermal expansion. *J. Am. Ceram. Soc.*, 34:87–90, 1951.
- [14] J. Petzold and W. Pannhorst. Chemistry and structure of glass-ceramic materials for high precision optical applications. *J. Non-Cryst. Solids*, 129:191–198, 1991.
- [15] R. M. Hovhannisyan. Rafaelites-new kind of glass ceramics with low thermal expansion and low melting temperatures on the basis of alkaline earth aluminium borates. *Glass Technol.*, 44:96-100, 2003.
- [16] C. Ravagnani, R. Keding, and C. Rüssel. The impedance of Na<sub>2</sub>O / B<sub>2</sub>O<sub>3</sub> / SiO<sub>2</sub> glass during phase separation. *Glastech. Ber. Glass Sci. Technol.*, 73 C2:166–175, 2000.
- [17] C. Ravagnani, R. Keding, and C. Rüssel. High temperature impedance spectroscopy of homogeneous and phase separated melts and glasses of the composition 48.5SiO<sub>2</sub>-48.5B<sub>2</sub>O<sub>3</sub>-3Na<sub>2</sub>O. *J. Non-Cryst. Solids*, 328:164–173, 2003.
- [18] C. Ravagnani, R. Keding, and C. Rüssel. Phase separation in a glass melt with the composition 6.5Na<sub>2</sub>O-33.5B<sub>2</sub>O<sub>3</sub>-60SiO<sub>2</sub> studied by impedance spectroscopy. *Glass Sci. Technol.*, 77:77–81, 2004.
- [19] K. C. Sobha and K. J. Rao. Investigation of phosphate glasses with the general formula A<sub>x</sub>B<sub>y</sub>P<sub>3</sub>O<sub>12</sub> where A=Li, Na or K and B=Fe, Ga, Ti, Ge, V or Nb. *J. Non-Cryst. Solids*, 201:52–65, 1996.
- [20] R. F. Bartholomew, D. M. Young, and A. J. G. Ellison. Electrical properties of new glasses based on the Li<sub>2</sub>S-SiS<sub>2</sub> system. *J. Non-Cryst. Solids*, 256-257:242, 1999.
- [21] N. Ye, R. Zeng, B. C. Wu, X. Y. Huang, and C. T. Chen. Crystal structure of barium aluminium borate, BaAl<sub>2</sub>B<sub>2</sub>O<sub>7</sub>. *Z. Kristallogr. NCS*, 213:452, 1998.
- [22] H. Scheidler and E. Rodek. Li<sub>2</sub>O-Al<sub>2</sub>O<sub>3</sub>-SiO<sub>2</sub> glass ceramics. *Ceram. Bull.*, 68:1926–1930, 1989.
- [23] W. Pannhorst, R. Müller, and H. Höness. Status of the production of 8 m ZERODUR mirror blanks. *SPIE*, 2018:226–236, 1993.

- [24] J. F. MacDowell and P. Yan. Alkaline earth aluminoborate glass-ceramics. US Patent: 4,861,734, Aug. 29 1989.
- [25] C. Lira, A. P. N. De Oliveira, and O. E. Alarcon. Sintering and crystallization of MgO-Al<sub>2</sub>O<sub>3</sub>-SiO<sub>2</sub> glass powders to produce cordierite glass ceramics. *Glass Technol.*, 45(12):43–48, 2004.
- [26] I. Szabo, B. Nagy, G. Völksch, and W. Höland. Structure, chemical durability and microhardness of glass-ceramics containing apatite and leucite crystals. *J. Non-Cryst. Solids*, 272:191–199, 2000.
- [27] R. Keding, D. Tauch, and C. Rüssel. Electrical impedance determination of phase transitions in glasses and melts. *J. Non-Cryst. Solids*, 348:123–130, 2004.
- [28] H. Scheidler. Herstellung und Eigenschaften von Glaskeramik-Werkstoffen. *Silika. J.*, 11:144–149, 1972.
- [29] W. Pannhorst. Glass ceramics: state-of-the-art. *J. Non-Cryst. Solids*, 219:198–204, 1997.
- [30] W. Pannhorst. Low expansion glass ceramics - Review of the glass ceramics Ceran and Zerodur and their applications. In *Nucleation and crystallization in liquids and glasses*, pages 267–276. Westerville, Ohio, 1993.
- [31] Without author. Schott Technische Gläser. Brochure, Mainz, 1999.
- [32] G. Tammann. *Kristallisieren und Schmelzen*. Barth Leipzig, 1903.
- [33] E. R. Plumat. Surface and bulk nucleation and phase separation in some vitreous systems. *Silic. Ind.*, 38:97–105, 1973.
- [34] S. D. Stookey. German patent no. 1045056, 1956.
- [35] T. Kokubo. Surface chemistry of bioactive glass ceramics. *J. Non-Cryst. Solids*, 120:138–151, 1990.
- [36] E. D. Zanotto. Surface crystallization kinetics in soda-lime-silica glasses. *J. Non-Cryst. Solids*, 129:183–190, 1991.
- [37] H. Scholze. *Glas*. Springer Berlin, Heidelberg, New York, 1988.
- [38] W. Vogel and K. Gerth. Model silicate glasses and their constitution. *Glastechn. Ber.*, 31:15–28, 1958.

- [39] A. Dietzel. Glass structure and glass properties. II. *Glastech. Ber.*, 22:81–86, 1948.
- [40] K.-H. Hübner. Untersuchungen im Dreistoffsystem BaO-Al<sub>2</sub>O<sub>3</sub>-B<sub>2</sub>O<sub>3</sub>. *N. Jb. Miner. Abh.*, 112:150–160, 1970.
- [41] W. Vogel. *Glass Chemistry*. Springer Berlin, Heidelberg, New York, 1994.
- [42] Wasserbeständigkeit von Glasgrieß bei 98 °C. DIN ISO 719, 1989.
- [43] A. Karamanov and M. Pelino. Evaluation of the degree of crystallization in glass-ceramics by density measurements. *J. Eur. Ceram. Soc.*, 19:649–654, 1999.
- [44] R. Müller, R. Naumann, and S. Reinsch. Surface nucleation of  $\mu$ -cordierite in cordierite glass: thermodynamic aspects. *Thermochim. Acta*, 280/281:191–204, 1996.
- [45] P. E. Hart, M. G. Mesko, and J. E. Shelby. Crystallization and phase equilibrium in the sodium barium metaphosphate system. *J. Non-Cryst. Solids*, 263/264:305–311, 2000.
- [46] T. G. Mayerhöfer, H. H. Dunken, R. Keding, and C. Rüssel. Interpretation and modeling of IR-reflectance spectra of glasses considering medium range order. *J. Non-Cryst. Solids*, 333:172–181, 2004.
- [47] J. A. Duffy, B. Harris, E. I. Kamitsos, G. D. Chryssikos, and Y. D. Yiannopoulos. Basicity variation in network oxides: distribution of metal ion sites in borate glass systems. *J. Phys. Chem. B*, 101:4188–4192, 1997.
- [48] V. C. Farmer, editor. *The infrared spectra of minerals*. Mineralogical Society, London, 1974.
- [49] V. G. Chekhovskii, Y. A. Petrov, S. Redala, and P. Pauks. Study of the crystallization of glasses of the strontia (or baria)-alumina-boric oxide system. *Fiz. Khim. Stekla*, 15:265–268, 1989.
- [50] J. Fukunaga, R. Ota, M. Shiroyama, and N. Yoshida. Raman and infrared spectroscopy and some physical properties of glasses in the MgO-Al<sub>2</sub>O<sub>3</sub>-B<sub>2</sub>O<sub>3</sub> system. *Nippon Kagaku Kaishi*, 12:1971–1976, 1988.
- [51] A. Daniel. *Untersuchungen zum strukturellen Einbau von Zinnionen in Erdalkali- und Zinkboratgläser sowie die Charakterisierung der Eigenschaften der Gläser*. PhD thesis, Friedrich-Schiller-Universität Jena, 1999.

- [52] P. Pernice, S. Esposito, A. Aronne, and V. N. Sigaev. Structure and crystallization behavior of glasses in the BaO-B<sub>2</sub>O<sub>3</sub>-Al<sub>2</sub>O<sub>3</sub> system. *J. Non-Cryst. Solids*, 258:1–10, 1999.
- [53] N. I. Leonyuk and E. P. Shvanskiy. X-ray powder diffraction study of solids in the CaO-Al<sub>2</sub>O<sub>3</sub>-B<sub>2</sub>O<sub>3</sub> system. *Mater. Sci. Forum*, 278-281:589–593, 1998.
- [54] K. Heide, E. Hartung, H. G. Schmidt, and I. Ottlinger. Study of evaporation of boron during melting of boron-containing glass batches. *Glastech. Ber.*, 59:59–63, 1986.
- [55] M. H. V. Fernandes and M. Cable. Reactive vaporization of sodium tetraborate with water vapor. *Glass Technol.*, 34:26–32, 1993.
- [56] C. Pentzel. Mechanism of volatilization of fluorides from E-glass melts. *Glass Sci. Technol.*, 67:213–219, 1994.
- [57] M. A. Villegas, A. de Pablos, and J. M. F. Navarro. Properties of CaO-TiO<sub>2</sub>-SiO<sub>2</sub>. *Glass Technol.*, 35:276–280, 1994.
- [58] T. Baak, C. F. Rapp, H. T. Hartley, and B. E. Wiens. Chemical durability of a soda-lime glass with titanium dioxide, germanium dioxide, zirconium dioxide, and aluminum phosphate partially substituted for silicon dioxide. *Am. Ceram. Soc. Bull.*, 47:727–730, 1968.
- [59] F. J. Parker and W. R. Grace. Aluminum titanate (Al<sub>2</sub>TiO<sub>5</sub>)-zirconium titanate (ZrTiO<sub>4</sub>)-zirconia composites: a new family of low-thermal-expansion ceramics. *J. Am. Ceram. Soc.*, 73:929–932, 1990.
- [60] P. Virro-Nic and J. Pilling. Thermal expansion and microstructures of melted Al<sub>2</sub>O<sub>3</sub>-ZrO<sub>2</sub>-TiO<sub>2</sub> ceramics. *J. Mater. Sci. Lett.*, 13:950–954, 1994.
- [61] F. D. Dönitz, E. Heidenreich, A. Röncke, and W. Vogel. Complex effect of zirconia and titania on the phase separation process in glass-ceramics. *Silikattechnik*, 33:81–84, 1982.
- [62] T. I. Barry, J. M. Cox, and R. Morrell. Cordierite glass-ceramics-effect of titanium dioxide and zirconium dioxide content on phase sequence during heat treatment. *J. Mater. Sci.*, 13:594–610, 1978.
- [63] W. Sack and H. Scheidler. Effects of the nucleating agents TiO<sub>2</sub> and ZrO<sub>2</sub> on crystal phases formed during development of glass-ceramics (pyroceram bodies). *Glastech. Ber.*, 39:126–130, 1966.

- [64] D. Tauch. Korrosion von Glasfasern. Master's thesis, Friedrich-Schiller-Universität Jena, 2001.
- [65] <http://plasma-gate.weizmann.ac.il/grace/>, 2004.
- [66] I. Gutzow and J. Schmelzer. *The Vitreous State*. Springer Berlin, Heidelberg, New York, 1995.
- [67] P. Hudon and D. R. Baker. The nature of phase separation in binary oxide melts and glasses. I. Silicate systems. *J. Non-Cryst. Solids*, 303:299–345, 2002.
- [68] P. Hudon and D. R. Baker. The nature of phase separation in binary oxide melts and glasses. III. Borate and germanate systems. *J. Non-Cryst. Solids*, 303:354–371, 2002.
- [69] I. J. M. Hermans. Fundamentals of glass science and technology. pages 558–564, Gotab, Stockholm, 1997.
- [70] W. J. Zachariasen. The atomic arrangement in glass. *J. Am. Ceram. Soc.*, 54:3841–3851, 1932.
- [71] P. Taylor, A. B. Campell, and D. G. Owen. Liquid immiscibility in the system  $X_2O$ - $MO$ - $B_2O_3$ - $SiO_2$  ( $X=Na, K$ ;  $M=Mg, Ca, Ba$ ) and sodium oxide-magnesium oxide-barium oxide-boron oxide-silicon dioxide. *J. Am. Ceram. Soc.*, 66:347, 1983.
- [72] J. W. Greig. Immiscibility in high-silica melts. *J. Soc. Glass Technol.*, 8:255–256, 1924.
- [73] C. Cramer and M. Buschner. Complete conductivity spectra of fast ion conducting silver iodite/silver selenate glass. *Solid State Ionics*, 105:109–120, 1998.
- [74] M. D. Ingram, B. Macmillan, A. J. Pappin, B. Roling, and J. M. Hitchinson. Effects on the ionic conductivity of  $AgI$ - $AgPO_3$  and  $KI$ - $AgPO_3$  glass. *Solid State Ionics*, 105:103–107, 1998.
- [75] M. Doreau, J. P. Malugani, and G. Robert. Silver phosphate-sodium iodide and -potassium iodide mixed glasses: vitreous domain, electrical conductivity, and a structural approach. *Electrochim. Acta*, 26:711–717, 1981.
- [76] A. S. Nowick, A. V. Vaysleyb, and W. Liu. Identification of distinctive regimes of behaviour in the ac electrical response of glass. *Solid State Ionics*, 105:121–128, 1998.

- [77] J. L. Souquet, M. Duclot, and M. Levy. Ionic transport mechanism in oxide based glasses in the supercooled and glassy states. *Solid State Ionics*, 105:237–242, 1998.
- [78] V. V. Ipat'eva, Z. U. Borisova, and V. S. Molchanov. Effect of the simultaneous presence of two alkali metal ions on the electric conductivity of silicate glasses (suppression effect in complex silicate glasses). *Zh. Prikl. Khim.*, 40:1424–30, 1967.
- [79] B. Roling. Scaling properties of the conductivity spectra of glasses and supercooled melts. *Solid State Ionics*, 105:185–193, 1998.
- [80] J. Setina and G. V. Lefand. Electrical properties of modified lead borate glasses. *Neorg. Stekla, Pokrytiya Mater.*, 6:77–83, 1983.
- [81] C. Hirayama. Properties of aluminoborate glasses of group II metal oxides: II. electrical properties. *J. Am. Ceram. Soc.*, 45:288–293, 1962.
- [82] E. Gough, J. O. Isard, and J. A. Topping. Electrical properties of alkali-free borate glasses. *Phys. Chem. Glasses*, 10:89–100, 1969.
- [83] I. Avramov, R. Keding, and C. Rüssel. The role of network rigidity on crystallization behaviour of glasses. *Glastech. Ber. Glass Sci. Technol.*, 73 C1:138–145, 2000.
- [84] N. Mishima, T. Wakasugi, and R. Ota. Nucleation behavior of  $\text{Li}_2\text{O-Na}_2\text{O-SiO}_2$  glass doped with platinum. *J. Ceram. Soc. Jpn.*, 112:350–353, 2004.
- [85] G. H. Frischat. Controlled nucleation and crystallisation of fluorozirconate glasses. *Ceram. Trans.*, 30:233–239, 1993.
- [86] H. Scholze. Chemical durability of glasses. *J. Non-Cryst. Solids*, 52:91–103, 1982.
- [87] A. Paul. Chemical durability of glasses; a thermodynamic approach. *J. Mater. Sci.*, 12:2246–2268, 1977.
- [88] D. Ehrt. Personal Communication, Jena, 2004.

# Danksagung

Mein besonderer Dank gilt Herrn Prof. Dr. Dr. C. Rüssel für die interessante Themenstellung und die fachliche Betreuung.

Ebenfalls möchte ich Frau Prof. Dr. D. Stachel für die Bereitschaft, ein Gutachten für die vorliegende Dissertation zu übernehmen, danken.

Mein Dank gilt auch Herrn Dr. R. Keding für die fachlichen Diskussionen und die praktische Unterstützung bei der Durchführung der Impedanzmessungen.

Des Weiteren möchte ich Herrn Dr. T. Mayerhöfer und Frau Weber vom Institut für Physikalische Chemie für die Durchführung der IR-Reflexionsmessungen und die vielen anregenden Diskussionen danken.

Frau S. Ebbinghaus danke ich für die Durchführung einiger Experimente, Frau E. Wagner für die Messungen der Röntgendiffraktogramme und Frau G. Möller für die sehr anspruchsvolle Probenvorbereitung.

Mein herzlicher Dank gilt auch allen weiteren Mitarbeitern des Otto-Schott-Instituts, die zum Gelingen dieser Arbeit beigetragen haben.

Danken möchte ich auch all meinen Freunden für die schöne Studienzeit in Jena, welche unvergessen bleiben wird. Insbesondere sei allen Korrekturlesern für die harte Arbeit an dieser Stelle gedankt.

Und nicht zuletzt gilt mein außerordentlicher Dank meiner Familie und meinem Freund Tommy Kaspar für die moralische Unterstützung während meines Studiums und der Promotionszeit.



## **Selbstständigkeitserklärung**

Ich erkläre, dass ich die vorliegende Arbeit selbständig und unter Verwendung der angegebenen Hilfsmittel, persönlichen Mitteilungen und Quellen angefertigt habe.

Jena, den 26.05.2005

# Lebenslauf

## Persönliche Daten

Name	Diana Tauch
Geburtsdatum	02.04.1977
Geburtsort	Jena
Familienstand	ledig

## Ausbildungsdaten

09/91 - 06/95	Sportgymnasium "Johann Chr. Fr. GutsMuths" Jena
06/95	Abitur
10/95 - 08/01	Studium der Chemie (Umweltchemie) an der Friedrich-Schiller-Universität Jena
09/98 - 05/99	Studium der Chemie an der McGill University Montreal, Kanada
08/01	Diplom in Chemie
seit 11/01	Wissenschaftlicher Mitarbeiter am Otto-Schott-Institut der Friedrich-Schiller-Universität Jena
01/04 - 04/04	Forschungsaufenthalt an der Nagaoka University of Technology, Japan

Jena, den 26.05.2005